TOPOLOGICAL SOLITONS IN MAGNETIC SYSTEMS

by

Anirban Ghosh

A dissertation submitted to The Johns Hopkins University in conformity with the requirements for the degree of Doctor of Philosophy.

Baltimore, Maryland

August, 2017

Abstract

A ferromagnet can often have inhomogeneous states that are protected from decaying into the uniform ground state due to topological reasons. Common examples of such states, known as topological solitons, are domain walls in a ferromagnetic wire and domain walls, vortices and skyrmions in two- and three-dimensional ferromagnets. In this dissertation, we study the statics and dynamics of multiple interacting topological solitons in one- and two-dimensional magnets.

The ferromagnetic spin-1/2 Ising chain has domain walls, also known as kinks, as its elementary excitations. Adding a weak transverse magnetic field endows kinks with an ability to move; an additional weak longitudinal field leads to their confinement. In particular, this gives rise to a hierarchy of two-kink bound states. We show that in a two-dimensional system of parallel Ising chains with weak antiferromagnetic interchain coupling, two confined pairs on adjacent chains can form a composite bound state. This work supports the interpretation of an experimentally observed excitation in the spectrum of the quasi one-dimensional magnet $CoNb_2O_6$ as a four-kink bound state.

ABSTRACT

Two domain walls in a classical ferromagnetic spin chain attract each other with a force that is exponentially weak at large separations but gets stronger as the domain walls approach each other. In the absence of energy dissipation this force simply causes a simultaneous precession of all magnetization vectors about the chain direction with a fixed angular velocity, owing to the gyrotropic nature of the dynamics of spins. Adding dissipation to the system then causes the two domain walls to approach each other and ultimately annihilate to create a uniform state. We develop an effective theory of the dynamics of the annihilation process by isolating four modes of the system, parametrized by four collective coordinates, that capture the essential physics of this process: the global position and orientation of the two domain walls and their relative position and orientation. The theoretical predictions are found to be in excellent agreement with micromagnetic simulations of the domain wall annihilation.

Finally, we present a theory of the annihilation process of a vortex and an antivortex in a ferromagnetic thin film.

Primary Reader: Oleg Tchernyshyov

Secondary Reader: Predrag Nikolic

Acknowledgments

Foremost, I owe deepest gratitude to my advisor Oleg Tchernyshyov for his patient guidance and continuous encouragement over all these years. I learned how to think like a theoretical physicist from him.

I would then like to thank Peter Armitage for engaging me in two of his experimental projects early on in my research. He helped broaden my perspective of physics by showing how experimentalists approach a problem.

I would then like to thank all my other research collaborators, especially Chris Morris, LiDong Pan, Se Kwon Kim, Kevin Huang, and Derek Reitz, for sharing their great physical insights on various problems with me.

I would then like to thank my many friends and colleagues at Hopkins, Yuan Wan, Olga Petrova, Imam Makhfudz, Se Kwon Kim, Jiadong Zang, Jake Mokris, Sayak Dasgupta, Shu Zhang, Hitesh Changlani and Michael Bjerngaard, with whom I had numerous stimulating physics discussions.

I made many other great friends at Hopkins over the long years, but alas there is only space to name a few here. Special thanks to Jiajia Wen, Prasenjit Bose, Arpit

ACKNOWLEDGMENTS

Gupta, Manu Madhav, Ravikrishnan P. Jayakumar, Subhransu Mishra and Linda Braun, among many others.

I would also like to thank my parents for their continuous support over Skype calls.

Lastly, I would like to thank all my friends who have made my graduate life a memorable experience - especially, Anirban Gangopadhyay, Madhura Joglekar, Srimoyee Sen, Kaji Rajubul Islam, Shantanu Debnath, Sumit Shekhar, again among many others.

Contents

List of Figures

Chapter 1

Introduction

In this chapter, we will introduce the concept of a magnetic soliton. The distinction between topological and non-topological solitons will be presented and the issue of stability of these solitons will be discussed. We will then proceed to a show how the various magnetic interactions found in condensed matter give rise to specific topological solitons in one- and two-dimensional systems.

1.1 Topological and Non-topological Solitons

The state of a classical magnet can be completely characterized by specifying the local magnetization vector $\mathbf{M}$ (magnetic dipole moment per unit volume) at every point in space, i.e. by the vector field $\mathbf{M}(\mathbf{r})$. In this dissertation, we will not study

phase transitions and will work at temperatures well below the Curie temperature of the material. Fluctuation effects are insignificant in this regime and the magnitude of $\mathbf{M}$ remains the same everywhere in space. As a result, we will simply use the unit vector $\mathbf{m}(\mathbf{r}) = \mathbf{M}(\mathbf{r})/|\mathbf{M}|$ to characterize the state of our system.

In this dissertation, we will be interested specifically in ferromagnets, in which the Heisenberg exchange interaction [1, 2] tries to align neighboring magnetic moments. Therefore, magnetization tends to be uniform in a ground state. For example, in a ferromagnetic wire, shape anisotropy caused by the dipolar interaction prefers $\mathbf{m}$ to point along the length of the wire in one of the two possible directions. This gives rise to two ground states $\mathbf{m}(z) = \pm\hat{\mathbf{z}}$, where the z-axis is along the length of the wire, as shown in Figure 1.1.

A magnetic soliton [3] can be defined as an localized configuration $\mathbf{m}(\mathbf{r})$ that approaches a ground state as $r \to \infty$. If the system has multiple ground states, like the ferromagnetic wire, the ground state at different points at infinity may or may not be the same (Figure 1.1). One can ask whether or not a soliton can be continuously deformed to one of the ground states. This forms the basis of a classification of solitons into topological and non-topological ones. In the rest of this section, we will illustrate these two types of solitons in the simple setting of a one-dimensional ferromagnet with an easy axis.

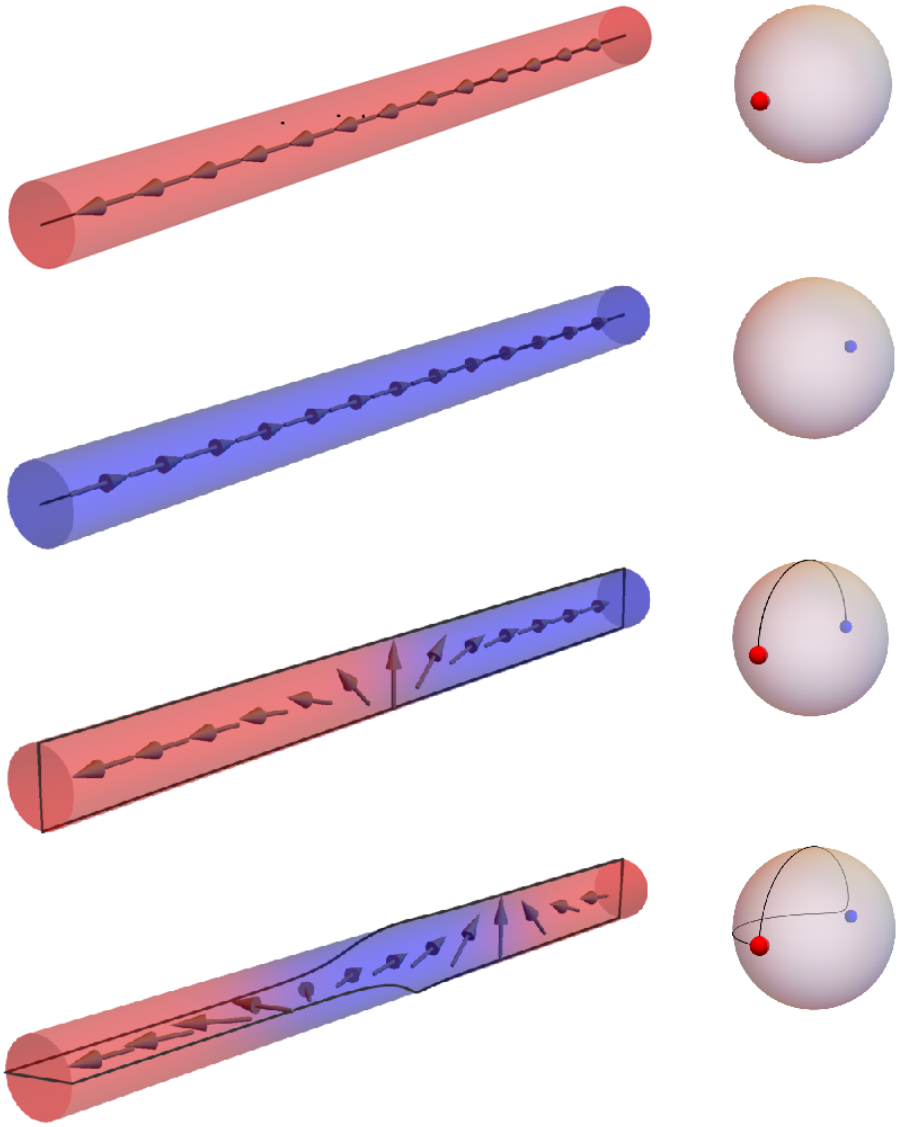

Figure 1.1: Left column: Four configurations of magnetization in the one-dimensional ferromagnetic wire with an easy axis along its length. The first two are the two ground states. The third one is a domain wall. The fourth one is a pair of domain walls with a $\pi/2$ twist between them in the azimuthal direction. Red and blue denote spins pointing along $+\hat{\mathbf{z}}$ and $-\hat{\mathbf{z}}$ respectively. Right column: Corresponding trajectories of the $\mathbf{m}$ vector on the unit magnetization sphere.

1.1.1 Solitons in One Dimension

The total potential energy of a ferromagnetic wire with exchange and anisotropy can be written as

$$U = \int_{-\infty}^{\infty} dz \left(A|\mathbf{m}'|^2 + K|\mathbf{m} \times \hat{\mathbf{z}}|^2 \right) /2. \tag{1.1}$$

Here $A > 0$ is the exchange constant, $K > 0$ is the anisotropy, $\hat{\mathbf{z}}$ is the direction of the easy axis in magnetization space, and $\mathbf{m}' \equiv \partial \mathbf{m}/\partial z$. We will use the spherical representation to characterize $\mathbf{m}(z)$ using the polar angle $\theta(z)$ and the azimuthal angle $\phi(z)$,

$$\mathbf{m} = (\sin\theta\cos\phi, \sin\theta\sin\phi, \cos\theta). \tag{1.2}$$

Any configuration $\mathbf{m}(z)$ can be represented by a trajectory on the unit sphere $\mathbb{S}^2$ that the tip of $\mathbf{m}$ traces as one moves from $z = -\infty$ to $z = \infty$ along the wire. A few such trajectories are illustrated in Figure 1.1.

Minimizing the potential energy (1.1), we find that the ferromagnetic wire has two uniform ground states $\mathbf{m}(z) = \pm\hat{\mathbf{z}}$. We can also minimize the potential energy (1.1) with boundary conditions $\mathbf{m}(\pm\infty) = \pm\hat{\mathbf{z}}$ or $\mathbf{m}(\pm\infty) = \mp\hat{\mathbf{z}}$. This yields solitons interpolating between the two ground states, known as domain walls or kinks:

$$\cos\theta(z) = \pm\tanh\frac{z - Z}{l_0}, \quad \phi(z) = \Phi, \tag{1.3}$$

where $l_0 = \sqrt{A/K}$ is the width of the domain wall and Z and Φ are two arbitrary

constants denoting the location of the center and the azimuthal plane of the wall. A typical domain wall is shown in the third row of Figure 1.1. As a local minimum of the potential energy, it is a static configuration.

One can also put two domain walls next to each other in a wire and thus obtain a configuration that approaches the same ground state at $z = \pm\infty$. Such a state, with $\mathbf{m}(\pm\infty) = \hat{\mathbf{z}}$ is shown in the fourth row of Figure 1.1. This state is clearly a non-topological soliton since it can be continuously deformed to the uniform state $\mathbf{m}(z) = \hat{\mathbf{z}}$. This is most easily seen by looking at its trajectory on the unit sphere, as shown in Figure 1.1, which is a closed loop starting and ending at the north pole and can thus be shrunk continuously to the north pole.

A domain wall, on the other hand, describes a trajectory that starts at the north pole and ends at the south pole. Since the ends of a trajectory are fixed (they are realized only at $z = \pm\infty$), the trajectory of the domain wall cannot be continuously shrunk to a point. It is thus a topological soliton. One can associate topological charges of ± 1 to domain walls that interpolate between $\pm\hat{\mathbf{z}}$ and $\mp\hat{\mathbf{z}}$, respectively. The non-topological soliton in Figure 1.1 is then just a pair of oppositely charged domain walls and hence has zero net topological charge, as expected.

A topological soliton is a stable object since it cannot be continuously deformed to a uniform state. As a result, adding a weak external perturbation won't cause it to decay into a ground state. A non-topological soltion, on the other hand, is usually unstable since it has no such topological protection. In some situations, it can be

stabilized by conserved integrals of motion such as energy, momentum or angular momentum. But as soon as these conservation laws are broken by a weak external perturbation such as a viscous force, the non-topological soliton decays into a uniform ground state. We will see an explicit example of how this happens in Chapter 3 of this dissertation.

In Chapter 2 we will study the nature of elementary excitations in the quantum magnet $CoNb_2O_6$, which can be modelled as a collection of weakly interacting ferromagnetic chains. We will see how weak interactions between domain walls in this material give rise to localized bound states of two and four domain walls.

We will then move on to study the decay of a pair of domain walls in a ferromagnetic wire into a uniform ground state. This process will be modeled as two domain walls approaching and ultimately annihilating each other. We'll develop an effective theory that describes this process and compare its predictions with numerical simulations.

1.2 Solitons in Two-Dimensional Systems

1.2.1 Vortices

A minimal model of a thin film again consists of two kinds of interactions: an isotropic exchange interaction that tries to align neighboring spins and an easy-plane

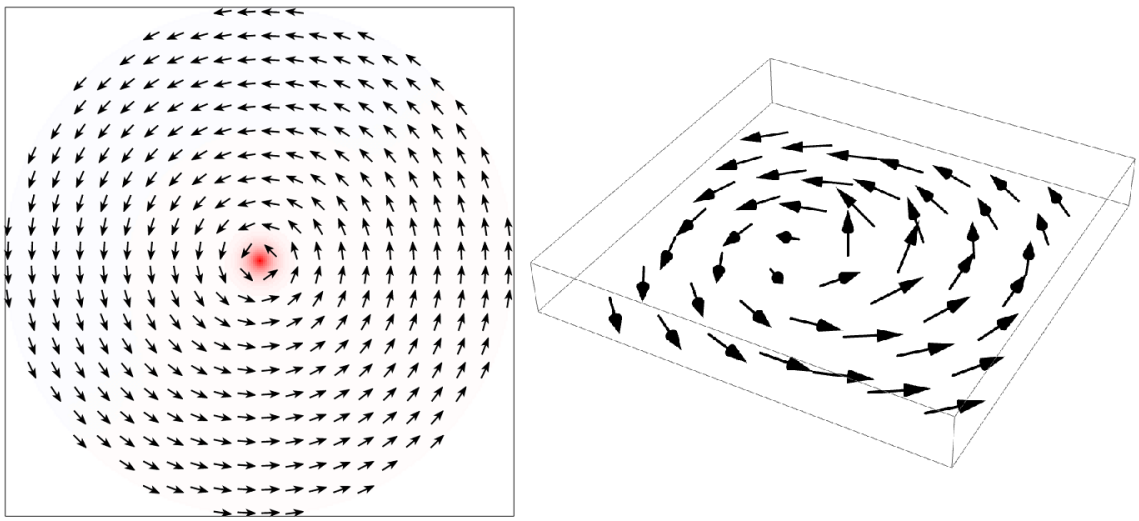

Figure 1.2: Left: A vortex in a ferromagnetic thin film with winding number $k = 1$ and core polarity $p = 1$. The arrows show the component of magnetization $\mathbf{m}_{||}$ parallel to the plane. The red color denotes a magnetization component $m_z > 1/e$ out of the plane of the film. Right: Structure of the vortex core. One can see that $\mathbf{m}$ points out of the plane at the center of the core.

anisotropy that penalizes any out-of-plane magnetization m_z:

$$U[\mathbf{m}] = U_{\text{ex}}[\mathbf{m}] + U_{\text{anis}}[\mathbf{m}] = \int dx\, dy \quad \left[\frac{A}{2}(\nabla \mathbf{m})^2 + \frac{K}{2} m_z^2\right]. \tag{1.4}$$

Here $A > 0$ is the exchange constant and $K > 0$ is the anisotropy. The characteristic length in this system is again the exchange length $l_0 = \sqrt{A/K}$. It readily follows from (1.4) that this system has a continuous family of degenerate ground states. In any of these ground states, all spins point in some specific direction in the x-y plane, i.e. $\mathbf{m}(x, y) = \cos\beta\, \hat{\mathbf{x}} + \sin\beta\, \hat{\mathbf{y}}$ for a fixed angle $0 \leq \beta < 2\pi$.

A well known class of solitons [4], known as vortices, that locally minimize (1.4)

is characterized by the following pattern of the azimuthal angle:

$$\phi(x, y) = k \arctan \frac{y - Y}{x - X} = k\varphi \tag{1.5}$$

where (X, Y) is the center of the vortex, k is a nonzero integer and (ρ, φ) are polar coordinates around the center of the vortex: $x = X + \rho\cos\varphi$ and $y = Y + \rho\sin\varphi$. Figure 1.2 shows a vortex with $k = 1$.

A nonzero k implies that the azimuthal angle ϕ is not well-defined at the center (X, Y). This means the magnetization vector, which has a fixed length of 1, has to be perpendicular to the x-y plane at that location, i.e. $\mathbf{m}(X, Y) = p\hat{\mathbf{z}}$, where $p = \pm 1$ is the polarity of the vortex core. In addition, the $U_{\text{anis}}[\mathbf{m}]$ term in (1.4) forces the magnetization to be completely in-plane far away from the core. Solving for the polar angle $\theta(x, y)$ with these constraints yields a radial function $\theta(\rho)$ with $\theta(0) = 0$ or π depending on the polarity of the vortex core $p = \pm 1$ and $\theta(\rho \gg l_0) - \pi/2 \sim e^{-\rho/l_0}$. Thus the characteristic size of the core is equal to the exchange length l_0 and m_z decays exponentially beyond this distance from the vortex center [5,6]. The structure of the vortex core is shown in Figure 1.2.

To understand the topological properties of the vortex, it is useful to introduce a quantity called the winding number. We can define the winding number k of a configuration as the net azimuthal angle ϕ described by the vector $\mathbf{m}$ as one traces a

closed loop (in counterclockwise fashion) in the x-y plane [4]. Mathematically,

$$k = \frac{1}{2\pi} \oint d\phi \tag{1.6}$$

Because the function $\mathbf{m}(x, y)$ is single valued, ϕ returns to the same value after an excursion around a loop, modulo 2π. So the winding number k can only take discrete integer values. As a result, configurations with different winding numbers cannot be continuously deformed into each other [4], making k a topological invariant. This splits up the set of all smooth configurations $\mathbf{m}(x, y)$ into distinct topological sectors, the totality of which is known as the first homotopy group of the circle $\pi_1(\mathbb{S}^1)$ [4]. The fact that k can only take integer values implies that $\pi_1(\mathbb{S}^1) = \mathbb{Z}$. Obviously all the ground states of the thin film have $k = 0$. On the other hand, profile of the vortex (1.5) implies that its winding number is just the nonzero integer k. This makes the vortex a topological soliton: one that cannot be continuously deformed to the ground state.

1.2.2 Skyrmions

While defining the winding number of a configuration, we were dealing with a mapping from a circle (a loop in real space) to a circle (the order-parameter space: the equatorial circle $\theta = \pi/2$ of the unit $\mathbf{m}$-sphere). For two-dimensional systems it is possible to define a second topological charge, which measures the number of times

the vector field $\mathbf{m}(x, y)$ wraps around the unit sphere [7]:

$$S = \frac{1}{4\pi} \int dx\, dy\, \mathbf{m} \cdot \left(\frac{\partial \mathbf{m}}{\partial x} \times \frac{\partial \mathbf{m}}{\partial y} \right). \tag{1.7}$$

This quantity is known as the skyrmion number. If we restrict ourselves to configurations that approach a uniform state at infinity, the mapping considered here is from a sphere (a plane with all points at infinity identified) to a sphere (the entire space of $\mathbf{m}$). By the same argument as with winding numbers, the skyrmion number S for such a mapping can take only integer values and splits up the set of all solitons into distinct topological sectors. The totality of these sectors are said to form the second homotopy group of the sphere $\pi_2(\mathbb{S}^2) = \mathbb{Z}$ [7].

A soliton with a nonzero skyrmion number is topological since it cannot be continuously deformed to a uniform state (which has $S = 0$). The simplest example of a soliton with a nonzero S (often simply known as a "skyrmion") is the configuration [8]

$$\theta = 2 \arctan \rho, \quad \phi = \varphi, \tag{1.8}$$

which is illustrated in Figure 1.3. In this soliton, the vector $\mathbf{m}$ points up at the center, down at infinity, and realizes every other orientation exactly once in between. Thus it wraps around the unit sphere exactly once and has a skyrmion number $+1$.

Vortices do not belong to the set of configurations considered above since they do not approach a uniform state at infinity. Instead, they map the circle at infinity to

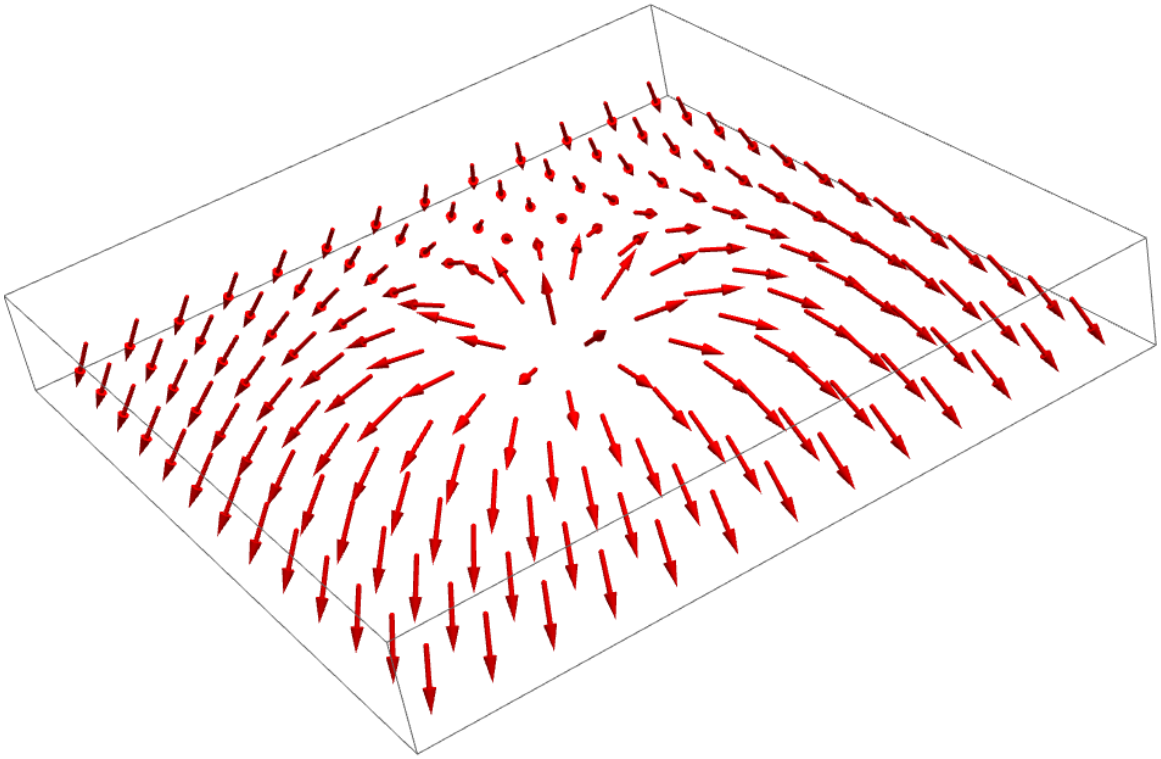

Figure 1.3: A localized soliton with skyrmion number $S = 1$. The magnetization vector points up at the center, down everywhere at infinity. Every other orientation is realized exactly once in the region between the center and the circle at infinity.

the equatorial circle $\theta = \pi/2$ of the **m**-sphere. Nevertheless, it is possible to define the skyrmion number of a vortex by looking at the portion of the **m**-sphere spanned by it. Since a vortex with winding number $k = 1$ and core polarity $p = 1$ wraps once around the north hemisphere of the magnetization sphere, it has a skyrmion number 1/2. This result can be readily generalized to a vortex with winding number $k \in \mathbb{Z}$ and polarity $p = \pm 1$. Such a configuration will have a skyrmion number $S = kp/2$. The skyrmion number of a vortex can thus take any integer or half-integer value.

1.2.3 Two Types of Topological Solitons

There is a fundamental distinction between solitons like skyrmions on one hand and those like domain walls and vortices on the other that is worth mentioning.

In the former **m** approaches the same ground state as $\mathbf{r} \to \infty$ along different directions. For example, in (1.8) $\mathbf{m}(r \to \infty) = -\hat{\mathbf{z}}$ irrespective of how one approaches the circle at infinity. As a result, one can transform this soliton to one that is in the same topological sector as the ground state $\mathbf{m}(\mathbf{r}) = -\hat{\mathbf{z}}$ by a local, albeit discontinuous, transformation of magnetization near the origin. Thus in a lattice model or at finite temperatures, where such local discontinuous processes are allowed, it is possible to destroy a skyrmion and return to a ground state of the system. By the same argument, it is also possible to nucleate a skyrmion in a lattice model or, at finite temperatures, even in a continuum model.

Solitons like domain walls and vortices are different. There **m** approaches different

ground states as $\mathbf{r} \to \infty$ along different directions. For example, in a domain wall configuration, two different ground states $\mathbf{m} = +\hat{\mathbf{z}}$ and $\mathbf{m} = -\hat{\mathbf{z}}$ are realized at $z = \pm\infty$. So one needs to modify an infinite number of degrees of freedom to convert a single domain wall or vortex to a ground state in an infinite system. Hence even on a lattice and at finite temperatures, such topological solitons will be stable, e.g. it is impossible to remove an uncompensated domain wall or nucleate a single vortex. One can only create a pair of them and separate them if they are deconfined.

In Chapter 4 of this dissertation, we will study the dynamics of a pair of solitons: a vortex (with winding number $k_1 = 1$ and polarity $p_1 = 1$) and an antivortex (with winding number $k_2 = -1$ and polarity $p_2 = -1$) in a ferromagnetic thin film. This system has a total winding number $k = k_1 + k_2 = 0$, which is identical to that of a uniform state. On the other hand, the total skyrmion number of the pair is $S = (k_1 p_1 + k_2 p_2)/2 = 1$, making it a topological soliton. We will see that in the presence of dissipation, the pair approaches each other, much like a domain wall pair. But unlike domain walls, the pair cannot annihilate to form a uniform state since a skyrmion is topologically protected in the continuum. As a result, as the separation between the pair approaches zero, the skyrmion keeps shrinking but it is always present in the system. It is worth mentioning that as the separation between the pair approaches the lattice scale, the topological argument breaks down and the skyrmion can unwind itself and ultimately disaapear. We will not address this final stage of the annihilation process in our work. Instead, we will discuss theoretical frameworks

that describe the dynamics of vortices when their separation is large compared to the lattice scale of the system.

Chapter 2

Kink Bound States in a Quasi One-Dimensional Magnet

Classical and quantum lattice spin models are ubiquitous in the study of magnetism. They are often simple enough to be understood theoretically using analytical and/or numerical techniques. At the same time, they capture well the essential physics of many real magnetic materials. The simplest of these is the ferromagnetic Ising model in one-dimension [9] in which the spins have two preferred orientations: up and down along some axis (say the z-axis). In addition, the nearest neighbor spins like to point in the same direction: hence a ferromagnet. As a result, this model has two ground states (also known as domains) in which all spins point along $+\mathbf{z}$ or $-\mathbf{z}$. Elementary excitations are kinks or domain walls separating an up domain and a down domain. In the presence of additional interactions, two such kinks can come

together and form a bound state.

In this chapter, we present a theoretical study of the nature of magnetic excitations in the quasi one-dimensional magnet columbite ($CoNb_2O_6$) and compare the findings with experimental results. This material can be modeled as a collection of parallel ferromanetic spin-1/2 Ising chains with weak antiferromagnetic inter-chain coupling. Previous neutron scattering experiments had revealed a hierarchy of two-kink bound states on a single Ising chain in this material [10]. High-resolution time-domain terahertz spectroscopy (TDTS) by the Armitage group at JHU [11] revealed the existence of more bound states in the same hierarchy and found a new sharp excitation of a different nature. Our theoretical calculations supported the interpretation of this new excitation as a novel bound state of two kink pairs on two adjacent Ising chains.

In Section 2.1, we will introduce the one-dimensional Ising chain, relate it to the material $CoNb_2O_6$ and discuss the previous and new experimental results. In Section 2.2, the theoretical framework for understanding the observed excitations will be presented. We will then proceed to the numerical calculations based on this theory and compare them with experimental observations. We will conclude the chapter by discussing our results. This work was done by collaboration with the experimental group of Professor N. Peter Armitage at the Johns Hopkins University and my advisor Professor Oleg Tchernyshyov and has been published in Phys. Rev. Lett. [11].

2.1 Introduction

2.1.1 Ferromagnetic Ising Chain and Kinks

The one-dimensional quantum Ising model consists of an infinite chain of spins-1/2 $\{\mathbf{S}_i\}$ interacting via the Hamiltonian

$$H_I = -J \sum_i S_i^z \, S_{i+1}^z - h_x \sum_i S_i^x, \tag{2.1}$$

where $J > 0$ is the exchange constant and $\mathbf{h} = h_x \hat{\mathbf{x}}$ is an external transverse magnetic field coupling to the spins through a Zeeman term. This was one of the first exactly soluble models of a quantum phase transition. It can be exactly solved via the Jordan-Wigner transformation [12] and exhibits a quantum phase transition at $J = h_x$. If the exchange is much stronger than the transverse field ($J \gg h_x$), the system has two ferromagnetic ground states $|\ldots\uparrow\uparrow\uparrow\ldots\rangle$ and $|\ldots\downarrow\downarrow\downarrow\ldots\rangle$ as shown in Figure 2.1, where $S^z|\uparrow\rangle = \frac{\hbar}{2}|\uparrow\rangle$ and $S^z|\downarrow\rangle = -\frac{\hbar}{2}|\downarrow\rangle$. If the transverse field is much stronger ($J \ll h_x$), the system becomes a paramagnet and there is just one polarized ground state $|\ldots\rightarrow\rightarrow\rightarrow\ldots\rangle$ in which all spins are aligned in the direction of the transverse field: $S^x|\rightarrow\rangle = \frac{\hbar}{2}|\rightarrow\rangle$.

An elementary excitation in the ferromagnetic phase in the limit $J \gg h_x$ [13, 14] is a state like $|\ldots\uparrow_{i-1}\uparrow_i\downarrow_{i+1}\downarrow_{i+2}\ldots\rangle$. Such a state is called a kink or a domain wall. The kink in this example is located between the sites i and $i+1$ and will be denoted

by $\left|i+\frac{1}{2}\right\rangle$ for brevity. (Note: for simplicity we shall use rational units, in which $\hbar = 1$ in everything that follows.) The transverse field term allows these kinks to hop from one site to another, thus endowing them with a kinetic energy.

It is impossible to apply a small perturbation to one of the ground states and excite a single kink. This is because a kink is a nonlocal excitation: one needs to flip infinitely many spins to create a single-kink state. This is related to the fact that the ground state and the single-kink state satisfy different boundary conditions at $i = \pm\infty$ and hence belong to different topological sectors, as can be clearly seen in Figure 2.1. A two-kink state, on the other hand, is a local excitation that requires only a finite number of spin flips and thus can be generated from a ground state by applying a small perturbation.

Time-domain terahertz spectroscopy (TDTS) uses photons to excite a system and can excite states only with total momentum $k = 0$. A photon, being a spin-1 object, can flip a single spin-1/2 from an up state to a down state (or vice-versa), thereby transferring a single unit of spin to the system. This creates a pair of adjacent kinks, as shown in Figure 2.1. In the presence of only an external transverse field, these kinks are free since there is no potential confining them. A single photon can excite two kinks with momenta k' and $-k'$, thus transferring an energy $E = E(k')+E(-k')$ to the system, where $E(k')$ is the dispersion of a single kink. Since k' can be any momentum here, the TDTS absorption spectrum would show a continuum of excitations at the total momentum $k = 0$ for a magnet that is described by (2.1).

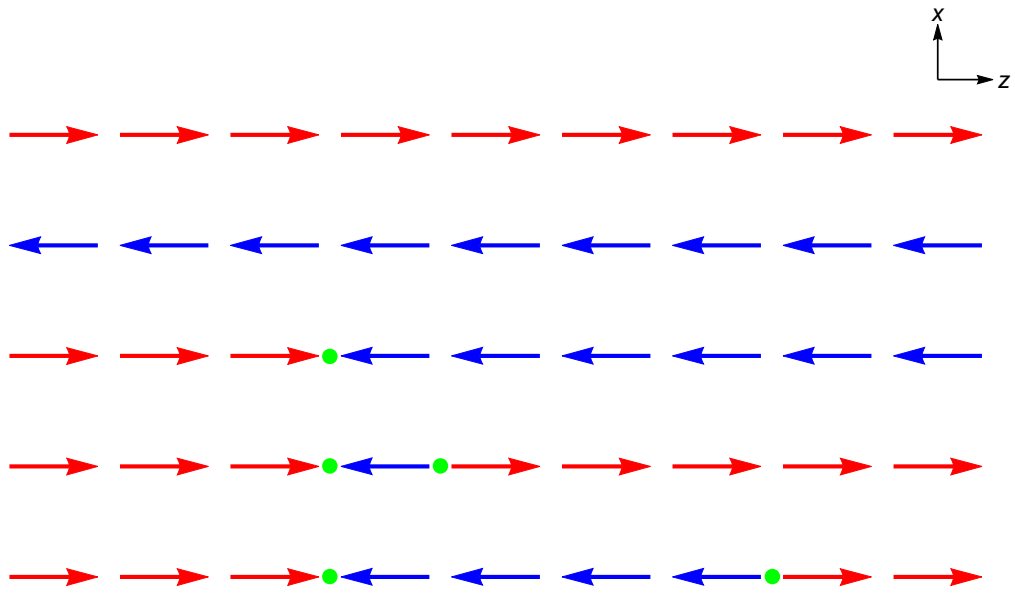

Figure 2.1: Five energy eigenstates of the one-dimensional Ising model H_I. Red and blue colors denote spins pointing along $+\mathbf{z}$ and $-\mathbf{z}$. The green circles denote kinks. The first two are the two ground states. The third one is a single-kink state and is topologically distinct from both ground states. The last two are two-kink states and are in the same topological sector as the first ground state.

We will introduce two different notations for a kink pair. Extending our way of denoting a single kink, a pair can be represented as $\left|i+\frac{1}{2}, j+\frac{1}{2}\right\rangle$. Alternatively, defining the "center-of-mass" $c = \frac{i+j+1}{2}$ and separation $n = j - i$, a two-kink state can also be denoted by $|c, n\rangle$. Here n, which is just the number of flipped spins, is a positive integer. If n is even, c can take any half-integer value. If n is odd, c can take any integer value.

To be concrete, let us now focus on two-kink states that are continuously connected to the "all up" ground state, like the ones shown in Figure 2.1. These kinks are deconfined since they can be separated indefinitely from each other at a finite energy cost (which is, in fact, zero in this case). One can confine them by applying a weak

external magnetic field $0 < h_z \ll J$ in the z-direction, also known as a longitudinal field. This modifies the Hamiltonian H_I to

$$H_{Ih_z} = -J \sum_i S_i^z \, S_{i+1}^z - h_x \sum_i S_i^x - h_z \sum_i S_i^z. \tag{2.2}$$

The second Zeeman term favors spins pointing in the $+\mathbf{z}$ direction and thus demands an extra energy h_z for every flipped spin-1/2. The two-kink state $\left|i+\frac{1}{2}, j+\frac{1}{2}\right\rangle$ costs an energy of $h_z(j-i)$, leading to confinement of kinks. This is expected to give rise to a hierarchy of two-kink bound states and hence change the excitation spectrum at $k = 0$ from a continuum to a discrete one.

With both longitudinal and transverse fields present, the Hamiltonian (2.2) is no longer exactly solvable. But the spectrum of two-kink bound states can still be obtained easily in the limit of weak longitudinal and transverse fields h_x, $h_z \ll J$. In this limit, one can stay within the subspace of two kink states $\left\{\left|i+\frac{1}{2}, j+\frac{1}{2}\right\rangle\right\}$ and treat the fields as perturbations.

The Ising term demands an energy equal to $4J$ for a kink pair. Since the transverse field flips a spin from "up" to "down" and vice-versa, it causes kinks to hop from a state $\left|i+\frac{1}{2}, j+\frac{1}{2}\right\rangle$ to a state like $\left|i+\frac{3}{2}, j+\frac{1}{2}\right\rangle$. The longitudinal field term, as we saw before, adds a potential energy of $h_z(j-i)$. So, the effective Hamiltonian in the

subspace of two-kink states looks like

$$\begin{aligned} H_{Ih_z}\left|i+\frac{1}{2},j+\frac{1}{2}\right\rangle =&(4J+(j-i)h_z)\left|i+\frac{1}{2},j+\frac{1}{2}\right\rangle - \frac{h_x}{2}\left[\left|i+\frac{3}{2},j+\frac{1}{2}\right\rangle\right. \\ &\left.+\left|i-\frac{1}{2},j+\frac{1}{2}\right\rangle+\left|i+\frac{1}{2},j+\frac{3}{2}\right\rangle+\left|i+\frac{1}{2},j-\frac{1}{2}\right\rangle\right] \end{aligned} \tag{2.3}$$

It is worth noting that the two-kink system described by H_{Ih_z} [15,16] has a simple physical interpretation. A kink pair can be thought of a string of flipped spins. This string is under constant tension (potential energy per unit length) h_z. Its length $n=(j-i)>0$ is subject to quantum fluctuations of amplitude $h_x/2$. Thus, in the continuum approximation, the spectrum of this system at zero total momentum is identical to that of a massive particle tied to the origin by a linear confining potential [17]

$$\begin{aligned} V(x) &= \lambda x, \text{ if } x>0 \\ &= \infty, \text{ if } x\leq 0. \end{aligned} \tag{2.4}$$

So, the spectrum of two-kink bound states can be obtained by solving the Schrodinger equation

$$-\frac{\hbar^2}{\mu}\frac{d^2}{dx^2}\psi_n(x)+V(x)\,\psi_n(x)=(E_n-4J)\psi_n(x). \tag{2.5}$$

Solutions to this equation are Airy functions with energy eigenvalues

$$E_n=4J+z_n\lambda^{2/3}\left(\frac{\hbar^2}{\mu}\right)^{1/3}, \quad n=1,2,3,... \tag{2.6}$$

Here $4J$ is the energy cost of misaligning two ferromagnetic bonds, λ and μ are two phenomenological parameters and z_n's are the negative zeroes of the Airy function of the first kind. As we'll see in the next section, this simple continuum model can reproduce a large part of the excitation spectrum of the quasi one-dimensional magnet $CoNb_2O_6$.

2.1.2 $CoNb_2O_6$: Experimental Results

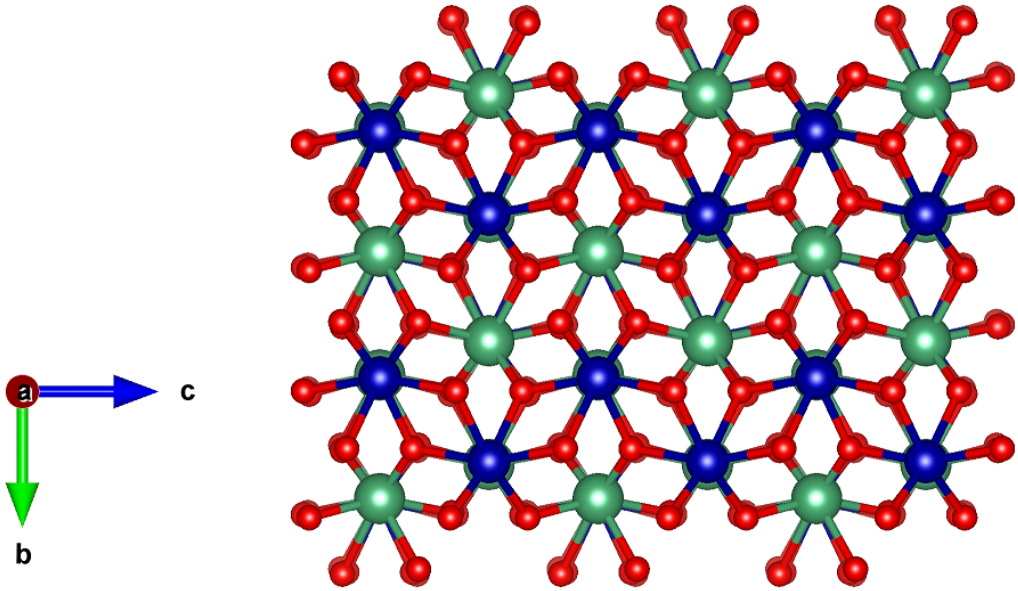

Figure 2.2: The crystal structure of $CoNb_2O_6$. The Co^{2+}, Nb^{2+} and O^{2-} ions are shown as blue, green and red spheres respectively. The magnetic cobalt ions form zigzag chains extending in the c-direction, two of which can be seen in this figure. These chains can be modeled as spin-1/2 ferromagnetic Ising chains with weak antiferromagnetic inter-chain coupling.

$CoNb_2O_6$, also known as columbite, crystallizes in the orthorhombic *Pbcn* space group. The crystal structure and the arrangement of various ions in columbite is

shown in Figure 2.2. Crystal field splitting produces an effective spin-1/2 moment on the Co^{2+} ions, with a strong anisotropy axis in the $a-c$ plane at an angle of $\pm 31^\circ$ to the c-axis [18, 19]. The Co atoms form zigzag chains along the c-axis. Ferromagnetic exchange interactions between nearest-neighbor Co^{2+} ions along this axis cause ferromagnetic correlations in these chains beginning at around 25 K [20]. Below 2.95 K weak antiferromagnetic interchain exchange interactions stabilize a spin-density wave along the b-direction with a temperature-dependent ordering wave vector Q. Below 1.97 K the spin-density wave becomes commensurate antiferromagnet along b with a temperature independent $Q_{AF} = (0, 1/2, 0)$ and an ordered moment of $3.05\,\mu_B$ [21].

We are interested in the properties of $CoNb_2O_6$ well into the ordered state, i.e. below 1.97 K. A simple physical model describing the magnetic properties of columbite in this regime is shown in Figure 2.3. The spins-1/2 (the Co^{2+} ions) lie on a triangular lattice in the $a-b$ plane. The full lattice is generated by stacking many of these triangular lattices exactly on top of each other in the c-direction. One thus obtains a set of parallel c-chains. These spins are Ising-like and their preferred axis is depicted to be along the a-direction in the figure for simplicity. The actual orientation of this axis, as noted before, is at an angle $\pm 31^\circ$ to the c-axis. The dominant interaction between spins is the ferromagnetic exchange in the c-direction with strength $J = 0.48\,\text{meV}$. There are two more exchange interactions, both antiferromagnetic: of strength $J_1 = 0.005J$ in the b-direction and of strength $J_2 < J_1$ along the diagonals in the ab-plane. The difference in strength of J_1 and J_2 lifts the geometrical frustration on

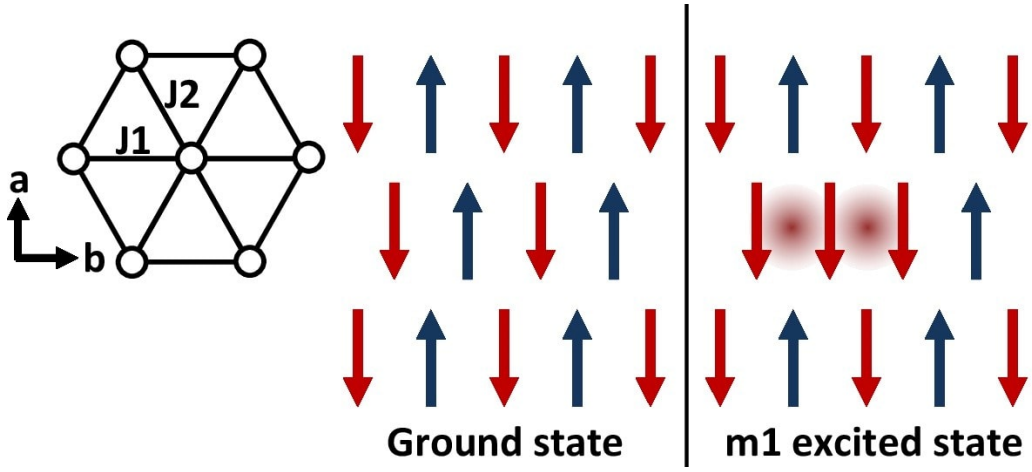

Figure 2.3: Diagram of the ground state and the single spin-flip excitation in the low temperature ordered state of $CoNb_2O_6$. The antiferromagnetic exchange interaction along the b-direction has a strength J_1, while along the diagonals in the ab-plane the interaction strength is $J_2 < J_1$. The flipped spin state breaks two J_1 exchange interactions while leaving the total energy due to J_2 exchange unchanged.

the triangular lattice and selects the grounds state depicted in Figure 2.3. All spins along a c-chain are parallel to each other in the ground state.

One can now create a kink-pair by flipping a single spin. It is clear from Figure 2.3 that this frustrates two J-bonds and two J_1-bonds but leaves the total energy due to J_2 exchange unchanged. This would be true for multiple spin flips as well. Hence, one can further simplify this model while studying properties of kinks on the c-chains by ignoring the J_2-interaction altogether. One is then left with a two-dimensional model in the $c-b$ plane that has parallel ferromagnetic Ising chains with weak antiferromagnetic inter-chain coupling.

We show a pair of kinks in this reduced model in Figure 2.4. For simplicity of depiction, the easy-axis is now chosen to point in the c-direction. One can see from Figure 2.4 that a two-kink state $|c, n\rangle$ frustrates $2n$ inter-chain bonds of strength J_1,

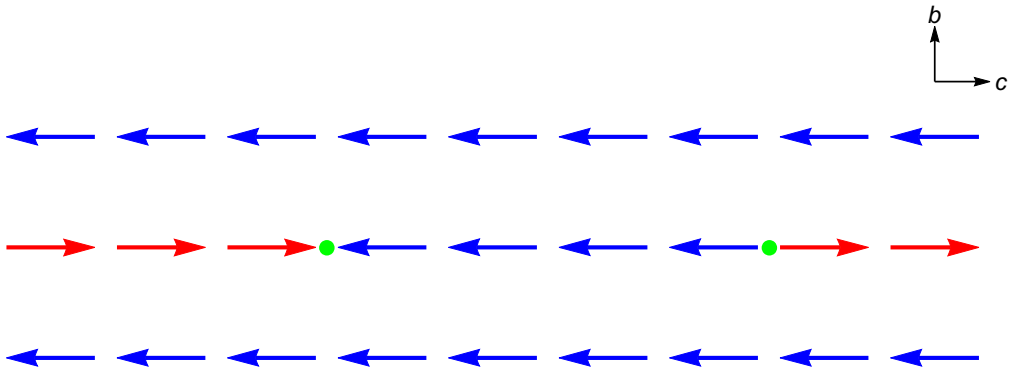

Figure 2.4: Two kinks on a single c-chain separated by $n = 4$ spin flips. The number of frustrated J_1 bonds is $2n = 8$.

thus incurring an energy cost of $2n \times 2J_1 = 4nJ_1$. Thus the inter-chain interaction can be modelled as a weak longitudinal field $h_z = 4J_1$ confining the kinks. There also exist weak non-Ising type interactions between the spins in this material that allow the kinks to hop along a c-chain and can thus be modeled as an effective weak transverse field h_x. Putting everything together, we can expect that the Ising model with weak transverse and longitudinal fields (2.2) to be a good effective theory for this material. In other words, $CoNb_2O_6$ is a nice playground for testing this theory.

The spectrum of two-kink bound states in $CoNb_2O_6$ was experimentally studied by Coldea et. al. [10] using inelastic neutron scattering. In particular, they observed five sharp excitations labelled $m1 - m5$ at zero momentum which show excellent agreement with the bound state energies given in terms of the first five zeroes of the Airy function in (2.6) with λ and μ as phenomenological parameters. Time domain terahertz spectroscopy (TDTS) can only probe excitations at $k = 0$, but with much greater resolution than neutron scattering. TDTS by the Armitage group at JHU

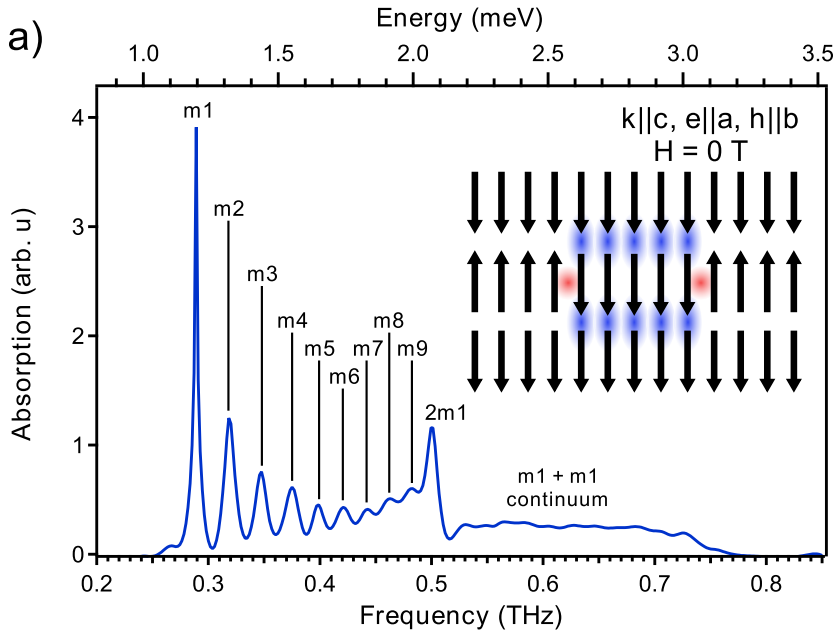

Figure 2.5: TDTS absorption spectrum at 1.6 K showing the hierarchy of excitations $m1 - m9$, the $2m1$ excitation and the continuum.

[11] revealed more bound states in the same hierarchy $m1 - m9$, all in excellent agreement with the energies calculated from (2.6). But in addition to these two-kink bound states, a sharp excitation mode $2m1$ was observed at an energy slightly less than twice the lowest bound state energy (bottom of the $m1 + m1$ contunuum) as depicted in Figure 2.5. This new mode, as seen in the figure, has a significantly higher spectral weight than the mode $m9$ just preceding it. It is unlikely that it is a tenth two-kink bound state $m10$, since the spectral weight of $m10$ is expected to be even lower than the $m9$ state. In the rest of this chapter, we'll develop a theory for understanding this mode starting with the hypothesis that it is an exotic bound state of two $m1$ bound states on two adjacent Ising c-chains.

2.1.3 $CoNb_2O_6$: Lattice Model

As we'll see in the next section, a detailed lattice model of $CoNb_2O_6$ is necessary to understand the properties of the $2m1$ excitation. Here we present the model used in [10]. It is identical to (2.3), with two additional phenomenological terms:

$$\begin{aligned} H_2 \left| i+\frac{1}{2}, j+\frac{1}{2} \right\rangle &= (4J + (j-i)h_z) \left| i+\frac{1}{2}, j+\frac{1}{2} \right\rangle - \alpha \left[\left| i+\frac{3}{2}, j+\frac{1}{2} \right\rangle \right. \\ &+ \left| i-\frac{1}{2}, j+\frac{1}{2} \right\rangle + \left| i+\frac{1}{2}, j+\frac{3}{2} \right\rangle + \left. \left| i+\frac{1}{2}, j-\frac{1}{2} \right\rangle \right] - \beta_0 \delta_{i+1,j} \left[\left| i+\frac{3}{2}, j+\frac{3}{2} \right\rangle \right. \\ &+ \left. \left| i-\frac{1}{2}, j-\frac{1}{2} \right\rangle \right] + \beta_1 \delta_{i+1,j} \left| i+\frac{1}{2}, j+\frac{1}{2} \right\rangle \end{aligned} \tag{2.7}$$

Here α is the phenomenological hopping parameter that plays the role of an effective transverse field, β_0 is the kinetic energy gain for two nearest neighbor kinks hopping together and β_1 is the extra energy cost for having two kinks next to each other (i.e. a single spin flip). These two terms do not qualitatively alter the spectrum of the Hamiltonian. But we need to add them as phenomenological terms to quantitatively reproduce the spectrum in $CoNb_2O_6$ at nonzero k, as observed in neutron scattering experiments.

To diagonalize H_2, we first write it in the basis of center-of-mass and relative

coordinates.

$$H_2 \left|c,n\right\rangle = (4J + nh_z) \left|c,n\right\rangle - \alpha \left[\left| c + \frac{1}{2}, n+1 \right\rangle + \left| c + \frac{1}{2}, n-1 \right\rangle + \left| c - \frac{1}{2}, n+1 \right\rangle + \left| c - \frac{1}{2}, n-1 \right\rangle \right] - \beta_0 \delta_{n,1} \left[|c-1,n\rangle + |c+1,n\rangle \right] + \beta_1 \delta_{n,1} \left|c,n\right\rangle \tag{2.8}$$

It is readily seen that the system has discrete translation invariance with respect to the c-coordinate. Thus H_2 can be partially diagonalized by going over to the momentum basis in the c-direction. Considering a finite chain of N-sites, we define a new basis:

$$\left|k,n\right\rangle = \frac{1}{\sqrt{N}} \sum_c e^{ick} \left|c,n\right\rangle \tag{2.9}$$

The Hamiltonian written in this basis is diagonal with respect to $k \in [-\pi, \pi]$. It now looks like:

$$H_2 \left|k,n\right\rangle = (4J + nh_z - 2\beta_0 \delta_{n,1} \cos k + \beta_1 \delta_{n,1}) \left|k,n\right\rangle - 2\alpha \cos(k/2) [|k,n+1\rangle + |k,n-1\rangle] \tag{2.10}$$

H_2 is symmetric under $k \mapsto -k$. For any $0 \leq k \leq \pi$, it becomes a sparse matrix in the n-coordinate which can be numerically diagonalized using *Mathematica*. This yields a hierarchy of two-kink bound states for each k-value. Figure 2.6 shows the dispersion of the lowest member of this hierarchy. Here we've used the coupling constants given in [10]: $4J = 1.94\,\text{meV}$, $\alpha = 0.12J$, $\beta_0 = 0.17J$, $\beta_1 = 0.21J$ and $h_z = 0.02J$.

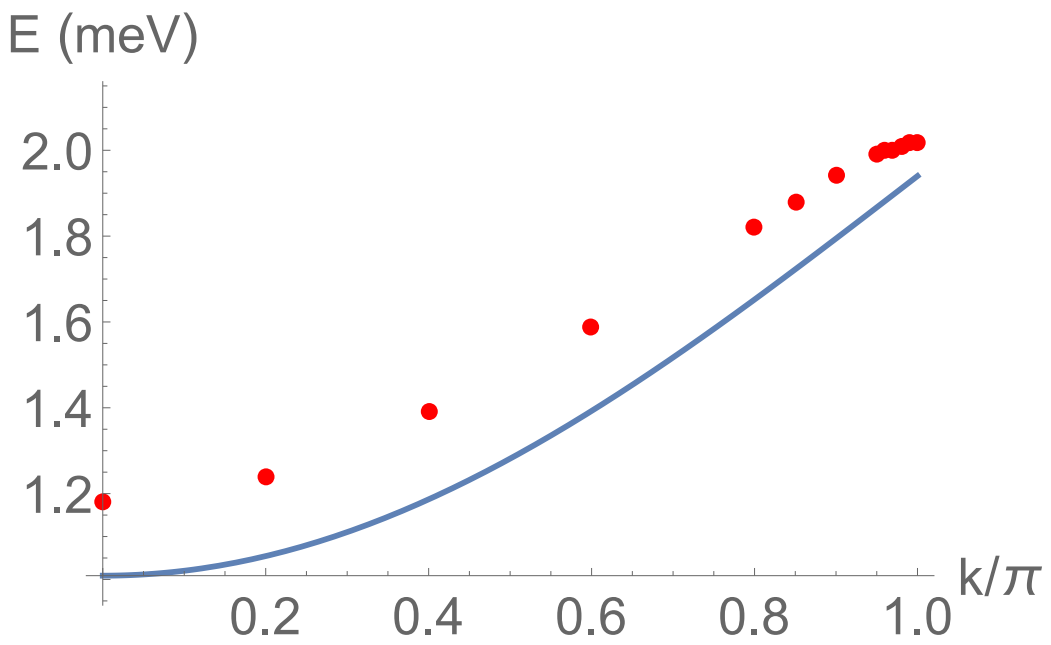

Figure 2.6: Dispersion of the ground state of the two-kink system [red points]. The dispersion is flat near the zone center and sharp near the edge, which match the features of the bottom of the continuum (at zero longitudinal field) [blue line].

It is also interesting to look at the two-kink spectrum in the absence of the confining longitudinal field and the beta terms ($h_z = \beta_0 = \beta_1 = 0$). In this case, the spectrum would form a continuum since the two kinks are free to move about in the chain. The bottom of this continuum has the dispersion $E_{\text{bottom}} = 4J - 4\alpha\cos(k/2)$ which is also shown in Figure 2.6. If a weak confining interaction is then turned on, the ground state dispersion is expected to track the bottom envelope of this continuum, which is indeed seen in the figure. In addition, the bottom of the continuum is flat at $k = 0$ and a has sharp edge at $k = \pi$. These features can also be seen in the bound state dispersion.

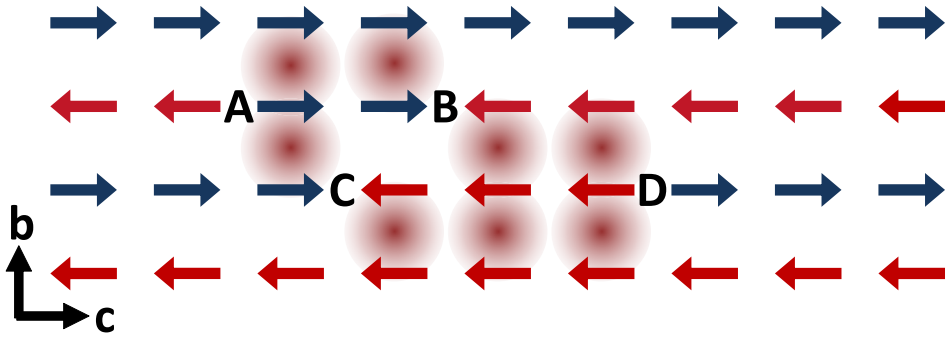

Figure 2.7: A typical four-kink configuration. The four kinks where the intra-chain order is broken at an energy cost of $2J$ each are labelled as A, B, C and D. Sites where inter-chain ordering is broken at an energy cost of $2J_1$ are shown by colored red clouds.

2.2 Four-Kink Bound State: Theory

The theoretical results described so far were obtained under the assumption that the photon incident on the system creates excitations on just one chain, while the neighboring chains remain perfectly ordered. Under that assumption, interchain interactions can be modeled as a confining longitudinal field. Here we reexamine this assumption and find that this mean-field model is inadequate because excitations can be created on adjacent chains as well. We then develop a description beyond the mean-field model to study the properties of such excitations.

To understand the nature of the experimentally observed $2m1$ excitation, we made a hypothesis that it is a bound state of two $m1$ kink pairs on two adjacent c-chains, as shown in Figure 2.7. The preliminary reason for this hypothesis was the fact that the $2m1$ excitation appears just below the $m1 + m1$ continuum. To see if such a bound state indeed exists, we started with a system of four such kinks, two each on two

adjacent Ising chains. As noted in the previous section, only the exchange interaction J_1 contributes to kink confinement. The four-kink potential then depends on which J_1 bonds are frustrated in a given configuration. One can read off this potential directly from Figure 2.7, which takes the form

$$\begin{aligned} V(z_A, z_B, z_C, z_D) &= 4J_1[(z_D - z_C) + (z_B - z_A)] \text{ if } z_D < z_A \text{ or } z_B < z_C, \\ &= 2J_1[|z_A - z_C| + |z_B - z_D|] + 2J_1[(z_D - z_C) + (z_B - z_A)] \\ &\text{otherwise,} \end{aligned} \tag{2.11}$$

where z_A, z_B, z_C, and z_D are the locations of the four kinks. In addition, there is the hard-wall constraint $z_B > z_A$ and $z_D > z_C$ between the kinks on any one Ising chain. Thus the effective Hamiltonian for this four-kink system consists of two copies of the two-kink Hamiltonian H_2 (2.8) with V replacing the simple linear two-kink attractive potential. It is interesting to note that the two flipped-spin-clusters (on the two adjacent c-chains) attract each other only when there is an overlap between them. Otherwise, they are essentially free. We found that this inter-cluster potential, despite having a strictly finite range, accommodates at least one bound state.

To see this, we first write the four-kink Hamiltonian in a basis labeled by the centres-of-mass (COMs) of the two clusters i and j and their lengths $m > 0$ and

$n > 0$.

$$
\begin{aligned}
H_4 \left|i, m; j, n\right\rangle = (8J + V(i,j,m,n)) \left|i, m; j, n\right\rangle - \alpha \Bigg[& \left| i + \frac{1}{2}, m+1; j, n \right\rangle \\
& + \left| i + \frac{1}{2}, m-1; j, n \right\rangle + \left| i - \frac{1}{2}, m+1; j, n \right\rangle + \left| i - \frac{1}{2}, m-1; j, n \right\rangle \\
& + \left| i, m; j + \frac{1}{2}, n+1 \right\rangle + \left| i, m; j + \frac{1}{2}, n-1 \right\rangle + \left| i, m; j - \frac{1}{2}, n+1 \right\rangle \\
& + \left| i, m; j - \frac{1}{2}, n-1 \right\rangle \Bigg] - \beta_0 \delta_{m,1} [|i-1, m; j, n\rangle + |i+1, m; j, n\rangle] \\
& - \beta_0 \delta_{n,1} [|i, m; j-1, n\rangle + |i, m; j+1, n\rangle] \\
& + \beta_1 \delta_{m,1} \left|i, m; j, n\right\rangle + \beta_1 \delta_{n,1} \left|i, m; j, n\right\rangle
\end{aligned}
\tag{2.12}
$$

One can now transform to a more natural set of coordinates: the COM of the whole system $u = (i + j)/2$ and the relative separation of the two clusters $v = (j - i)$. The Hamiltonian again has a discrete translational symmetry with respect to u and hence can be partially diagonalized by Fourier transforming from the basis $\{|u, v; m, n\rangle\}$ to the basis $\{|k, v; m, n\rangle = \sum_u e^{iku} |u, v; m, n\rangle\}$. Here m and n are positive integers. If both of them have the same even/odd parity, v can be any integer. If they have opposite parity v can be any half-integer. The problem now becomes a 3D lattice model, $\{v, m, n\}$ being the lattice coordinates, for every wavevector k within the first Brillouin zone $[-\pi, \pi]$. The exact form of H_4 in this basis, which is a sparse matrix, is given in Appendix A.

Since two non-overlapping spin clusters on adjacent chains are essentially free, the

spectrum of the four kink system definitely has a continuum. We wanted to know if the spectrum has bound states in addition to this continuum. We investigated this by numerically diagonalizing the sparse matrix H_4 for a fixed k-value on a finite-size lattice and checking the convergence of the result with varying system size, as discussed in the next section.

2.3 Four-Kink Bound State: Numerics

We first had to decide how big a system we need to choose for our numerical diagonalization. To this end we made some estimates of the size of a possible four-kink bound state. We first studied a two-kink system on one Ising chain which can be easily solved numerically. We found that the two kinks in the ground state of this system are well localized within $L \sim 10$ lattice units from each other. This implies that if there are four-kink bound states, the values of m and n in the lowest-lying state will be localized approximately within the same distance L. In that case, the range of the inter-cluster potential is $v \in [-L, L]$ and outside this range the four-kink wave-function should fall off exponentially.

Thus, if there is a bound state, the wave function will be localized within $[-aL, aL]$ in the v-direction for some a. Because the v coordinate can assume half integer values, this means that we now need to find the lowest eigenvalue and the corresponding eigenstate of our reduced model within a $L \times L \times 4aL$ lattice with hard wall boundary

conditions at the six faces. We can then vary L and a to check convergence of the energy. For $L = 10$ and $a = 2$ this reduces to the diagonalization problem of a 8000×8000 sparse matrix which can be easily done numerically using *Mathematica*.

We first looked at the $k = 0$ sector of the Hilbert space since time-domain terahertz spectroscopy can probe only the zero momentum states. As a starting point, we took $a = 2$. It turned out that the ground state energy converges to $2.33\,\text{meV} = 564\,\text{GHz}$ for $L = 8$ and stays constant (up to the second decimal place) for $L = 8, 9, 10, 11$. Increasing a to 3 doesn't change the energy either (up to the fifth decimal place, in meV). Also, $E_{bound}(k = 0)$ thus obtained is less than the bottom of the (theoretical) $m1 + m1$ continuum 572 GHz. This indicates that we are seeing a stable bound state here.

The calculation was repeated for finite wavevectors and the dispersion of this bound state $E(k)$ in the first Brillouin zone was obtained. A plot of this dispersion is shown in Figure 2.8. (Due to symmetry of the Hamiltonian under inversion, $E(k) = E(-k)$.) By comparing with Figure 2.6, it can be seen that $E(k)$ has a lesser curvature for the four-kink state than the two-kink state. This is expected because in the absence of any interaction between kinks, the four-kink spectrum forms a continuum with the bottom envelope given by $E_{\text{bottom}}(k) = 8J - 8\alpha\cos(k/4)$. If a weak interaction is then turned on, the ground state dispersion is expected to track this bottom envelope. It is easily seen that the bottom of the four kink continuum is indeed flatter than the two kink one. In addition, these continua are flat at $k = 0$

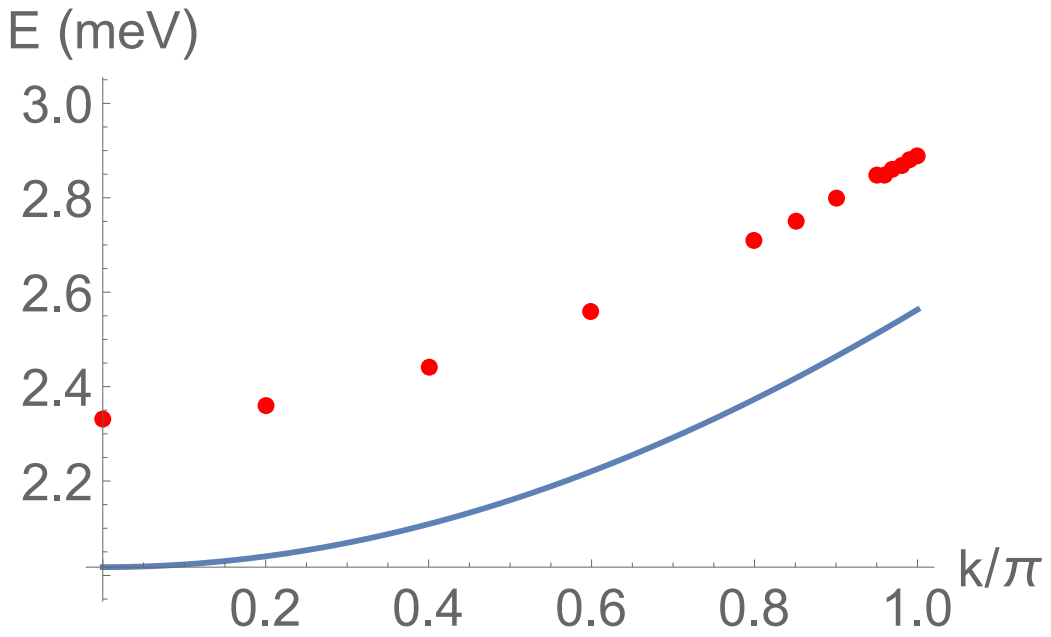

Figure 2.8: Dispersion of the ground state of the four-kink system [red points]. The dispersion is flat near the zone center and sharp near the edge, which match the features of the bottom of the four-kink continuum (at zero longitudinal field) [blue line].

and have sharp edges at $k = \pi$. These features can also be seen in the bound state dispersions.

2.4 Comparison with Experiment

The four-kink bound state obtained above has an energy of 564 GHz. In comparison, the experimentally observed $2m1$ excitation has an energy 500 GHz.

As noted in the introduction, time-domain terahertz spectroscopy uses photons to excite a system. A photon flips a single spin. Also, the momentum transferred by it to the system is negligible. Thus the state it excites is $|k = 0, n = 1\rangle$ in our notation.

So, the experimental spectral weight of any state $|s\rangle$ is proportional to its overlap with $|k=0, n=1\rangle$ and is given by $S = \frac{|\langle k=0,n=1|s\rangle|^2}{|\langle s|s\rangle|^2}$.

If we strictly confine ourselves to the four-kink Hilbert space, the spectral weight of the four-kink bound state obtained in the previous section vanishes. But the Hamiltonian H_4 (2.12) has a set of α-terms which flip an $|\uparrow\rangle$ to a $|\downarrow\rangle$ and vice-versa. As a result, they can flip a spin in a completely aligned c-chain and thus create a kink-pair out of the kink-vacuum. This provides a tunneling mechanism between the four-kink and the two-kink bound states. The four-kink bound state acquires a finite spectral weight because of this which can be calculated in first-order perturbation theory. The details of this calculation is given in Appendix A.

The spectral weight thus obtained for the $2m1$ excitation is 0.17 which lies roughly halfway between the (theoretical) $m1$ and $m2$ spectral weights (0.20 and 0.13 respectively). This theoretical spectral weight is greater than what is observed experimentally from the absorption spectrum. However, it qualitatively supports the interpretation of the $2m1$ peak as a separate excitation from the $m1 - m9$ series, not a tenth $m10$ bound state. The theoretically predicted spectral weights for the $m1$, $m2$, etc. excitations decrease monotonically, with the $m9$ and $m10$ spectral weights being only 0.037 and 0.033, respectively. The significantly increased spectral weight of the $2m1$ excitation compared to the $m9$ excitation therefore supports the interpretation of the $2m1$ excitation as a bound state of $m1$ bound states on adjacent chains.

2.5 Discussion

We studied the properties of elementary excitations in columbite ($CoNb_2O_6$). Columbite can be modeled as a collection of parallel ferromagnetic spin-1/2 Ising chains in two dimension, with weak antiferromagnetic inter-chain coupling. The inter-chain coupling gives rise to an effective longitudinal magnetic field felt by the spins on any single chain. A ferromagnetic Ising chain has kinks (domain walls) as its most elementary excitation. Previous authors [15, 16] had pointed out that a weak longitudinal magnetic field can confine the kinks and give rise to a hierarchy of two-kink bound states. Previous experimental studies on columbite [10] had found a hierarchy of sharp excitations that were in excellent agreement with this two-kink bound state picture.

High-resolution time-domain terahertz spectroscopy (TDTS) by the Armitage group at JHU [11] revealed more bound states at $k = 0$ (named $m1 - m9$) in the same hierarchy. But in addition they found a sharp excitation mode (named $2m1$) at an energy slightly lower than the continuum of two $m1$ excitations. We started with the hypothesis that the $2m1$ state is a bound state of two $m1$ pairs of kinks on two adjacent Ising chains confined by the antiferromagnetic inter-chain coupling. We wrote an effective Hamiltonian in the four-kink Hilbert space and carried out a numerical exact diagonalization on a finite lattice. A four-kink bound state was indeed found at $k = 0$ at an energy comparable to but higher than the experimentally observed energy. The dispersion of this state was found to be flatter than the lowest

two-kink state. Its spectral weight was also calculated and was found to be of the same order as the experimental weight. These findings support the interpretation of the $2m1$ state as a bound state of two $m1$ modes.

Chapter 3

Annihilation of Domain Walls in a Ferromagnetic Wire

In this chapter we will continue to explore the one-dimensional ferromagnetic spin chain. This time we'll treat the spins at a classical level, regarding them as vectors of a fixed length that can point in any direction in the three-dimensional magnetization space. Such a treatment is often sufficient to account for the properties of magnetic nanostructures such as nanowires and thin films and even three-dimensional ferromagnets. We will focus specifically on the one-dimensional system, the ferromagnetic wire, for which many analytical results can be obtained. In this system the spins prefer to point along the length of the wire due to shape anisotropy induced by the magnetic dipolar interaction. As a result, one ends up with two ground states/domains like before: uniform states with all spins pointing along the length of the wire in one of

the two possible directions as shown in Figure 3.1. Once again, one can have two domains separated by a domain wall. But this domain wall is different from the kink we saw before since now the spins are vectors varying continuously in space instead of being discretely either $|\uparrow\rangle$ or $|\downarrow\rangle$. So the domain wall is no longer located precisely at one point but is extended over a finite width. The local spin direction changes continuously from up to down over this width.

A domain wall is a topological soliton [3] since it is protected from decaying into any of the ground states for topological reasons: it cannot be continuously deformed into a uniform state. Study of the dynamics of such solitons is important for potential technological applications like magnetic memory devices (e.g. the racetrack memory [22]), but is also of fundamental interest. A soliton has infinitely many modes (since it has a spin variable at every point in space) that are coupled nonlinearly [23, 24]. As a result, an exact solution for the dynamics is unavailable in most cases. But in many situations, it is possible to distinguish between "soft" and "hard" modes of the system. A soft mode is one that has a relaxiation time much larger than the typical time scale over which the system is observed. A hard mode, on the other hand, relaxes much faster and thus can be viewed as instantaneously adjusting its value to the local conditions. As a result, we need to focus only on the soft modes while trying to understand the behavior of the system under a weak external perturbation. Inspired by this observation, a powerful approach has been developed in which one isolates a small number of relevant soft modes of the system, parametrizes

them by collective coordinates, and writes an effective theory only in terms of these [25, 26]. This method has been quite successful in describing the dynamics of solitons in ferromagnets [27–31] and antiferromagnets [32–35].

A mode corresponding to a global symmetry of a system doesn't change its energy. For example, if a system is translationally invariant in a certain direction, any translation in that direction won't cost any energy. These modes, known as zero modes of the system, have infinite relaxation time and hence are the softest ones. Thus, any description of the dynamics in terms of collective coordinates must include these modes. In most of the previous literature, only the zero modes have been used as collective coordinates. Going beyond the zero mode approximation and including other modes as dynamical degrees of freedom often poses significant challenges [36]. In the present chapter we will study a problem whose description fundamentally requires going beyond the zero-mode approximation: the annihilation of two domain walls in a ferromagnetic wire.

In Section 3.1 we will introduce the basic equations that govern the dynamics of spins in a classical magnet. We'll discuss the method of collective coordinates and illustrate it for the case of a single domain wall in an external magnetic field. In Section 3.2, the new problem we want to address will be described: the annihilation of two domain walls. This will also include a discussion of the role of conserved momenta as collective coordinates in our analysis. We'll then proceed to discuss a class of exact solutions for domain wall pairs that will be used as the starting point of

our main analysis. The theoretical calculations and results for the annihilation process will be presented in Section 3.4. This will be followed by a discussion of numerical micromagnetic simulations which were done to check the theoretical predictions. We'll conclude with a discussion of our results. This work was done by collaboration with high-school student Kevin S. Huang and my advisor Professor Oleg Tchernyshyov and has been published in Phys. Rev. B as a Rapid Communication [37].

3.1 Introduction

3.1.1 The Landau-Lifshitz-Gilbert Equation

A magnetic texture can be characterized by a three-dimensional vector field $\mathbf{M}(\mathbf{r})$ where $\mathbf{M}$ is the local magnetization vector (magnetic dipole moment per unit volume). If the magnitude of $\mathbf{M}$ stays constant throughout the sample, which is often the case in a magnetically ordered system well below the Curie temperature, one can instead use the unit-vector field $\mathbf{m}(\mathbf{r}) = \mathbf{M}/|\mathbf{M}|$. The time evolution of magnetization $\mathbf{m}(\mathbf{r}, t)$ is then given by the Landau-Lifshitz-Gilbert (LLG) equation [23, 24]

$$\mathcal{J}\dot{\mathbf{m}} = \mathbf{m} \times \mathbf{h}_{\text{eff}} + \alpha|\mathcal{J}|\dot{\mathbf{m}} \times \mathbf{m}. \tag{3.1}$$

Here $\mathcal{J} = |\mathbf{M}|/\gamma$ is the angular momentum density where $\gamma = ge/2mc$ is the gyromagnetic ratio, $\mathbf{h}_{\text{eff}}(\mathbf{r}) = -\delta U/\delta\mathbf{m}(\mathbf{r})$ is the effective magnetic field obtained from the

potential energy functional $U[\mathbf{m}(\mathbf{r})]$ and $\alpha \ll 1$ is the Gilbert damping constant [24]. The first term on the right hand side of (3.1) describes the precession of $\mathbf{m}$ about an effective magnetic field $\mathbf{h}_{\text{eff}}$. The second term represents the energy loss due to viscous forces in the system that cause $\mathbf{m}$ to align with $\mathbf{h}_{\text{eff}}$ at long time.

Alternatively, one can use a Lagrangian formulation of the theory. Equation (3.1), without the damping term, can be derived from the Lagrangian

$$L = \mathcal{J} \int \mathbf{a}(\mathbf{m}) \cdot \dot{\mathbf{m}}\, dV - U[\mathbf{m}]. \tag{3.2}$$

Here the first term is the so-called Berry phase with a monopole vector potential $\mathbf{a}(\mathbf{m})$ which obeys $\nabla_{\mathbf{m}} \times \mathbf{a} = -\mathbf{m}$ [9]. This can be easily seen by substituting (3.2) into the Eular-Lagrange equation, written in component notation,

$$\frac{\partial}{\partial t}\left(\frac{\delta L}{\delta \dot{m}_i}\right) = \frac{\delta L}{\delta m_i} \tag{3.3}$$

Evaluating the functional derivatives on the two sides, one obtains

$$\mathcal{J}\frac{\partial a_i}{\partial m_j}\dot{m}_j = \mathcal{J}\frac{\partial a_j}{\partial m_i}\dot{m}_j - \frac{\delta U}{\delta m_i}, \tag{3.4}$$

which can be rearranged to give

$$\epsilon_{ijk}\mathcal{J}\dot{m}_j(\nabla \times \mathbf{a})_k = \frac{\delta U}{\delta m_i}. \tag{3.5}$$

Remembering that $\mathbf{a}(\mathbf{m})$ is the vector potential of a monopole located at the origin and using the definition of the effective magnetic field $\mathbf{h}_{\text{eff}}$, the above equation transforms to

$$\mathcal{J}(\dot{\mathbf{m}} \times \mathbf{m}) = \mathbf{h}_{\text{eff}}. \tag{3.6}$$

Finally, taking cross product of both sides with $\mathbf{m}$ and using the relation $\mathbf{m} \cdot \dot{\mathbf{m}} = 0$ (since $\mathbf{m}$ is a unit vector), one recovers the LLG equation (3.1) without the damping term.

The Gilbert damping term can be handled within this framework by using the Rayleigh dissipation function

$$R = \frac{\alpha|\mathcal{J}|}{2} \int |\dot{\mathbf{m}}|^2 \, dV. \tag{3.7}$$

The Euler-Lagrange equations then get modified to

$$\frac{\partial}{\partial t}\left(\frac{\delta L}{\delta \dot{m}_i}\right) - \frac{\delta L}{\delta m_i} + \frac{\delta R}{\delta \dot{m}_i} = 0. \tag{3.8}$$

Using both the Lagrangian (3.2) and the Rayleigh function (3.7) in (3.8) readily reproduces the full LLG equation (3.1).

The field of a magnetic monopole has a nonzero divergence and hence cannot be globally captured by a vector potential [9]. Thus any choice of the vector potential $\mathbf{a}(\mathbf{m})$ will be singular at (at least) one point on the unit sphere. This is the entry point

for the Dirac string that ensures that the total flux of the magnetic field described by $\mathbf{a}(\mathbf{m})$ is zero thorough the sphere. One is free to choose the exact location of this singular point. In our study of the annihilation of two domain walls, we will use the boundary condition $\mathbf{m}(\pm\infty) = \hat{\mathbf{z}}$ and the magnetization will not point exactly along $-\hat{\mathbf{z}}$ anywhere on the wire. It would thus be convenient for us to choose a vector potential that is singular at the south pole $\mathbf{m} = -\hat{\mathbf{z}}$ of the unit sphere. This corresponds to the choice

$$a_\theta = 0, \qquad a_\phi = \frac{\cos\theta - 1}{\sin\theta}, \tag{3.9}$$

where we have used the polar and azimuthal angles θ and ϕ to characterize $\mathbf{m}$,

$$\mathbf{m} = (\sin\theta\cos\phi, \sin\theta\sin\phi, \cos\theta). \tag{3.10}$$

Since Equation (3.1) is a nonlinear partial differential equation in $\mathbf{r}$ and t, a full analytic solution for $\mathbf{m}(\mathbf{r}, t)$ is unavailable for most initial conditions. But one can often extract the dynamics at long time-scales by identifying a small number of relevant soft modes of the system, parametrized by collective coordinates. We will illustrate this approach with the simple example of the motion of a domain wall in an external magnetic field in the next subsection. We'll then proceed to give a general formulation of the method, as applicable to any soliton.

3.1.2 Domain Wall in External Magnetic Field

The simplest setting for the study of topological solitons is an easy-axis ferromagnet in one spatial dimension $\mathbf{m} = \mathbf{m}(z,t)$ with the potential energy

$$U = \int_{-\infty}^{\infty} dz \left(A|\mathbf{m}'|^2 + K|\mathbf{m} \times \hat{\mathbf{z}}|^2 \right) /2. \tag{3.11}$$

Here A is the exchange constant, K is the anisotropy, $\hat{\mathbf{z}}$ is the direction of the easy axis, and $m' \equiv \partial m/\partial z$. The unit of length is the width of the domain wall $\ell_0 = \sqrt{A/K}$ and the unit of time is the inverse of the ferromagnetic resonance frequency, $t_0 = 1/\omega_0 = \mathcal{J}/K$. In what follows, we will work in these natural units and set $\mathcal{J} = A = K = \ell_0 = t_0 = 1$. Using the polar and azimuthal angles $\theta(z)$ and $\phi(z)$ to characterize $\mathbf{m}$, the Lagrangian (3.2) can be written as

$$L = \int_{-\infty}^{\infty} dz \, (\cos\theta - 1)\, \dot{\phi} - U. \tag{3.12}$$

As discussed in the previous subsection, this Lagrangian completely captures the conservative part of the dynamics as long as $\mathbf{m}$ doesn't point exactly in the $-\hat{\mathbf{z}}$ direction anywhere on the wire. The potential energy $U[\mathbf{m}]$ has the two uniform states $\mathbf{m}(z) = \pm\hat{\mathbf{z}}$ as its ground states. One can obtain topological solitons interpolating between these two ground states by minimizing $U[\mathbf{m}] = U[\theta, \phi]$ with the boundary condition $\mathbf{m}(\pm\infty) = \pm\hat{\mathbf{z}}$ or $\mathbf{m}(\pm\infty) = \mp\hat{\mathbf{z}}$. This yields domain wall profiles (Figure

3.1)

$$\cos\theta(z) = \pm\tanh(z - Z), \quad \phi(z) = \Phi. \tag{3.13}$$

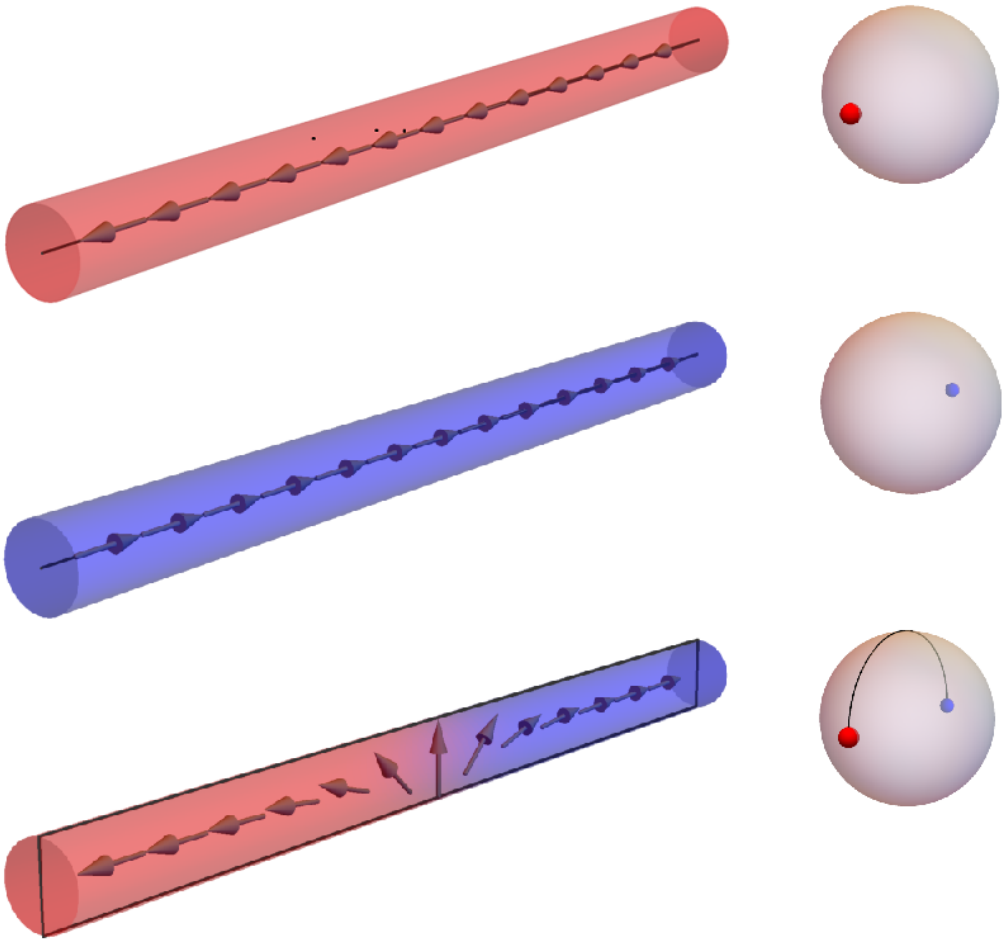

Figure 3.1: Left column: three configurations of the one-dimensional ferromagnetic wire with an easy axis along its length. The first two are the two ground states. The third one is a domain wall. Red and blue denote spins pointing along $+\hat{\mathbf{z}}$ and $-\hat{\mathbf{z}}$ respectively. Right column: Corresponding trajectories of the spin vector on the unit magnetization sphere.

A domain wall, being a local minimum of the total energy, is a static configuration. The position of the center of the domain wall $-\infty < Z < \infty$ and its azimuthal angle $-\pi \leq \Phi \leq \pi$ are the two zero modes of the system. These correspond to the

translational ($\mathbf{m}(z) \mapsto \mathbf{m}(z - Z)$) and rotational ($\phi(z) \mapsto \phi(z) + \Phi$) symmetries of the energy U (3.11) of the wire. Since changing these modes doesn't cost any energy, they are the easiest ones to perturb by a weak external force. Schryer and Walker [25] showed that the dynamics of a domain wall at long time scales can be captured by assuming that a weak external perturbation just makes these two parameters in Equation (3.13) time dependent: $Z(t)$ and $\Phi(t)$. Strictly speaking, Schryer and Walker's model also included an anisotropy in Φ, i.e. an easy azimuthal plane. In their model they also included variations of the domain wall width l_0 in time (it gets wider when Φ is away from the easy plane). This mode is hard, so, on time scales long compared to its relaxation time, it can be viewed as instantaneously adjusting to the local conditions (value of the effective anisotropy constant $K(\Phi)$). So l_0 is time-dependent but not an independent dynamical variable. These variations can be neglected if the anisotropy in Φ is weak. In our model this anisotropy is exactly zero and hence we can safely treat l_0 as a constant.

Substituting this domain-wall ansatz into either the LLG equation (3.1) or the Lagrangian (3.2), one obtains an effective theory for the domain wall motion in terms of the two "collective coordinates" Z and Φ. Their equations of motion look like

$$F_\Phi \pm 2\dot{Z} - 2\alpha\dot{\Phi} = 0, \tag{3.14a}$$

$$F_Z \mp 2\dot{\Phi} - 2\alpha\dot{Z} = 0. \tag{3.14b}$$

Here the force $F_Z = -\partial U/\partial Z$ and the torque $F_\Phi = -\partial U/\partial \Phi$ come from the external perturbation that is now contained in U.

To give a concrete example, let us focus on the special case of a domain wall in the sector $\mathbf{m}(\pm\infty) = \pm\hat{\mathbf{z}}$ in an external magnetic field $\mathbf{H} = H\hat{\mathbf{z}}$ which corresponds to $U_{\text{ext}} = -\int dz\, \mathbf{m}\cdot\mathbf{H}$. The domain-wall ansatz (3.13) gives $U_{\text{ext}} = 2HZ$. This in turn gives a force $F_Z = -2H$ and a torque $F_\Phi = 0$. Substituting these into the equations of motion (3.14), one obtains the steady-state motion of the domain wall:

$$\dot{Z} = V = -\frac{\alpha H}{1+\alpha^2}, \tag{3.15a}$$

$$\dot{\Phi} = \Omega = -\frac{H}{1+\alpha^2}. \tag{3.15b}$$

In the absence of dissipation ($\alpha = 0$) the domain wall just precesses about the external field at a constant angular velocity $\Omega_0 = -H$. Once dissipation is turned on it starts to lose energy and, as a result, begins to move opposite to the magnetic field with a velocity proportional to the damping coefficient α: $V = \alpha\Omega$. Note that the rotational velocity Ω is zeroth order in the Gilbert damping $\alpha \ll 1$, while the linear velocity is first. This dependence on the small parameter α allows us to separate the dynamics into fast ($O(\alpha^0)$) and slow ($O(\alpha^1)$), which will be useful in what follows. Note also the somewhat counter-intuitive response of the domain wall to an external force: it mostly rotates. Conversely, the application of an external torque would produce mostly translational motion! This happens because a domain wall is made out of

magnetic moments, which behave like spinning tops and precess in response to an external perturbation.

3.1.3 The Collective Coordinates Formalism

We can generalize the above technique to the case of a general magnetic soliton by assuming that its time dependence $\mathbf{m}(\mathbf{r},t)$ can be described by a set of collective coordinates $\mathbf{q}(t) = \{q_1(t), q_2(t), \ldots, q_N(t)\}$, i.e. $\mathbf{m}(\mathbf{r},t) = \mathbf{m}_0(\mathbf{r},\mathbf{q}(t))$ where $\mathbf{m}_0$ is a known ansatz for the profile of the soliton. Substituting this ansatz into the LLG equation (3.1) gives a set of equations of motion for the collective coordinates [26],

$$F_i + G_{ij}\dot{q}_j - \Gamma_{ij}\dot{q}_j = 0, \tag{3.16a}$$

$$F_i = -\frac{\partial U}{\partial q_i}, \tag{3.16b}$$

$$G_{ij} = -\mathcal{J}\int dV\, \mathbf{m_0}\cdot\left(\frac{\partial \mathbf{m_0}}{\partial q_i}\times\frac{\partial \mathbf{m_0}}{\partial q_j}\right), \tag{3.16c}$$

$$\Gamma_{ij} = \alpha|\mathcal{J}|\int dV\, \frac{\partial \mathbf{m_0}}{\partial q_i}\cdot\frac{\partial \mathbf{m_0}}{\partial q_j}. \tag{3.16d}$$

Here F_i is the conservative force conjugate to collective coordinate q_i, G_{ij} is the antisymmetric gyrotropic tensor, and Γ_{ij} is the symmetric viscosity tensor. Equation (3.16a) describes the balance of three forces acting on the soliton: conservative, gyrotropic and viscous. It is important to note that there is no inertial term in the equation of motion (3.16a). This is because a ferromagnetic soliton is made of spins, which behave like spinning gyroscopes whose dynamics (in the absence of dissipation)

is governed solely by a gyrotropic term involving a first order time derivative. This is in contrast with antiferromagnetic solitons in which the spins in two sublattices are almost antiparallel. In such solitons, the Berry phases gathered by two neighboring spins almost cancel each other and what remains behaves like an effective inertial term in the Lagrangian [3]. Thus antiferromagnetic solitons do have inertia but ferromagnetic ones don't. In this dissertation we will deal exclusively with ferromagnetic solitons.

One can also obtain a Lagrangian formulation of this effective theory by substituting the collective-coordinates ansatz into the Lagrangian (3.2). This yields the following Lagrangian for the collective coordinates [36]:

$$L(\mathbf{q}, \dot{\mathbf{q}}) = \mathbf{A}(\mathbf{q}) \cdot \dot{\mathbf{q}} - U(\mathbf{q}), \tag{3.17}$$

The vector potential in the Berry phase term becomes $A_i(\mathbf{q}) = \int \mathbf{a}(\mathbf{m}) \cdot (\partial \mathbf{m}/\partial q_i)\, dV$. The curvature of the gauge potential $\mathbf{A}(\mathbf{q})$ is just the gyrotropic tensor: $\partial A_j/\partial q_i - \partial A_i/\partial q_j = G_{ij}$. The same substitution also gives the Rayleigh dissipation function in the space of collective coordinates,

$$R(\mathbf{q}, \dot{\mathbf{q}}) = \frac{1}{2} \dot{\mathbf{q}}^{\mathrm{T}} \mathbf{\Gamma}(\mathbf{q}) \dot{\mathbf{q}}. \tag{3.18}$$

3.2 Two Domain Walls

3.2.1 The Problem: Annihilation of Domain Walls

As noted in the previous section, past applications of the method of collective coordinates have mostly been limited to the zero modes of the system. Going beyond the zero mode approximation and including hard modes as dynamical degrees of freedom often poses significant challenges [36]. The present work will address a problem that fundamentally requires going beyond the zero-mode approximation: the annihilation of two domain walls in a one-dimensional ferromagnet with an easy axis. We start with a state that has two domain walls located far from each other compared to the width of an individual wall (which is $l_0 = \sqrt{\frac{A}{K}} = 1$ in our rational units), as shown in Figure 3.2. The two domain walls might lie in the same azimuthal plane or might have a relative twist. We then ask the question: what happens once we let this system evolve in time?

Two-domain-wall configurations satisfy the boundary condition $\mathbf{m}(\pm\infty) = \hat{\mathbf{z}}$ or $\mathbf{m}(\pm\infty) = -\hat{\mathbf{z}}$ and thus live in the same topological sector as one of the two ground states of the system. Hence, in the presence of energy dissipation, one can expect the domain walls to approach each other and eventually annihilate to form a uniform state $\mathbf{m}(z) = \hat{\mathbf{z}}$ or $\mathbf{m}(z) = -\hat{\mathbf{z}}$ respectively. Our goal will be to develop a theoretical understanding of this annihilation process.

The potential energy U of our system is still given by the same expression (3.11)

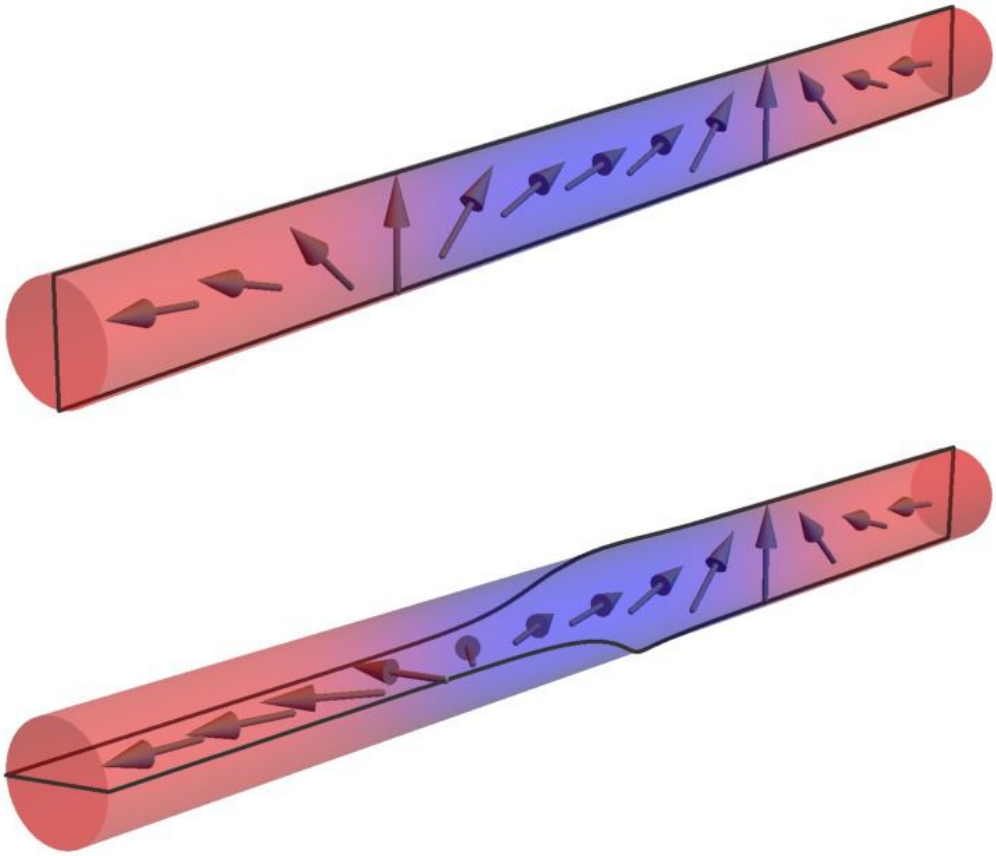

Figure 3.2: Two configurations of a pair of domain walls. The wire frames depict the local plane tangential to the magnetization field. The first configuration has both domain walls in the same azimuthal plane. The second one has two domain walls in two orthogonal azimuthal planes. Both configurations are in the same topological sector as the "red" ground state.

as in the previous section. When two domain walls are far apart, they behave like rigid objects and can be described by two independent pairs of collective coordinates: two positions Z_1 and Z_2 and two azimuthal angles Φ_1 and Φ_2. Alternatively, we may use the average position $Z = (Z_1 + Z_2)/2$ and the average angle $\Phi = (\Phi_1 + \Phi_2)/2$ and two relative coordinates, the separation $\zeta = Z_2 - Z_1$ and the twist $\varphi = \Phi_2 - \Phi_1$. The average coordinates Z and Φ still represent exact zero modes associated with the symmetries of U under translation and rotation. On the other hand, the relative coordinates ζ and φ are only approximate zero modes in the large separation limit. They affect the energy (3.11) and thus harden as the domain walls get closer and their interaction increases.

For concreteness, let us work with the boundary condition $\mathbf{m}(\pm\infty) = \hat{\mathbf{z}}$. We may anticipate how the annihilation proceeds in the limit of large separation, $\zeta \gg 1$, when the domain walls retain their individual character and are described by Eq. 3.14. In this limit the forces and torques on the two domain walls can be obtained from the potential energy expressed in terms of the collective coordinates $U(Z_1, \Phi_1, Z_2, \Phi_2)$.

We observe that the potential energy U of the system must decrease as the separation $\zeta = Z_2 - Z_1$ is decreased, since this brings the configuration closer to the uniform state. This implies that the domain walls attract each other with equal and opposite forces. It is also important to note that one of the two domain walls interpolates from the $+\hat{\mathbf{z}}$ to the $-\hat{\mathbf{z}}$ state and the second one does the opposite. So they satisfy equations of motion that differ in the sign of the second term, as shown in (3.14).

Let us first look at the situation where $\alpha = 0$ (no dissipation). The two domain walls experience equal and opposite F_Z forces, and thus precess in a rigid manner with the same angular velocity $\dot{\Phi}$, as dictated by the second equation in (3.14). Adding dissipation (a small nonzero α) to the system then causes the two domain walls to move slowly in the direction of the forces, i.e. toward each other. A similar analysis involving the relative twist $\varphi = \Phi_2 - \Phi_1$ implies that a pair with a twist also applies equal and opposite aligning torques F_Φ on each other that cause the system to translate rigidly with a fixed linear velocity $\dot{Z}$ in the absence of dissipation. Adding dissipation then causes the azimuthal planes of the pair to slowly rotate toward each other.

It is clear at this point that a minimal description of the annihilation process has to include at least two hard modes: the relative separation and the relative twist. In the large separation limit, this does not pose a problem as one can still use the single domain wall picture. At this level the hardness of the two relative modes enters the description only through $U(\zeta, \phi)$. But as the domain walls approach each other and begin to overlap, they lose their ideal shape (3.13) and the equations of motion (3.14) no longer apply. This is illustrated in Figure (3.3). The two average coordinates Z and Φ, being exact zero modes, are still well-defined. But since the precise positions and azimuthal angles of overlapping domain walls are now ill-defined, previous definitions of the two relative coordinates ζ and φ become meaningless.

At this point, the two conserved momenta of the system corresponding to the

global rotational and translational symmetries of (3.12)—angular J and linear P—come to our rescue. As we'll see in the next subsection, these two quantities, which are always well defined, can be used as proxies for the separation and the twist respectively. Fortunately this redefinition of the relative coordinates will preserve much of our previous intuition about the physical meaning of these quantities, as we'll also see in the next subsection.

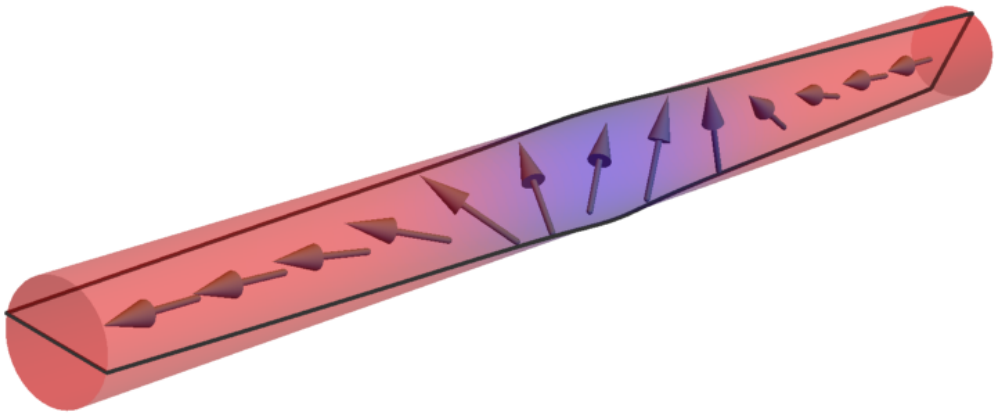

Figure 3.3: A pair of domain walls that have started to overlap. The individual domain walls have lost their ideal shape. The naive definitions of the two relative coordinates $\zeta = Z_2 - Z_1$ and $\varphi = \Phi_2 - \Phi_1$ are not applicable in this regime.

3.2.2 Conserved Momenta

The Lagrangian of the ferromagnetic wire (3.12) is invariant under a global rotation $\phi(z) \mapsto \phi(z) + \Phi$ and a global translation $\mathbf{m}(z) \mapsto \mathbf{m}(z - Z)$. So, in the absence of dissipation ($\alpha = 0$), the momenta J and P conjugate to the two zero modes Φ and Z are constants of motion. One can read off the cannonical mo-

mentum corresponding to any collective coordinate q_i from the Lagrangian (3.17): $p_i = A_i(\mathbf{q}) = \int \mathbf{a}(\mathbf{m}) \cdot (\partial \mathbf{m}/\partial q_i)\, dV$ [38]. This indicates that the definition of cannonical momentum of a soliton might be problematic since there are multiple ways of choosing the gauge field $A_i(\mathbf{q})$ for the same physical situation. This ambiguity is indeed present for the case of a topological soliton like a single domain wall and has been discussed extensively in the literature [3, 38–43]. Fortunately for us, a pair of domain walls can be continuously deformed to the uniform state and is thus a non-topological soliton, in which case this ambiguity does not arise [38]. As a result, the cannonical momenta we will deal with are always well defined.

3.2.2.1 Angular Momentum

The momentum conjugate to Φ can be obtained from (3.12) [3]:

$$J = p_\Phi = \int_{-\infty}^{\infty} dz\, \mathbf{a}(\mathbf{m}) \cdot \frac{\partial \mathbf{m}}{\partial \Phi} = \int_{-\infty}^{\infty} dz\, (\cos\theta - 1) \frac{\partial \phi}{\partial \Phi} = \int_{-\infty}^{\infty} dz\, (\cos\theta - 1). \quad (3.19)$$

According to quantum mechanics, the angular momentum about the z-axis should be the total spin in the z-direction $S^z_{\text{tot}} = \int dz\, \cos\theta$. But since $\mathbf{m}(\pm\infty) = \hat{\mathbf{z}}$, S^z_{tot} diverges and it is more convenient to measure the total spin with respect to the uniform state $\mathbf{m}(z) = \hat{\mathbf{z}}$. This is exactly what Equation (3.19) does.

As noted above, the angular momentum is a constant of motion for our system. It also has a simple geometric meaning in the limit when the two domain walls are

far apart ($\zeta \gg 1$). In this limit, $\cos\theta \approx -1$ in the space between the domain walls and ≈ 1 in the space outside, so $J \approx -2\zeta$. Turning this around, we can *define* the separation in terms of the angular momentum (3.19), $\zeta \equiv -J/2$. This definition agrees with the previous definition of separation in the large ζ limit, is valid for any configuration and goes to zero as the two domain walls merge.

3.2.2.2 Linear Momentum

The momentum conjugate to Z can be obtained as [3]:

$$P = p_Z = \int_{-\infty}^{\infty} dz\, \mathbf{a}(\mathbf{m}) \cdot \frac{\partial \mathbf{m}}{\partial Z} = -\int_{-\infty}^{\infty} dz\, (\cos\theta - 1)\frac{\partial \phi}{\partial z} = \oint d\phi\, (1 - \cos\theta). \quad (3.20)$$

Here we have used the fact $\partial/\partial Z = -\partial/\partial z$ since Z corresponds to a rigid translation of the soliton: $\mathbf{m} = \mathbf{m}(z - Z)$. The linear momentum is the area subtended by the vector $\mathbf{m}(z)$ on the unit sphere as z goes from $-\infty$ to $+\infty$ [41]. For two well-separated domain walls with a twist φ, this area is 2φ. Again, we turn things around and *define* the twist in terms of the linear momentum (3.20), $\varphi \equiv P/2$. Once again, this definition agrees with the previous definition of twist in the large ζ limit, is valid for any configuration and goes to zero as the two domain walls merge. Pairs of domain walls with several values of separation ζ and twist φ are shown in Fig. 3.4.

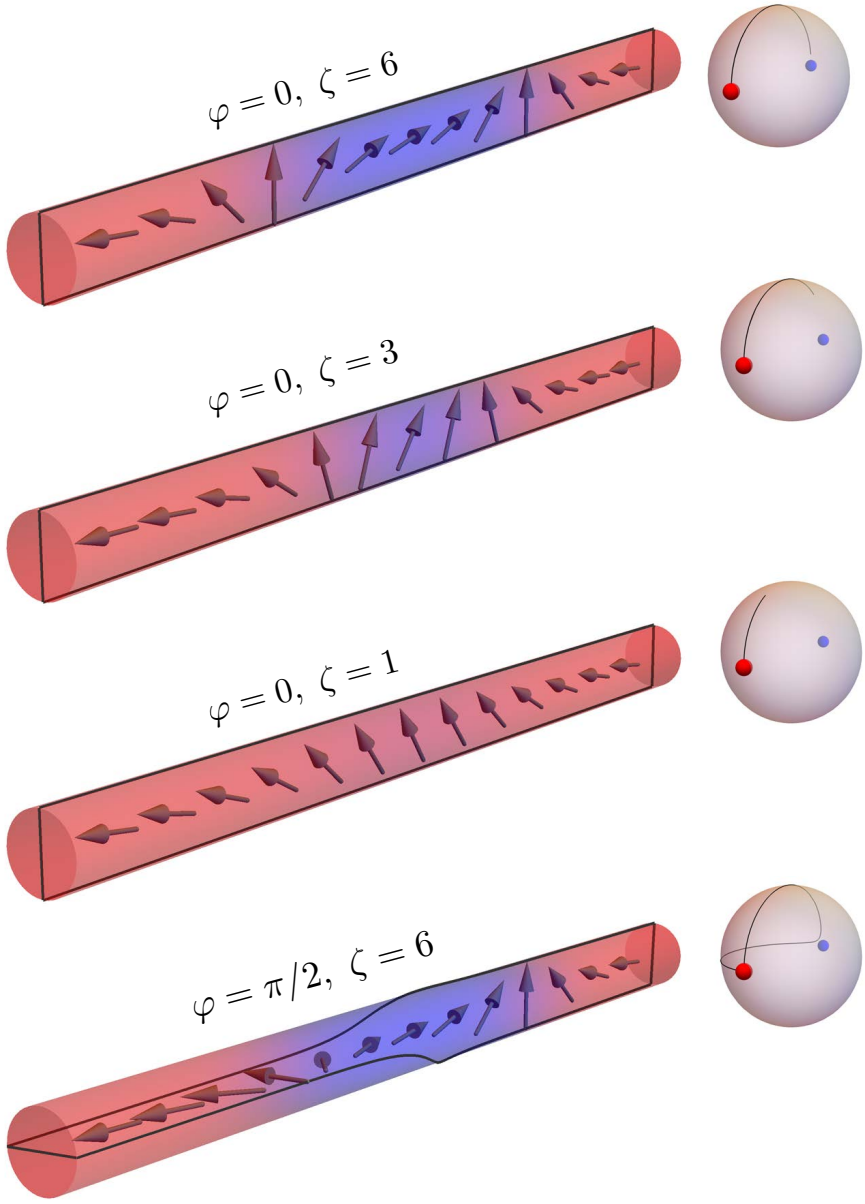

Figure 3.4: Several configurations of a pair of domain walls with shown values of separation ζ and twist φ. The red and blue colors denote positive and negative magnetization component m_z along the axis of the cylinder. The wire frames depict the local plane tangential to the magnetization field. Spheres on the right show the path of the magnetization field $\mathbf{m}(z)$ as z goes from $-\infty$ to $+\infty$, beginning from and ending at the north pole (red). The south pole (blue) can only be reached if the separation of the domain walls $\zeta = \infty$.

3.3 Non-Dissipative Case: Uniformly Moving Solitons

Unlike single domain walls, which are stable for topological reasons, pairs of domain walls are unstable: minimization of the energy (3.11) in the topologically trivial sector with $\mathbf{m}(\pm\infty) = \hat{\mathbf{z}}$ yields a uniform ground state $\mathbf{m}(z) = \hat{\mathbf{z}}$. Both conserved momenta are zero in the uniform state: $J = P = 0$. To obtain a solution for a pair of domain walls, we may rely on conservation of linear and angular momenta and minimize the energy U at fixed P and J. Such a minimization is expected to yield a domain wall pair with separation $\zeta = -J/2$ and twist $\varphi = P/2$. As we'll see below, this minimization can be carried out analytically and yields a class of exact solutions for domain wall pairs parametrized by two independent collective coordinates $0 < \zeta < \infty$ and $-\pi < \varphi \leq \pi$. This class of solutions was first obtained by Kosevich *et. al.* [44] and by Long and Bishop [45]. In this section we'll present a derivation that makes the role of conserved quantities more explicit and is thus better suited for our further analysis of the annihilation process. The analysis in this section assumes the system follows a conservative dynamics, i.e. the Gilbert damping constant $\alpha = 0$.

3.3.1 Two Domain Walls: Planar Case

For simplicity, we'll start with the special case where the two domain walls lie in the same azimuthal plane. Such a planar soliton does not describe any area on the

unit magnetization sphere and thus has zero linear momentum P. So, to obtain the planar configuration we just need to minimize the energy U (3.11) with respect to a fixed angular momentum J (3.19) in the sector $\mathbf{m}(\pm\infty) = \hat{\mathbf{z}}$. This would yield a domain wall pair with separation $\zeta = -J/2$ and twist $\varphi = 0$. The minimization can be done by defining a modified energy

$$\tilde{U} = U - J\Omega, \tag{3.21}$$

where Ω is a Lagrange multiplier, and minimizing it with respect to $\mathbf{m}(z)$. The corresponding Lagrangian,

$$\tilde{L} = \int_{-\infty}^{\infty} dz\,(\cos\theta - 1)(\dot{\phi} + \Omega) - U, \tag{3.22}$$

describes the dynamics of magnetization in a new frame rotating at the angular velocity Ω. This can be easily seen by carrying out the coordinate transformation $\phi = \tilde{\phi} + \Omega t$ in (3.12). Minimization of the new potential energy (3.21) yields a static soliton in the new frame. In the static frame, this soliton is rigidly rotating at the angular velocity Ω. By explicitly calculating the angular momentum of this soliton, one can find the angular velocity Ω in terms of J, or equivalently, the collective coordinate $\zeta = -J/2$.

To explicitly solve the minimization problem, we write everything in terms of the two angles $\theta(z)$ and $\phi(z)$. The modified potential energy (3.21) becomes

$$\tilde{U}[\theta,\phi] = \int_{-\infty}^{\infty} dz \left\{ \frac{1}{2}\left[\left(\frac{d\theta}{dz}\right)^2 + \sin^2\theta \left(\frac{d\phi}{dz}\right)^2 \right] + \frac{1}{2}\sin^2\theta - \Omega(\cos\theta - 1) \right\} \quad (3.23)$$

We can now minimize this expression by setting $\delta\tilde{U}/\delta\phi = 0$ and $\delta\tilde{U}/\delta\theta = 0$. The first yields a constant azimuthal angle $\phi(z) = \Phi$: hence a planar soliton. The second differential equation can now be solved with the boundary condition $\theta(\pm\infty) = 0$ to obtain the profile of the soliton. The details of this calculation are given in Appendix B. We quote below the final expressions for the shape of the soliton and its angular velocity as functions of the three collective coordinates: separation $\zeta = -J/2$ and the two zero modes Φ and Z. Here the separation can take any positive value: $0 < \zeta < \infty$.

$$\begin{aligned} \cos\theta(z) &= \frac{2\,\mathrm{sech}^2\frac{\zeta}{2}}{1 - \tanh^2\frac{\zeta}{2}\tanh^2\left((z-Z)\tanh\frac{\zeta}{2}\right)} - 1 \\ \phi(z) &= \Phi \\ \text{Angular velocity: } \Omega &= -\,\mathrm{sech}^2\frac{\zeta}{2} \end{aligned} \quad (3.24)$$

The first three solitons in Figure 3.4 are illustrations of this solution for relative separations $\zeta = 6, 3$ and 1. It is also interesting to note that the angular velocity is very small and negative for large separations and approaches a finite limiting value of -1 (in rational units) as the domain walls merge to form the uniform state. (In these units, 1 is the lowest frequency of spin waves in this model. Thus the rotational frequency of a pair of domain walls is always below this threshold.)

3.3.2 Two Domain Walls: General Case

We'll now look at the general case where the domain wall pair may form a non-coplanar structure. A non-coplanar soliton describes a nonzero area on the unit magnetization sphere (Figure 3.4) and thus has a finite linear momentum P. So, now we need to minimize the energy U (3.11) with respect to a fixed angular momentum J (3.19) and a fixed linear momentum P (3.20) in the sector $\mathbf{m}(\pm\infty) = \hat{\mathbf{z}}$. This would yield a domain wall pair with separation $\zeta = -J/2$ and twist $\varphi = P/2$. The minimization can be done by defining a modified energy

$$\tilde{U} = U - J\Omega - PV, \tag{3.25}$$

where Ω and V are Lagrange multipliers, and minimizing it with respect to $\mathbf{m}(z)$. The corresponding Lagrangian,

$$\tilde{L} = \int_{-\infty}^{\infty} dz\,(\cos\theta - 1)(\dot{\phi} - V\phi' + \Omega) - U, \tag{3.26}$$

describes the dynamics of magnetization in a new frame rotating at the angular velocity Ω and moving at the linear velocity V. This can be easily seen by carrying out the coordinate transformation $\phi = \tilde{\phi} + \Omega t$ and $z = \tilde{z} + Vt$ in (3.12). Minimization of the modified potential energy (3.25) yields a static soliton in the moving and rotating frame. In the static frame, this soliton is rigidly rotating at the angular

velocity Ω and rigidly translating at the linear velocity V. By calculating the angular and linear momenta, one can find the velocities Ω and V of this dynamical soliton in terms of $\{J, P\}$, or equivalently, the collective coordinates $\{\zeta, \varphi\}$.

To explicitly solve the minimization problem, we again write everything in terms of the two angles $\theta(z)$ and $\phi(z)$. The modified potential energy now becomes

$$\tilde{U}[\theta,\phi] = \int_{-\infty}^{\infty} dz \left\{ \frac{1}{2}\left[\left(\frac{d\theta}{dz}\right)^2 + \sin^2\theta \left(\frac{d\phi}{dz}\right)^2 \right] + \frac{1}{2}\sin^2\theta - \Omega(\cos\theta - 1) + V(\cos\theta - 1)\phi' \right\} \tag{3.27}$$

We can minimize this expression by setting $\delta\tilde{U}/\delta\phi = 0$ and $\delta\tilde{U}/\delta\theta = 0$. The first gives the derivative of the azimuthal angle in terms of the polar angle,

$$\phi' = \frac{V}{1+\cos\theta} \tag{3.28}$$

With the help of this relation, the differential equation $\delta\tilde{U}/\delta\theta = 0$ can be solved with the boundary condition $\theta(\pm\infty) = 0$ to obtain the profile of the soliton. We present the details of the calculation in Appendix B. Here we quote the final expressions for the shape of the soliton and its velocities as functions of the four collective coordinates: separation $\zeta = -J/2$, twist $\varphi = P/2$ and the two zero modes Φ and Z. The separation can take any positive value: $0 < \zeta < \infty$ and the twist can be any angle $-\pi < \varphi \leq \pi$.

It is convenient to first write the solution in a symbolic form:

$$\cos\theta(z) - 1 = \quad f(z - Z; \zeta, \varphi) \tag{3.29a}$$

$$\phi(z) = \quad \Phi + g(z - Z; \zeta, \varphi) \tag{3.29b}$$

To express the functions f and g in a compact way we define:

$$a(\zeta, \varphi) = 2\Big(1 - \cos^2\tfrac{\varphi}{2}\operatorname{sech}^2\tfrac{\zeta}{2}\Big) \tag{3.30a}$$

$$b(\zeta, \varphi) = 2\Big(1 + \sin^2\tfrac{\varphi}{2}\operatorname{csch}^2\tfrac{\zeta}{2}\Big) \tag{3.30b}$$

The expressions for f and g are then given by:

$$f(z; \zeta, \varphi) = -b + \frac{b-a}{1 - \frac{a}{b}\tanh^2\left(\frac{\sqrt{ab}}{2}z\right)} \tag{3.31a}$$

$$g(z; \zeta, \varphi) = \tfrac{\sin\varphi}{\sinh\zeta}z + \operatorname{sgn}\varphi\tan^{-1}\left[\sqrt{\tfrac{a(b-2)}{b(2-a)}}\tanh\left(\tfrac{\sqrt{ab}}{2}z\right)\right] \tag{3.31b}$$

The angular and linear velocities of the soliton as functions of the relative separation ζ and relative twist φ are

$$\dot{Z} = V = \frac{2\sin\varphi}{\sinh\zeta}, \quad \dot{\Phi} = \Omega = \frac{\sin^2\frac{\varphi}{2}}{\sinh^2\frac{\zeta}{2}} - \frac{\cos^2\frac{\varphi}{2}}{\cosh^2\frac{\zeta}{2}}. \tag{3.32}$$

These equations reduce to the planar case (3.24) if we set $\varphi = 0$, as expected. It is

interesting to note that unlike the momenta ζ and φ, the velocities Ω and V are not completely independent of each other. For example, in the limit of the uniform state $\zeta \to 0, \varphi \to 0$ Equations (3.32) become $V_0 = 2\varphi/\zeta$ and $\Omega_0 = -1+\varphi^2/\zeta^2$. This implies the constraint $\Omega_0 = -1+V_0^2/4$ in this limit. A closer inspection of (3.32) reveals that for any fixed value of V, Ω can only take values in the range $-1 + V^2/4 < \Omega < \infty$. Like in the planar case, the angular velocity of the pair always lies below the lowest frequency of spin waves. This implies that a pair of approaching domain walls will not emit spin waves, which is consistent with our approximation that only the four collective coordinates Z, Φ, ζ, and φ are dynamical in this system.

3.4 Dissipative Case: Annihilating Solitons

We are now ready to derive the equations of motion for a pair of domain walls with four collective coordinates Φ, Z, φ, and ζ by using the general formalism discussed in Section 3.1.3. The gyrotropic coefficients and the forces can be directly read off from the results about stationary solitons we have already discussed. The viscosity coefficients can be obtained by direct integration of (3.16d). We will present these results in the following subsections.

3.4.1 Gyrotropic Tensor

The gyrotropic coefficients G_{ij} are most easily derived from the Berry phase term in the effective Lagrangian for the collective coordinates (3.17). The collective coordinates form two pairs of conjugate variables, Φ and $J = -2\zeta$ for rotational motion and Z and $P = 2\varphi$ for translational. We thus infer that the effective Lagrangian includes the Berry-phase terms [36]

$$L_B = -2\zeta\dot{\Phi} + 2\varphi\dot{Z} = A_i\dot{q}_i. \tag{3.33}$$

We can derive this result more explicitly as follows. We start with the symbolic form of the general solution for the domain wall pair (3.29). Differentiating (3.29b) with respect to time gives

$$\begin{aligned} \dot{\phi} &= \dot{\Phi} + \tfrac{\partial g}{\partial Z}\dot{Z} + \tfrac{\partial g}{\partial \zeta}\dot{\zeta} + \tfrac{\partial g}{\partial \varphi}\dot{\varphi} \\ &= \dot{\Phi} - \phi'\dot{Z} + \tfrac{\partial g}{\partial \zeta}\dot{\zeta} + \tfrac{\partial g}{\partial \varphi}\dot{\varphi} \end{aligned} \tag{3.34}$$

Substituting this into the Berry phase part of the full Lagrangian given by (3.2) gives

$$\begin{aligned} L_B &= \dot{\Phi}\int dz\,(\cos\theta - 1) - \dot{Z}\int dz\,(\cos\theta - 1)\phi' + \dot{\zeta}\int dz\, f\frac{\partial g}{\partial \zeta} + \dot{\varphi}\int dz\, f\frac{\partial g}{\partial \varphi} \\ &= -2\zeta\dot{\Phi} + 2\varphi\dot{Z} + A_\zeta\dot{\zeta} + A_\varphi\dot{\varphi} \end{aligned} \tag{3.35}$$

The first two terms denote the expected gyrotropic couplings between pairs of cannonically conjugate variables. On the other hand, the gauge connections $A_\zeta(\zeta,\varphi)$ and $A_\varphi(\zeta,\varphi)$ indicate the gyrotropic coupling between ζ and ϕ. The corresponding curvature is

$$F_{\zeta\varphi} = \partial_\zeta A_\varphi - \partial_\varphi A_\zeta = \int dz \left(\frac{\partial f}{\partial \zeta}\frac{\partial g}{\partial \varphi} - \frac{\partial f}{\partial \varphi}\frac{\partial g}{\partial \zeta}\right) \tag{3.36}$$

Since $f(g)$ is an even(odd) function of z the integrand is an odd function, implying $F_{\zeta\varphi} = 0$. This basically means that under a transport in the ζ-φ plane in an infinitesimally closed loop, Berry phases gathered by the spins at equal distances from the center on either side are equal and opposite. This is in agreement with our intuition of what should happen in the large separation limit, when the two domain walls stay rigid under an infinitesimal translation and rotation. Hence the Berry phase part of the effective Lagrangian reduces to (3.33).

From L_B we read off the Berry connections $A_\Phi = -2\zeta$, $A_Z = 2\varphi$, and $A_\zeta = A_\varphi = 0$. The gyrotropic coefficients are the Berry curvatures $G_{ij} = \partial_i A_j - \partial_j A_i$. The nonzero coefficients of the gyrotropic tensor are

$$G_{\Phi\zeta} = -G_{\zeta\Phi} = G_{\varphi Z} = -G_{Z\varphi} = 2. \tag{3.37}$$

3.4.2 Conservative Forces

To deduce conservative forces F_i, we turn off dissipation. Equations (3.16) now read $F_i + G_{ij}\dot{q}_j = 0$. Conservation of linear and angular momenta implies the absence of the external force and torque, $F_Z = F_\Phi = 0$. The relation (3.32) between the velocities $\dot{Z} = V$ and $\dot{\Phi} = \Omega$ and the momenta $P = 2\varphi$ and $J = -2\zeta$ together with the results for the gyrotropic tensor (3.37) yield the internal force and torque:

$$F_\zeta = 2\left(\frac{\sin^2\frac{\varphi}{2}}{\sinh^2\frac{\zeta}{2}} - \frac{\cos^2\frac{\varphi}{2}}{\cosh^2\frac{\zeta}{2}}\right), \quad F_\varphi = -\frac{4\sin\varphi}{\sinh\zeta}. \tag{3.38}$$

In the limit of large separation $\zeta \gg 1$, one can expand this expressions and observe that $F_\zeta \approx -8e^{-\zeta}\cos\varphi$, $F_\varphi \approx -8e^{-\zeta}\sin\varphi$. Thus the interaction between domain walls is exponentially small in the separation in this limit, as expected.

3.4.3 Viscosity Coefficients and Predictions of Effective Theory

3.4.3.1 Planar Case

The viscosity coefficients Γ_{ij} are obtained by directly evaluating the integrals in Equation (3.16d) by using the explicit solutions for the solitons (3.31). We first focus on the simpler case of zero twist, $\varphi = 0$. In this case, only two collective coordinates, Φ and ζ, evolve in time, whereas Z and φ remain constant. To the lowest non-vanishing

order in α,

$$G_{\Phi\zeta}\dot{\zeta} - \Gamma_{\Phi\Phi}\dot{\Phi} = 0, \quad F_\zeta + G_{\zeta\Phi}\dot{\Phi} = 0, \tag{3.39}$$

where $F_\zeta = -2\,\mathrm{sech}^2\,\frac{\zeta}{2}$ for $\varphi = 0$. We thus need just one viscosity coefficient, $\Gamma_{\Phi\Phi} = 4\alpha\tanh\frac{\zeta}{2}(1 + \frac{\zeta}{\sinh\zeta})$ for $\varphi = 0$. The resulting equations of motion are

$$\dot{\Phi} = F_\zeta/2, \quad \dot{\zeta} = \Gamma_{\Phi\Phi}F_\zeta/4. \tag{3.40}$$

From Equations (3.40) we see that the global rotation angle Φ is a fast variable whose leading-order behavior is determined by the dissipation-free limit (zeroth order in α). Separation ζ is a slow variable, whose dynamics arises at the first order in α and is dissipational in nature. For large initial separation $\zeta_0 \gg 1$, the attraction is exponentially suppressed, $F_\zeta \approx -8e^{-\zeta}$, and the viscosity is approximately constant, $\Gamma_{\Phi\Phi} \approx 4\alpha$. The separation slowly decreases as $\zeta(t) \approx \ln\bigl(e^{\zeta_0} - 8\alpha t\bigr)$ until the walls overlap. This initial approach takes an exponentially long time $t_i \approx e^{\zeta_0}/8\alpha$. The final stage, in which the "separation" (or angular momentum) decays as $\zeta(t) \sim Ce^{-2\alpha t}$, has a characteristic time scale $t_f = 1/2\alpha$. The global rotation frequency initially grows as $\dot{\Phi}(t) \approx -4/(e^{\zeta_0} - 8\alpha t)$ until the walls overlap, then approaches the asymptotic value $\dot{\Phi}_\infty = -1$.

To check the accuracy of our approach, we compared the solution of Equations (3.40) against numerical simulations of magnetization dynamics in a one-dimensional easy-axis ferromagnet performed with the aid of the micromagnetic solver OOMMF

[46]. In the simulations, separation ζ was obtained from the angular momentum along the easy axis, whereas the angle Φ was measured in the middle of the combined soliton. The results for the initial twist $\varphi_0 = 0$, initial separation $\zeta_0 = 4$, and Gilbert damping $\alpha = 0.01$ are shown as red dots (micromagnetic simulations) and red lines (effective theory, Eqs. 3.40) in Fig. 3.5. We found excellent agreement between the two. The technical details of the micromagnetic simulation are discussed in Section 3.5.

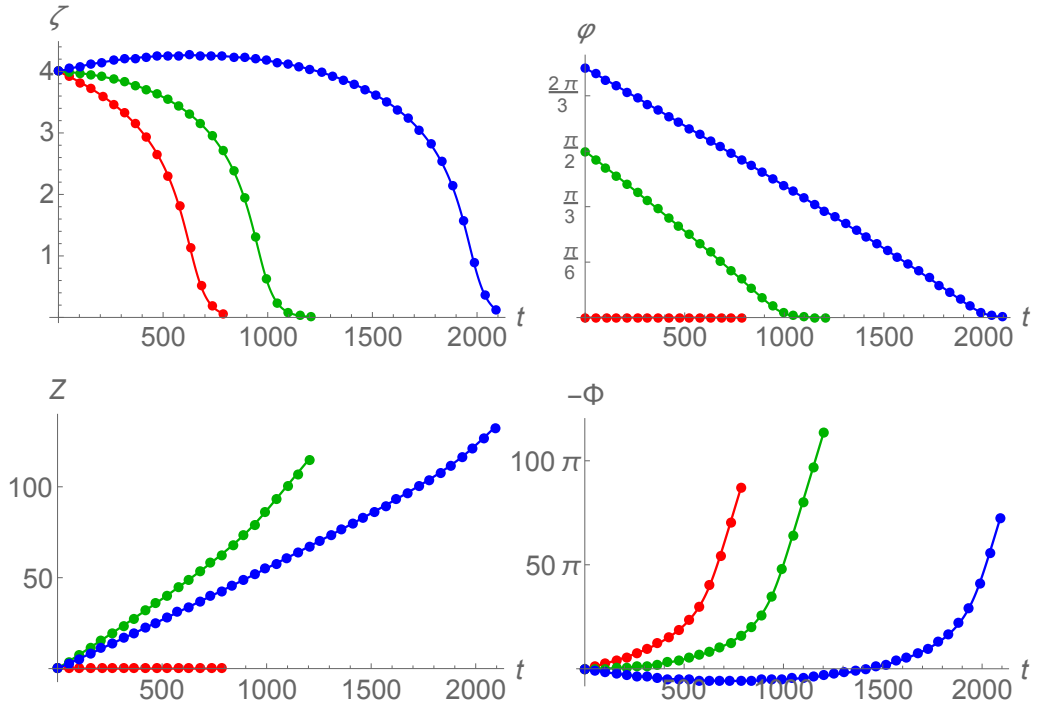

Figure 3.5: Collective coordinates $\zeta(t)$, $\varphi(t)$, $Z(t)$, and $\Phi(t)$ for initial separation $\zeta_0 = 4$ and initial twists $\varphi_0 = 0$ (red), $\pi/2$ (green), and $3\pi/4$ (blue). All quantities are in natural units. Dots are results of micromagnetic simulations, lines are predictions of the effective theory. The Gilbert damping coefficient is $\alpha = 0.01$.

3.4.3.2 General Case

In the general case, with both an initial twist $\varphi_0 \neq 0$ and separation $\zeta_0 \neq 0$, the equations of motion to the leading order in α have the following form:

$$\dot{\Phi} = F_\zeta/2, \qquad \dot{\zeta} = (\Gamma_{\Phi\Phi} F_\zeta - \Gamma_{\Phi Z} F_\varphi)/4, \tag{3.41a}$$

$$\dot{Z} = -F_\varphi/2, \qquad \dot{\varphi} = (-\Gamma_{Z\Phi} F_\zeta + \Gamma_{ZZ} F_\varphi)/4. \tag{3.41b}$$

Forces F_i are given in Eq. 3.38; components of the viscosity tensor Γ_{ij} can be found in Appendix C.

During the initial approach ($\zeta \gg 1$), the domain walls interact weakly, $F_\zeta \approx -8e^{-\zeta}\cos\varphi$, $F_\varphi \approx -8e^{-\zeta}\sin\varphi$, and retain their individual character, so that the dissipation tensor is diagonal, with $\Gamma_{\Phi\Phi} \approx \Gamma_{ZZ} \approx 4\alpha$. The twist angle decreases slowly and linearly in time:

$$\varphi(t) \approx \varphi_0 - 8\alpha t\, e^{-\zeta_0} \sin\varphi_0. \tag{3.42}$$

The separation evolves as

$$\zeta(t) \approx \zeta_0 + \ln\frac{\sin\varphi(t)}{\sin\varphi_0}. \tag{3.43}$$

Notably, for a large initial twist $\varphi_0 > \pi/2$, the force F_ζ is repulsive and the domain walls initially move apart until φ decreases to $\pi/2$. At that point, the force F_ζ vanishes

and the walls reach their maximum separation $\zeta_{\max} \approx \zeta_0 - \ln \sin \varphi_0$. This happens at

$$t_{\max} \approx \frac{(\varphi_0 - \pi/2)e^{\zeta_0}}{8\alpha \sin \phi_0}. \tag{3.44}$$

The total duration of the initial approach is

$$t_i \approx \frac{\varphi_0 e^{\zeta_0}}{8\alpha \sin \varphi_0}. \tag{3.45}$$

Both the linear trend in $\varphi(t)$ and the backward initial relative motion for $\varphi_0 > \pi/2$ are clearly visible in the micromagnetic simulation data in Figure 3.5.

During the final stage, the separation and twist decrease to zero. Expanding physical quantities in powers of ζ and φ yields $U \approx 2(\zeta^2 + \varphi^2)/\zeta$, $\Gamma_{\Phi\Phi} \approx 4\alpha\zeta$, $\Gamma_{Z\Phi} = \Gamma_{\Phi Z} \approx -4\alpha\varphi$, and $\Gamma_{ZZ} \approx 4\alpha\varphi^2/\zeta$. Equations (3.41) read

$$\dot{\Phi} \approx -1 + \varphi^2/\zeta^2, \qquad \dot{\zeta} \approx -2\alpha\zeta(1 + \varphi^2/\zeta^2), \tag{3.46}$$

$$\dot{Z} \approx 2\varphi/\zeta, \qquad \dot{\varphi} \approx -2\alpha\varphi(1 + \varphi^2/\zeta^2). \tag{3.47}$$

During this stage, the ratio φ/ζ remains constant. Both average velocities attain their terminal values $\dot{Z}_\infty = V_\infty$ and $\dot{\Phi}_\infty = -1 + V_\infty^2/4$, where $V_\infty = 2\varphi/\zeta$. It is interesting to note that, as the domain walls annihilate and the energy decreases toward zero, the pair does not slow down and keeps moving and rotating at constant rates. The

relative coordinates $\zeta(t)$ and $\varphi(t)$ decay exponentially with the characteristic time

$$t_f \approx \frac{1}{2\alpha(1+V_\infty^2/4)}. \tag{3.48}$$

Again, all these trends are clear in Figure 3.5. The micromagnetic data and the effective theory (Equations 3.41) show excellent agreement.

3.5 Numerical Simulation

So far we have been working with a continuum model of the ferromagnetic wire and have developed an effective theory of the annihilation of a domain wall pair within the framework of this model. This theoretical approach, also known as micromagnetics, is complemented by micromagnetic simulations of the corresponding lattice model. If the lattice period is small compared to the characteristic sizes in the problem (e.g. the exchange length and the relative separation between the domain wall pair in our problem), the simulation should reproduce the predictions of the continuum theory. The advantage of doing a computer simulation lies in the fact that one can solve the full microscopic equations of motion, retaining all the degrees of freedom of the system, instead of working only with a few effective variables as in the continuum theory.

Micromagnetic simulations of the annihilation process with initial conditions $\zeta_0 = 4$ (in natural units) and $\varphi_0 = 0, \pi/2 \,\text{and}\, 3\pi/4$ were performed using the Object Ori-

ented MicroMagnetic Framework [46]. The parameters used (written as 3-dimensional quantities) are: exchange constant $A = 2 \times 10^{-10}$ J/m, anisotropy constant $K = 2 \times 10^4$ J/m^3 and magnetization $M_s = 10^6$ A/m. A linear chain with lattice constant $a = 10$ nm and length $L = N_s a$ was used, N_s being the number of spins in the chain. N_s was taken to be 1000 for $\varphi_0 = 0$ and 2000 for $\varphi_0 = \pi/2$ and $3\pi/4$. The angular momentum density of this system is $\mathcal{J} = M_s/\gamma = 5.68 \times 10^{-6}$ Js/m^3. This gives a characteristic time scale $t_0 = \mathcal{J}/K = 0.284\,\text{ns}$ and a characteristic length scale (exchange length) $l_0 = \sqrt{A/K} = 100\,\text{nm}$, the latter greatly exceeding the lattice period.

Finite-size effects become important toward the end of the simulation for two reasons. Firstly, the width of the soliton diverges as the two domain walls merge, as discussed in Appendix C. Once it becomes comparable to the system size, the transverse component of magnetization $m_\perp$ is no longer zero at the edges of the wire. Secondly, for nonzero φ_0 the soliton has an overall translational motion (in the $+z$ direction for our φ_0 values), which causes it to run into one of the edges. To tackle the second issue, we started the simulation with $Z_0 = -L/4$ for $\varphi_0 = \pi/2$ and $3\pi/4$. (With respect to the origin at the center of the wire of length L.) For $\varphi_0 = 0$, $Z_0 = 0$ was used. Moreover, to minimize the finite-size effects, we truncated the simulation data when the value of $m_\perp$ at the edge became greater than 0.01.

We used $\Delta t = 0.082\,\text{ns} = 0.289 t_0$ for each iteration step. The four collective coordinates were extracted from the magnetization profile at each iteration. Since we

chose the boundary condition $m_z(z \to \pm\infty) = 1$,

$$Z = \frac{ia}{l_0} \text{ where } m_{zi} = \min_{j\in\{1,\ldots,N_s\}} m_{zj}. \tag{3.49}$$

Φ is the azimuthal angle of the spin at this location.

$$\cos\Phi = \frac{m_{xi}}{\sqrt{m_{xi}^2 + m_{yi}^2}} \tag{3.50}$$

The two relative coordinates were obtained by evaluating the discretized versions of their defining expressions (3.19) and (3.20).

$$\zeta = -\frac{a}{2l_0}\sum_{j=1}^{N_s}(m_{zj} - 1) \tag{3.51}$$

$$\varphi = -\frac{1}{2}\sum_{j=1}^{N_s-1}(m_{zj} - 1)(\phi_{j+1} - \phi_j) \tag{3.52}$$

Figure 3.5 clearly shows an excellent agreement between the results of numerical simulation with the predictions of the effective theory for all three initial conditions. Although the agreement looks almost exact, it is important to mention that our theory involving four collective coordinates is an approximate description of the annihilation process. It seems the almost exact nature of the agreement stems from our specific choice of collective coordinates. In the numerical simulations, we also looked at the evolution of the soliton along other directions in the parameter space, beyond the four collective coordinates. Such an inspection revealed deviations of the trajectory of the

soliton from the expected path as the two domain walls came closer. For example, we visually compared the full profile of $\mathbf{m}(z)$ from the effective theory and the numerical simulation at various instants of time. In early stages of the annihilation process they were virtually identical. But the difference between these profiles increased as the two domain walls approached each other. In other words, we saw that the full trajectory of the soliton in the multi-dimensional space of all parameters does deviate from the predictions of the effective theory toward the end of the annihilation process, while its projection in the four-dimensional space $\{Z, \Phi, \zeta, \varphi\}$ stays quite faithful to the theoretical prediction at all times.

3.6 Discussion

In this chapter we have considered the annihilation of two domain walls in a ferromagnetic wire. A minimal description of the process requires the use of 4 physical variables. The average coordinates of the combined soliton, position Z and azimuthal orientation Φ, are zero modes on account of global translational and rotational symmetries; the relative coordinates, separation ζ and twist φ, harden as the domain walls merge. We obtained the equations of motion for these variables using the method of collective coordinates [26] and showed that the relative separation ζ and twist φ of two domain walls exhibit purely viscous dynamics, whereas the average position Z and azimuthal angle Φ are driven by the torque $F_\varphi(\zeta, \varphi)$ and force $F_\zeta(\zeta, \varphi)$, even in

the absence of dissipation. These equations of motion (3.41) predict the dynamics of the 4 variables in excellent agreement with the results of numerical micromagnetic simulations (Figure 3.5).

Our approach can be applied beyond the specific idealized model considered in this chapter. For instance, we relied explicitly on symmetries of translation and rotation and used the corresponding conserved momenta. However, these conservation laws already break in the presence of dissipation in the form of local Gilbert damping and the momenta change in time. In a similar way, weak violations of translational and rotational symmetries will produce additional terms in the equations of motion in the form of global forces F_Z and F_Φ directly impacting the dynamics of the slow variables φ and ζ conjugate to Z and Φ. As long as these forces are small, the separation of time scales between the slow and fast variables remains and the general approach remains applicable.

We hope that the method can be successfully extended to the dynamics of other magnetic solitons.

Chapter 4

Vortex-Antivortex Annihilation in a Ferromagnetic Thin Film

Having explored the annihilation of topological solitons in a one-dimensional system, we will now move to one higher dimension and study a similar annihilation process in a two-dimensional thin film. Vortices and antivortices (see Figure 4.1 and 4.2) are common topological solitons found in a variety of two-dimensional systems, including ferromagnets. A vortex and an antivortex typically have an attractive interaction between them [4]. So, in the presence of viscous losses, a vortex-antivortex pair is expected to lose energy, approach each other and eventually annihilate to form a uniform ground state. This chapter presents an analytic framework for understanding this annihilation process in terms of collective coordinates.

In Section 4.1 we will introduce the system and discuss the properties of a single

isolated vortex. In Section 4.2 the new problem we want to address will be described: vortex-antivortex annihilation. In this section we'll discuss the dynamics in the limit where the vortex and the antivortex are far from each other and also explain why they approach each other and ultimately annihilate. We will then proceed to develop a theoretical framework for the opposite limit: just before annihilation when the relative separation of the pair is small. We will conclude with a discussion of our present results and and of the future plans for this work. These results form part of an ongoing project, being done by collaboration with undergraduate student Derek Reitz and my advisor Oleg Tchernyshyov.

4.1 Introduction: Single Vortex

The magnetization of a ferromagnetic thin film can be characterized by a unit-vector field $\mathbf{m}(x, y)$ in two dimension. The total energy of this system includes two components: an isotropic exchange interaction that tries to align neighboring spins and an easy-plane anisotropy, caused by the dipolar interaction, that penalizes any out-of-plane magnetization m_z:

$$U[\mathbf{m}] = U_{\text{ex}}[\mathbf{m}] + U_{\text{anis}}[\mathbf{m}] = \int dx\, dy \;\; \left[\frac{A}{2}(\nabla \mathbf{m})^2 + \frac{K}{2} m_z^2\right]. \tag{4.1}$$

Here $A > 0$ is the exchange constant and $K > 0$ is the anisotropy. It is important to note that the local U_{anis} is a crude approximation for the essentially nonlocal dipolar

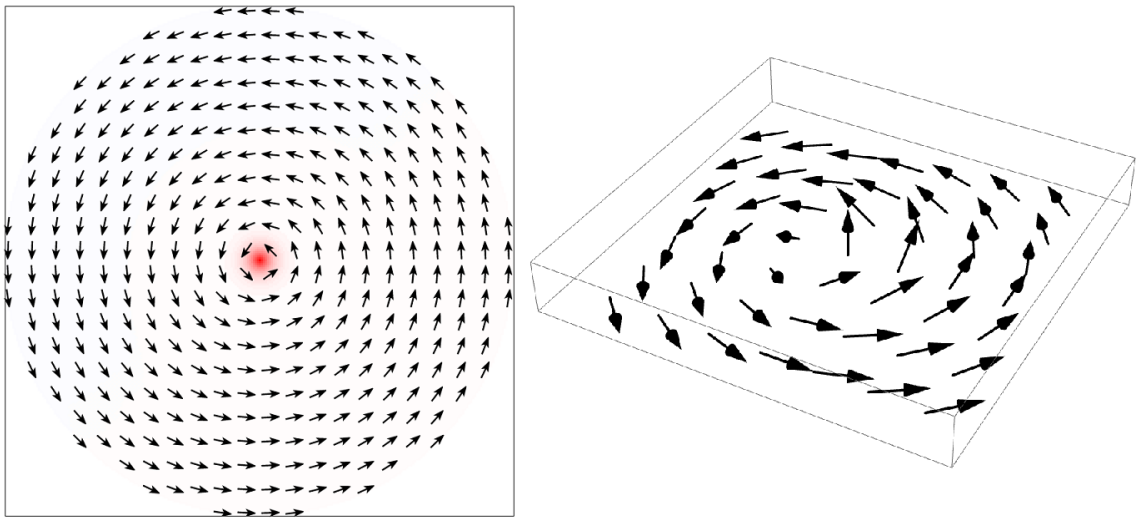

Figure 4.1: Left: A vortex in a ferromagnetic thin film with winding number $k = 1$ and core polarity $p = 1$. The arrows show the component of magnetization $\mathbf{m}_{||}$ parallel to the plane. The red color denotes a magnetization component $|m_z| > 1/e$ out of the plane of the film. Right: Structure of the vortex core. One can see that $\mathbf{m}$ points out of the plane at the center of the core.

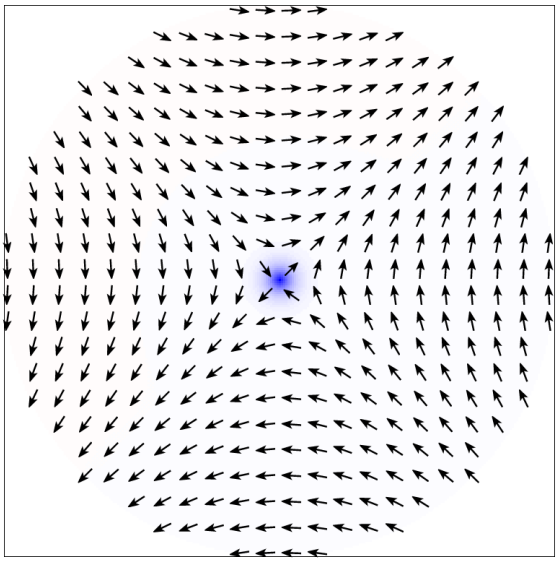

Figure 4.2: An antivortex in a ferromagnetic thin film with winding number $k = -1$ and core polarity $p = -1$. The arrows show the component of magnetization $\mathbf{m}_{||}$ parallel to the plane. The blue color denotes a magnetization component $|m_z| > 1/e$ going into the plane of the film.

anisotropy. In addition, there might be a separate physical mechanism in the system generating a local anisotropy term in the total potential energy.

The unit of length here is the exchange length $\ell_0 = \sqrt{A/K}$ and the unit of time is $t_0 = \mathcal{J}/K$ where $\mathcal{J}$ is the density of angular momentum of the film. Like in the one-dimensional case, we will work in these natural units and set $\mathcal{J} = A = K = \ell_0 = t_0 = 1$ in the rest of this chapter. Also, we'll often use the polar and azimuthal angles $\theta(x, y)$ and $\phi(x, y)$ to characterize the magnetization field,

$$\mathbf{m} = (\sin\theta\cos\phi, \sin\theta\sin\phi, \cos\theta). \tag{4.2}$$

It readily follows from (4.1) that this system has a continuous family of degenerate ground states. In any of these ground states, all spins point in some specific direction in the x-y plane, i.e. $\mathbf{m}(x, y) = \cos\beta\,\hat{\mathbf{x}} + \sin\beta\,\hat{\mathbf{y}}$ for a fixed angle $0 \leq \beta < 2\pi$. As discussed in Chapter 1, we can define the winding number $k \in \mathbb{Z}$ of a configuration as the net azimuthal angle ϕ described by the vector $\mathbf{m}$ as one traces a closed loop (in counterclockwise fashion). Mathematically, $k = \frac{1}{2\pi}\oint d\phi$. Configurations with different winding numbers cannot be continuously deformed into each other [4], making k a topological invariant.

All the ground states of this system obviously have $k = 0$. We will now find a class of configurations that are local minima of U and have a pre-assigned nonzero winding number k [5, 6]. These are known as vortices. Since these configurations

are expected to be rotationally symmetric, it is convenient to use polar coordinates $x = \rho\cos\varphi$ and $y = \rho\sin\varphi$. The conditions for minima are

$$\begin{aligned} 0 &= \frac{\delta U}{\delta \phi} = -\nabla\cdot\left(\sin^2\theta\,\nabla\phi\right), \\ 0 &= \frac{\delta U}{\delta \theta} = \frac{1}{2}\sin 2\theta\left[(\nabla\phi)^2 - 1\right] - \nabla^2\theta. \end{aligned} \tag{4.3}$$

Since $U[\theta,\phi]$ is translationally invariant in the x-y plane we can assume, without any loss of generality, that the vortex is centered at the origin. So, we make the ansatz

$$\theta = \theta_0(\rho) \quad \text{and} \quad \phi = k\varphi + \Phi = k\arctan\frac{y}{x} + \Phi, \tag{4.4}$$

where Φ is a global azimuthal angle. These satisfy both the winding number constraint and the first equation in (4.3) and generate an ordinary differential equation for $\theta_0(\rho)$,

$$\frac{d^2\theta_0}{d\rho^2} + \frac{1}{\rho}\frac{d\theta_0}{d\rho} - \frac{k^2}{2}\frac{\sin 2\theta_0}{\rho^2} + \frac{1}{2}\sin 2\theta_0 = 0. \tag{4.5}$$

A nonzero winding number implies that the azimuthal angle ϕ is not well-defined at the origin. This means the magnetization vector has to be perpendicular to the x-y plane at that location, i.e. $\mathbf{m}(0,0) = p\hat{\mathbf{z}}$, where $p = \pm 1$ is the polarity of the vortex core. This implies $\theta_0(\rho = 0) = (1-p)\pi/2$. The easy-plane anisotropy U_{anis} forces $\mathbf{m}$ to lie in the x-y plane far away from the origin: $\theta_0(\infty) = \pi/2$. This latter condition can be used to find the asymptotic behavior of the polar angle from (4.5):

$\theta_0(\rho \gg 1) - \pi/2 \sim e^{-\rho}$. We will not attempt to explicitly solve (4.5) here. For our purposes it will be sufficient to observe that the vortex is mostly a planar configuration with a three-dimensional core of radius $r_c \sim 1$ at the center, as shown in Figure 4.1.

A vortex has two zero modes corresponding to the invariance of the potential energy (4.1) under translations $\mathbf{m}(x) \mapsto \mathbf{m}(x - X)$ and $\mathbf{m}(y) \mapsto \mathbf{m}(y - Y)$. This implies that under a weak external perturbation, the motion of the vortex can be described by two time-dependent collective coordinates $X(t)$ and $Y(t)$, for reasons discussed in Section 3.1. This dynamics is completely governed by the gyrotropic coefficient G_{XY}, the dissipation coefficients Γ_{XX}, Γ_{YY} and Γ_{XY} and the external forces F_X and F_Y. The gyrotropic coefficient, obtained using (3.16c), is given by

$$\begin{aligned} G_{XY} &= -\int dx\, dy\, \mathbf{m} \cdot \left(\frac{\partial \mathbf{m}}{\partial X} \times \frac{\partial \mathbf{m}}{\partial Y} \right) \\ &= -\int dx\, dy\, \mathbf{m} \cdot \left(\frac{\partial \mathbf{m}}{\partial x} \times \frac{\partial \mathbf{m}}{\partial y} \right). \end{aligned} \tag{4.6}$$

In the second step we have used $\partial/\partial X = -\partial/\partial x$ and $\partial/\partial Y = -\partial/\partial y$ since X and Y correspond to rigid translations of the vortex $\mathbf{m}(x, y) \mapsto \mathbf{m}(x - X, y - Y)$. This expression for G_{XY} is simply equal to $-4\pi S$ where S is the skyrmion number of the vortex, as discussed in Chapter 1. Since a vortex with winding number $k = 1$ and core polarity $p = 1$ wraps once around the north hemisphere of the magnetization sphere, it has a skyrmion number $1/2$. This result can be readily generalized to a vortex with winding number $k \in \mathbb{Z}$ and polarity $p = \pm 1$. Such a configuration will have a skyrmion number $S = kp/2$ and hence a gyrotropic coefficient $G = -G_{XY} = G_{YX} = 2\pi kp$.

The dissipative part of the dynamics (controlled by the Gilbert damping constant α) can be handled by introducing the dissipation tensor Γ_{ij}, as defined in Equation (3.16d). To calculate the dissipation tensor, we first look at its diagonal components. They are equal due to the rotational symmetry of the vortex: $\Gamma_{XX} = \Gamma_{YY} = \Gamma$. Using the relations $\partial/\partial X = -\partial/\partial x$ and $\partial/\partial Y = -\partial/\partial y$ in the definition of the dissipation tensor (3.16d),

$$\begin{aligned} \Gamma &= \alpha \int dx\, dy \, \left[\left(\frac{\partial \theta}{\partial X} \right)^2 + \sin^2 \theta \left(\frac{\partial \phi}{\partial X} \right)^2 \right] \\ &= \frac{\alpha}{2} \int dx\, dy \, \left[(\nabla \theta_0)^2 + \sin^2 \theta_0 \, (\nabla \phi)^2 \right] \end{aligned} \tag{4.7}$$

Here we'll assume that the vortex is located at the center of a circular film of radius $R \gg 1$. The first term is nonzero only in the core region with radius $r_c \approx 1$. It is small compared to the second term which is nonzero everywhere in the bulk and in fact diverges with the system size, as we'll see below. So it is permissible to ignore the contribution of the core altogether and assume $\theta_0(1 < \rho < R) \approx \pi/2$. This, together with the form of the vortex profile given by (4.4), implies

$$\Gamma \approx \frac{\alpha}{2} \int\limits_{r_c \approx 1}^{R} \rho \, d\rho \, d\varphi \, \frac{k^2}{\rho^2} \approx \alpha \pi k^2 \ln R \tag{4.8}$$

It is easy to see from the form of the vortex profile (4.4) that symmetries of the integrand make the off-diagonal component vanish: $\Gamma_{XY} = 0$.

Thus in the presence of external forces F_X and F_Y, the equations of motion of a

single vortex look like [40],

$$\begin{aligned} -G\dot{Y} - \Gamma\dot{X} + F_X = 0, \\ G\dot{X} - \Gamma\dot{Y} + F_Y = 0. \end{aligned} \tag{4.9}$$

These equations can be written in a more compact form by defining a gyrotropic vector $\mathbf{G} = G\hat{\mathbf{z}}$. The equation of motion for the center of the vortex $\mathbf{R} = X\hat{\mathbf{x}} + Y\hat{\mathbf{y}}$ then becomes the celebrated Thiele equation [40],

$$\mathbf{G} \times \dot{\mathbf{R}} - \Gamma\dot{\mathbf{R}} + \mathbf{F} = 0. \tag{4.10}$$

The motion described by this equation is identical to that of a massless particle with unit positive charge under the influence of an external magnetic field equal to $-\mathbf{G}$, a viscous force of strength D and a conservative force $\mathbf{F}$. In particular, a vortex confined in a parabolic potential well $U(X, Y) = K(X^2 + Y^2)/2$ moves in a circle with frequency $\omega = K/G$ if there is no dissipation. In the presence of dissipation, it spirals down to the bottom of the well $\mathbf{R} = 0$ with a time constant $\tau = \Gamma/K$.

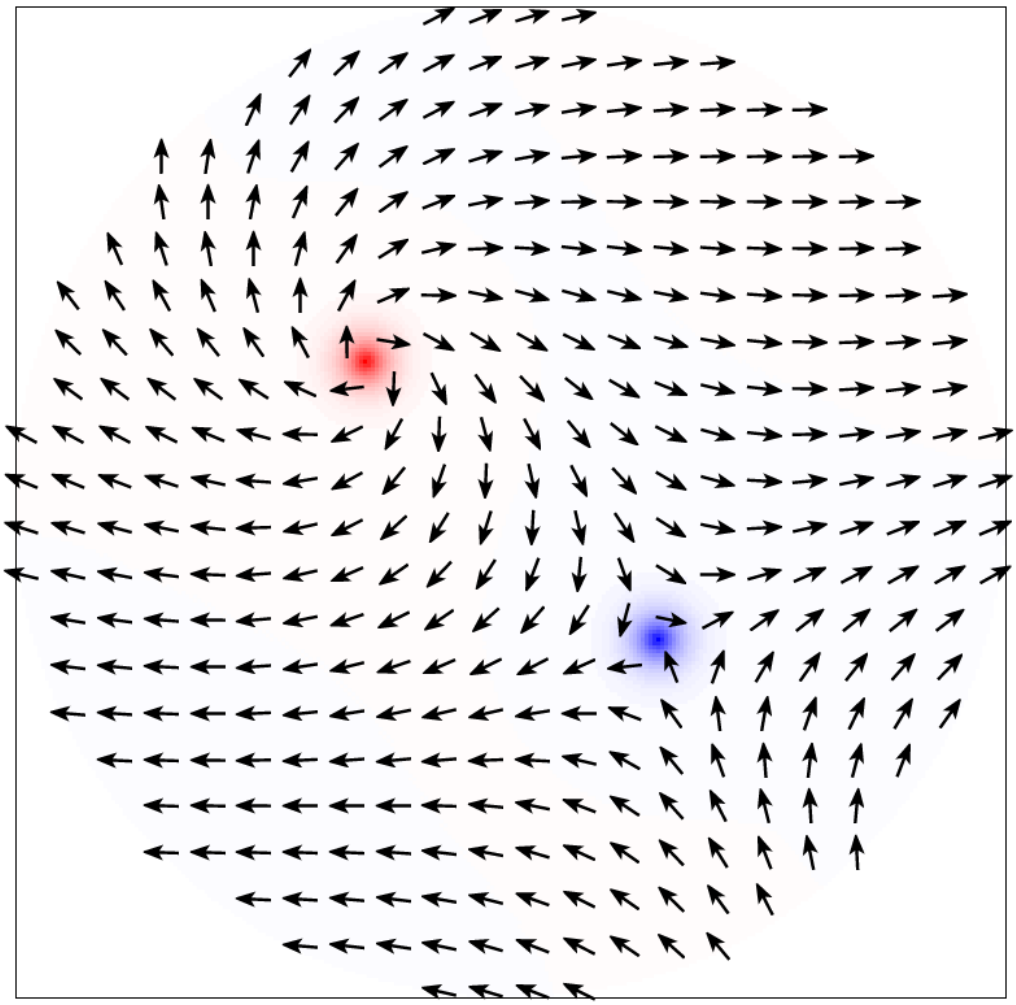

Figure 4.3: A vortex-antivortex pair in a circular thin film in the limit of large separation. Here the separation between the core centres is $r = 25$ in rational units.

4.2 Vortex-Antivortex Pair: Large Separation Limit

The problem we will address here is similar to the one studied in Chapter 3. We start with a state that has a vortex [with winding number $k_1 = 1$ and polarity $p_1 = 1$, centered at $\mathbf{a} = (a_1, a_2)$] and an antivortex [with winding number $k_2 = -1$ and polarity $p_2 = -1$, centered at $\mathbf{b} = (b_1, b_2)$] located far from each other compared to the core size, as shown in Figure 4.3. If we denote the separation between the centers of the vortex and the antivortex by $r = |\mathbf{a} - \mathbf{b}|$, this implies $r \gg r_c \approx 1$. We then ask the question: what happens once we let this system evolve in time?

As we'll see in the following paragraphs, the choice of core polarities $p_{1,2}$ influences the dynamics of the pair in a fundamental way. In the absence of dissipation, a pair with $p_1 = p_2$ moves in parallel paths in the same direction. On the other hand, a pair with $p_1 = -p_2$ moves in a circular path about their geometrical center. The total skyrmion number of a vortex-antivortex pair also depends on the choice of core polarities. A pair with same core polarities has $S = 0$ and is thus topologically identical to the ground state. A pair with opposite core polarities, on the other hand, has $S = 1$. The nonzero skyrmion number for the $p_1 = -p_2$ case has interesting physical consequences that are absent in the $p_1 = p_2$ situation.

A couple of other issues are worth mentioning before we get into the technical details of the theory. The spin waves in an easy-axis magnet are gapped, the gap

being $\omega_0 = K/\mathcal{J}$ where K is the anisotropy and $\mathcal{J}$ is the angular momentum density. Our discussion of the dynamics of a domain wall pair in Chapter 3 could safely ignore spin waves since the frequency of rotation $\Omega = \dot{\Phi}$ of the soliton never exceeded ω_0. But the spin wave spectrum in an easy-plane ferromagnet is gapless. Thus here there is a possibility that moving vortices might generate spin waves, and it is known from past numerical simulations that this indeed happens when the separation between the vortex cores is comparable to the lattice scale [47]. In our theory, we will not address this very small separation limit and will make the assumption that spin waves do not play a significant role at larger separations.

In the case of domain walls, we had a single class of analytic expressions spanning all possible values of the collective coordinates, that we took as a starting point for our analysis of the annihilation process. Here we do not have a class of expressions for vortex-antivortex pair configurations that span the entire range of core separations $0 < r < \infty$. But we do have such analytic expressions in two limiting situations. The large separation limit ($r \gg l_0 = 1$) can be handled by treating the vortex and antivortex cores as rigid objects and promoting the parameters $\{a_1, a_2, b_1, b_2\}$ to time-dependent quantities. In this section, we will analyze the motion in this limit. In the next section, we will develop a theoretical framework for the opposite limit when the separation between the pair is much smaller than the exchange length of the system: $r \ll l_0 = 1$.

The expressions for $\theta(x, y)$ and $\phi(x, y)$ in the large separation limit are easy to

obtain. Since the cores are well-localized around the points **a** and **b**, we can obtain $\theta(x, y)$ by simply adding the contributions of an isolated vortex and an isolated antivortex, that separately satisfy Equation (4.5):

$$\theta(x, y) = \theta_0 \left(\sqrt{(x - a_1)^2 + (y - a_2)^2} \right) + \theta_0 \left(\sqrt{(x - b_1)^2 + (y - b_2)^2} \right). \tag{4.11}$$

Moreover, since the second equation in (4.3) reduces to the Laplace equation $\nabla^2 \phi = 0$ outside the well-locaized vortex cores, we can simply add the two separate contributions to the azimuthal angle as well:

$$\phi(x, y) = \arctan \frac{y - a_2}{x - a_1} + \arctan \frac{y - b_2}{x - b_1}. \tag{4.12}$$

Since the core sizes are small in comparison to the distance between the vortex and antivortex, the dominant contribution to the energy of the pair in this limit comes from the bulk, where the spins lie in the x-y plane. As a result, the potential energy U (4.1) can be well-approximated by the energy of a vortex-antivortex pair in a two-dimensional XY ferromagnet [4]: $U(r) = 2\pi \ln r$. Thus the vortex and the antivortex act like two particles with charges ± 1 attracting each other via the Coulomb interaction in two-dimension, the attractive force being $\mathbf{F}(r) = -\partial U/\partial r = -2\pi \hat{\mathbf{r}}/r$ [6].

As seen in Section 4.1, only the core of an isolated vortex contributes to its gyrotropic coefficient. So, the G-tensor derived previously for a single vortex with

winding number k and polarity p applies separately to the vortex and the antivortex in this limit: $G_1 = G_2 = 2\pi$. Hence in the absence of dissipation ($\alpha = 0$), the dynamics of the system is governed by a pair of Thiele equations (4.10): $\mathbf{G}_i \times \dot{\mathbf{R}}_i + \mathbf{F}_i = 0$ for $i = 1, 2$. Here we have used the notation $\mathbf{R}_1 = \mathbf{a}$ and $\mathbf{R}_2 = \mathbf{b}$ to write the pair of equations in a compact form. It is easy to see that the two vortices move in opposite directions with equal speeds $v(r) = 2\pi/rG = 1/r$ and hence describe a common circular path about their center-of-mass. It is also easily seen that a pair with $p_1 = p_2$ will have $G_1 = -G_2 = 2\pi$ and will thus move in the same direction, as mentioned before.

It is worth mentioning here that a ferromagnetic (anti)vortex lacks inertia (see Section 3.1.3) and its dynamics, in the absence of dissipation, is governed solely by a gyrotropic term. As a result, equations of motion of the vortex-antivortex pair contain only a single time derivative and a specification of the initial positions is sufficient to completely determine the trajectories. One can only have circular trajectories in this case, as demonstrated in the previous paragraph. In contrast, for the more familiar inertial particles, one can independently specify both positions and velocities. In that situation, a Coulomb attraction can result in various kinds of trajectories (linear, circular, parabolic, hyperbolic) depending on the initial velocities of the pair.

It is clear at this point that a minimal description of the motion of the pair requires four collective coordinates: the locations of the centers of the vortex $(a_1(t), a_2(t))$ and the antivortex $(b_1(t), b_2(t))$. But since the geometrical center of the combined system

stays stationary during this process, one can set $\mathbf{R}_{\rm com} = (\mathbf{a} + \mathbf{b})/2 = 0$ and work only with the two relative coordinates: the magnitude r and the orientation ϑ of the relative separation vector $\mathbf{r} = \mathbf{a} - \mathbf{b}$. From the above analysis,

$$\dot{r} = 0 \quad \text{and} \quad \dot{\vartheta} = -v/(r/2) = -2/r^2 \tag{4.13}$$

in our rational units. Thus the pair maintains their relative separation and rotates at a fixed angular velocity that increases as the separation is decreased.

If we now add dissipation to this moving system, it will start to lose energy and the relative separation r will start decreasing. As a result, the pair will move toward their geometrical center in two symmetric spiral trajectories. Like in the domain wall case, here we have a separation of the motion into slow and fast modes. The angular velocity of the pair $\dot{\vartheta}$ is an $O(\alpha^0)$ quantity and hence is a fast mode. The linear velocity $\dot{r}$, on the other hand is purely dissipational. Hence it is a slow mode that is an $O(\alpha^1)$ quantity. This separation of slow and fast modes will help us solve the equations of motion, as we'll see in the next section when we treat the small separation limit.

The rigid core picture starts to break down once the separation becomes comparable to the core size ($r \approx r_c \approx 1$) and the cores begin to overlap, as shown in Figure 4.5. But the general idea of the two vortex centers approaching each other in spiral paths can be expected to be qualitatively correct even when the core separa-

tion is small. We will develop a theoretical framework for the dynamics in the small separation limit in Section 4.3.

As we discussed in Chapter 1, we can use two topological charges to characterize $\mathbf{m}(x, y)$: the vortex winding number k and the skyrmion number S. The total winding number of the vortex-antivortex pair is $k = k_1 + k_2 = 0$, same as a uniform state. So for a given core separation r, the magnetization in the region far from the geometrical center $\mathbf{m}(\rho \gg r)$ can be continuously deformed to a uniform state. Thus, as the system loses energy and r decreases, the magnetization everywhere except near $\rho = 0$ is expected to approach one of the ground states. This is also observed in Figure 4.5. But at the same time, the total skyrmion number of the pair is $S = S_1 + S_2 = k_1 p_1 + k_2 p_2 = 1$, implying that this configuration belongs to a different topological sector than the uniform states (that have zero skyrmion number). Thus in the later stages of the evolution of the pair there is a skyrmion localized in the region $0 \leq \rho < l_0$, where $l_0 = 1$ is the exchange length of the system, beyond which $\mathbf{m}$ approaches one of the uniform states.

In the continuum model, a configuration with skyrmion number $S = 1$ cannot continuously evolve to the uniform state. In this model, the size of the aforementioned skyrmion will continue to shrink, but it will always be present in the system and the configuration will remain topologically distinct from the uniform ground state. This topological argument works only if the magnetization field $\mathbf{m}$ is defined in the $\mathbb{R}^2$ continuum. But our continuum model is only an approximation to an underlying

lattice system and is reliable only till the core separation r is much greater than the lattice constant a. Once these two become comparable, the skyrmion spans only a few lattice unit cells, and ultimately just one unit cell. At this point, unwinding the skyrmion only involves flipping a few spins, which can easily happen. Such unwinding cannot happen in continuum models. Thus the system truly evolves into a uniform state in the lattice system. The unwinding of the skyrmion will release energy (equal to the energy of a single skyrmion), which is expected to radiate out in the form of spin waves. This radiation of spin waves has indeed been observed in numerical micromagnetic simulations [47].

One also expects generation of spin waves before the separation of the pair reaches the lattice scale. Using the analogy with electrodynamics discussed before, the rotating vortex-antivortex pair can be thought as a rotating electric dipole. Thus, it can be expected to generate spin waves just like a rotating dipole radiates out electromagnetic waves. This radiation of spin waves would be a second mechanism of energy loss in the system, in addition to the viscous loss. The spin wave radiation can be theoretically handled in this situation using the analogy with electrodynamics. However, in the numerical simulations [47], significant spin wave radiation is observed only when the separation of the pair reaches the lattice scale. Based on this numerical observation, we will make the simplifying assumption of ignoring spin waves in our subsequent theoretical treatment.

To handle the dissipative case in the large separation limit, one needs to calculate

the three dissipation coefficients Γ_{rr}, $\Gamma_{r\vartheta}$ and $\Gamma_{\vartheta\vartheta}$ by substituting the profile of the the pair in (3.16d) and evaluating the integrals. These can then be used to write the equations of motion for the two collective coordinates. We will not discuss this final piece of the theory for the large separation limit here, since it is a part of the currently ongoing work on this project. Instead, in the rest of the chapter, we will develop a theoretical framework for the opposite limit when the separation between the pair is much smaller than the exchange length of the system: $r \ll l_0 = 1$.

4.3 Vortex-Antivortex Pair: Small Separation Limit

4.3.1 Complex Representation of Magnetization

So far we have been representing the unit vector of magnetization $\mathbf{m} = (m_x, m_y, m_z)$ by the polar and the azimuthal angles θ and ϕ. There exists an alternative representation in terms of complex numbers that will be quite useful for the present discussion. In this representation one performs a stereographic projection of the unit magnetization sphere onto the complex plane, as shown in Figure 4.4. Under this mapping, the vector $\mathbf{m} = (m_x, m_y, m_z)$ becomes the complex number [48]

$$\psi = \frac{m_x + i m_y}{1 + m_z} = \tan\frac{\theta}{2}\, e^{i\phi} \tag{4.14}$$

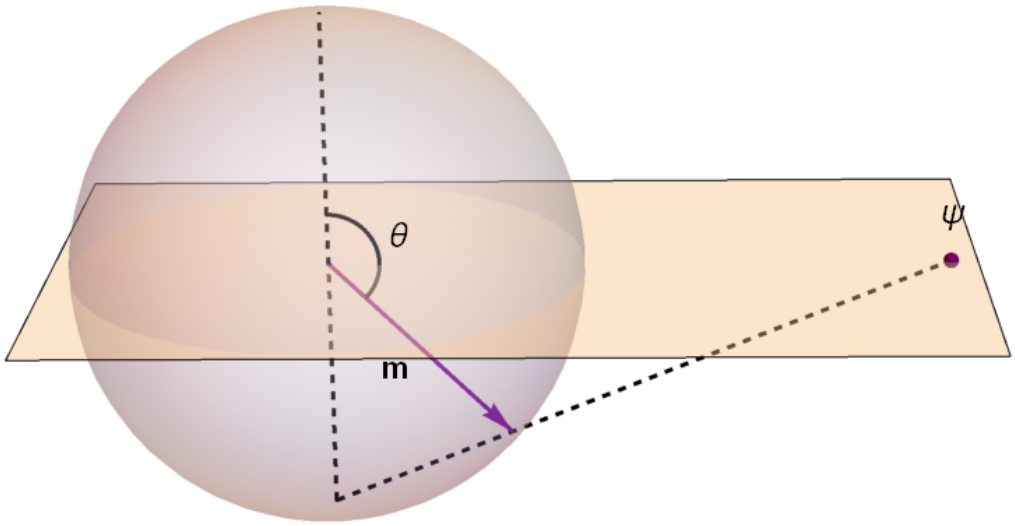

Figure 4.4: Stereographic projection from the unit magnetization sphere to the complex plane. The unit vector $\mathbf{m}$ maps to the complex number ψ.

It is clear from Figure 4.4 that this mapping is one-to-one: the north pole $\mathbf{m}_N = (0, 0, 1)$ maps to the origin of the complex plane $\psi = 0$, the south pole $\mathbf{m}_S = (0, 0, -1)$ to the point at infinity $\psi = \infty$ and the equator $\mathbf{m}_E = (\cos\phi, \sin\phi, 0)$ to the unit circle $\psi = e^{i\phi}$.

Using (4.14), one can easily rewrite the expressions for gyrotropic tensor G_{ij} and the dissipation tensor Γ_{ij} as given in Equation (3.16) in the complex representation. The details of this derivation are given in Appendix D. The results are:

$$\begin{aligned} G_{ij} &= -\int d\bar{z}dz\, \frac{\partial_i\psi\partial_j\bar{\psi} - \partial_i\bar{\psi}\partial_j\psi}{(1+\bar{\psi}\psi)^2} \\ \Gamma_{ij} &= -i\alpha \int d\bar{z}dz\, \frac{\partial_i\psi\partial_j\bar{\psi} + \partial_i\bar{\psi}\partial_j\psi}{(1+\bar{\psi}\psi)^2} \end{aligned} \tag{4.15}$$

where $z = x + iy$, $\bar{z} = x - iy$, $\bar{\psi}$ is the complex conjugate of ψ, $\partial_i = \partial/\partial q_i$ and $d\bar{z}dz \equiv 2i\, dxdy$ is the integration measure in the complex plane.

4.3.2 Belavin-Polyakov Soliton

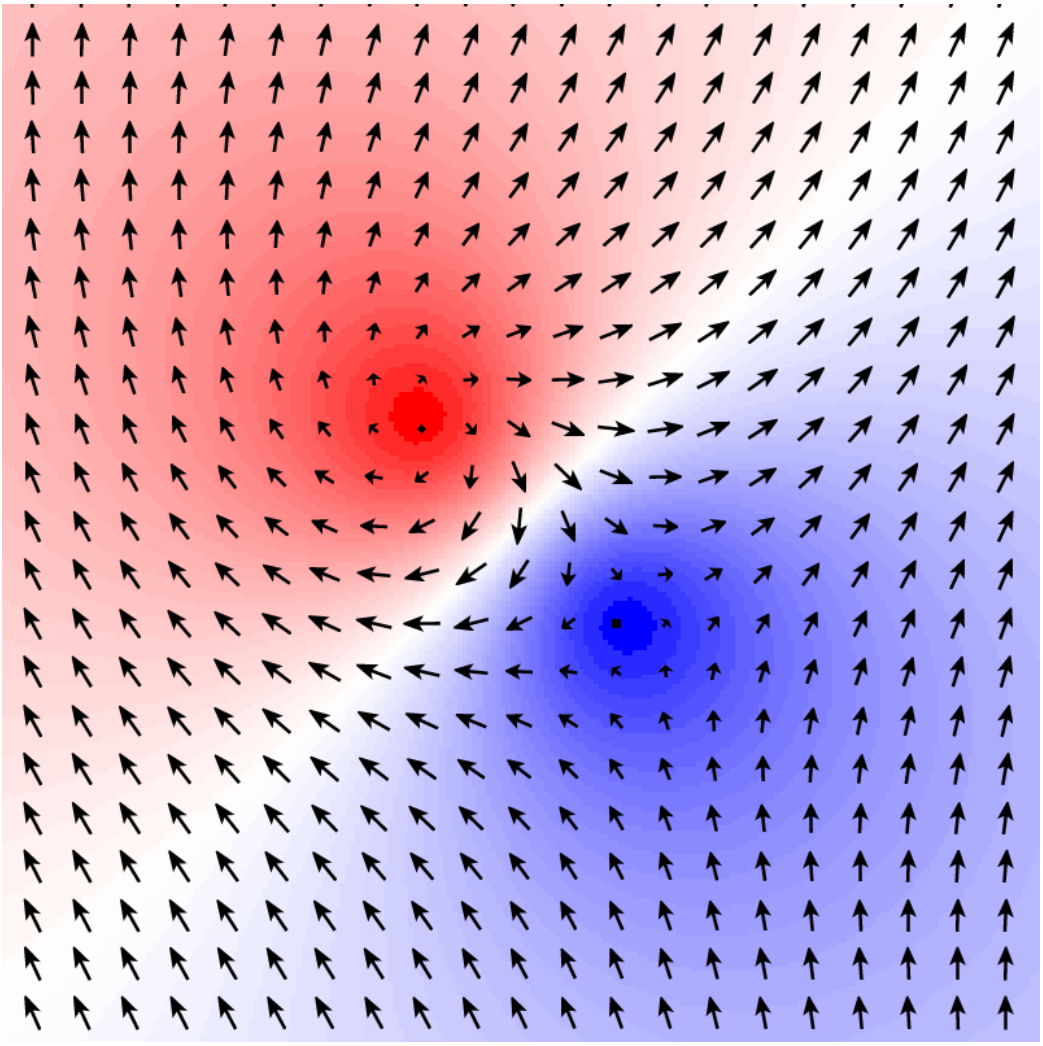

Figure 4.5: A Belavin-Polyakov soliton with separation $r = 0.15$ in rational units. This configuration closely resembles the profile of an annihilating vortex-antivortex pair in the small separation limit, as seen in micromagnetic simulations.

To find a class of exact solutions for vortex-antivortex pair configurations in the

small separation limit, we turn off anisotropy and consider the isotropic Heisenberg ferromagnet in two dimensions. Retaining only the first term in (4.1), one obtains the Heisenberg model ($A = 1$ in our rational units),

$$U_{\rm ex}[\mathbf{m}] = \int dx\, dy\ \frac{1}{2}(\nabla \mathbf{m})^2 = -2i \int \frac{d\bar{z}dz}{(1+\bar{\psi}\psi)^2} \left(\frac{\partial \bar{\psi}}{\partial \bar{z}} \frac{\partial \psi}{\partial z} + \frac{\partial \bar{\psi}}{\partial z} \frac{\partial \psi}{\partial \bar{z}} \right), \tag{4.16}$$

where in the second expression we have used the complex representation. Belavin and Polyakov [8] found a large class of configurations locally minimizing the exchange energy. All these configurations, being exact local minima of the potential energy, are static in a isotropic Heisenberg ferromagnet. They also showed that the total exchange energy of any of these configurations depends only on its skyrmion number S and is equal to $4\pi S$. One of these configurations, that will be useful for studying the vortex-antivortex annihilation, is given by

$$\psi(z) = \frac{z-a}{z-b} \tag{4.17}$$

where $a = (a_1, a_2)$ and $b = (b_1, b_2)$ are any two complex numbers. The configuration $\psi(z)$ is illustrated in Figure 4.5. It is easy to see that this configuration has $\mathbf{m}(a_1, a_2) = \hat{\mathbf{z}}$, $\mathbf{m}(b_1, b_2) = -\hat{\mathbf{z}}$ and $\mathbf{m}(\infty) = \hat{\mathbf{x}}$. Thus it resembles a vortex with core polarity $p = 1$ at location a and an antivortex with core polarity $p = -1$ at location b. Moreover, the mapping $z \mapsto \psi$ is one-to-one and thus $\psi(z)$ has a skyrmion number $S = 1$, just like the vortex-antivortex pair.

Based on these observations, we make the hypothesis that at later stages of the annihilation process, when the core separation $r \ll 1$, one can model the shape of the vortex-antivortex pair using (4.17). This hypothesis will be justified only if the anisotropy term in (4.1) is small (compared to U_{ex}) in this limit, i.e. $|U_{\text{anis}}| \ll U_{\text{ex}} = 4\pi$. If that is the case, one can regard U_{anis} as a weak perturbation that causes the otherwise static configuration $\psi(z) = (z-a)/(z-b)$ to evolve in time through the collective coordinates $a(t)$ and $b(t)$, approach each other, and ultimately annihilate. To be sure, the annihilation of the skyrmion itself, accompanied by a burst of spin waves, involves physics at the lattice scale a (where $a \ll 1$ is the lattice constant) and this continuum theory will not applicable in that regime. One can thus expect the Belavin-Polyakov (BP) soliton to faithfully model the dynamics in the regime $a \ll r \ll 1$, provided that exchange represents the dominant term in energy. We will verify that the anisotropy is indeed small and generates an attractive force in the next subsection.

It is also important to note that for the BP soliton (4.17) $m_z(\rho) \sim 1/\rho$ as $\rho \to \infty$. Thus the out-of-plane magnetization only decays weakly at large distances as the configuration approaches a uniform in-plane limit. This makes the integrals in the gyrotropic tensor G_{ij}, the dissipation tensor Γ_{ij} and the force components F_i diverge logarithmically as the system size, as we'll see in the next subsection. But rigorously speaking, the description of the vortex-antivortex pair in terms of (4.17) is valid only up to some length scale $\Lambda = Cl_0 = C$, where C is an unknown constant. Beyond this

length scale $m_z \sim e^{-\rho}$, as seen in the asymptotic analysis done in Section 4.1. So the divergence in these quantities is not physical and all of these divergent integrals should be cut-off at $\rho = C$.

Also, like before, we will assume that the thin film has a circular shape of radius $R \gg 1$. The geometric center of the pair $\mathbf{R}_{\rm com} = (\mathbf{a}+\mathbf{b})/2 = 0$ stays stationary at the center of this circle. The two collective coordinates will be the relative separation r and the relative orientation ϑ corresponding to $\mathbf{r} = \mathbf{a} - \mathbf{b}$. Also, because of rotational symmetry of the system about the z-axis, the quantities $G_{r\theta}, \Gamma_{rr}$, $\Gamma_{\vartheta\vartheta}$, $\Gamma_{r\vartheta}$, and U will be independent ϑ and depend only on r. As a result, we can safely assume $\mathbf{a} = (r/2, 0)$ and $\mathbf{b} = (-r/2, 0)$ while calculating these quantities.

4.3.3 Anisotropy Energy: Attractive Force

Using the mapping $\mathbf{m} \mapsto \psi$ (4.14), we can substitute the BP soliton (4.17) into the expression for the anisotropy energy given by (4.1):

$$U_{\rm anis}(r) = \frac{1}{2}\int dx\, dy \left(\frac{|z-b|^2 - |z-a|^2}{|z-b|^2 + |z-a|^2}\right)^2 . \tag{4.18}$$

Taking $b = (-r/2, 0)$ and $a = (+r/2, 0)$ and switching to polar coordinates (ρ, θ):

$$U_{\rm anis}(r) = \frac{r^2}{2}\int_0^{2\pi} d\theta \int_0^C \rho d\rho \frac{\rho^2 \cos^2\theta}{(\rho^2 + r^2/4)^2} = \frac{\pi r^2}{2}\left(-1/2 + \ln\frac{C}{r/2}\right). \tag{4.19}$$

In the last step we have used the approximation $r \ll C$. From here obtains the force

$$F(r) = -\frac{\partial U}{\partial r} = -\pi r \left(-1 + \ln \frac{C}{r/2} \right) \tag{4.20}$$

Thus the force is indeed attractive and approaches 0 as the relative separation vanishes. Thus our initial hypothesis of U_{anis} being small and generating an attractive force for the BP soliton is self-consistently justified. We also see that the force depends logarithmically on the unknown constant C, as anticipated before. Also, owing to the rotational symmetry of the system, there is no force in the angular direction $F_\vartheta = 0$.

4.3.4 Gyrotropic and Dissipation Tensor

It turns out that it is easier to calculate the components of the gyrotropic tensor for the original four collective coordinates $\{a_1, a_2, b_1, b_2\}$ and then transform these to the relative coordinates r and ϑ. To this end we first obtain the transformation rules between the two sets of partial derivatives using the relations $\mathbf{a} = r(\cos\vartheta, \sin\vartheta)/2$ and $\mathbf{b} = -r(\cos\vartheta, \sin\vartheta)/2$. These are:

$$\begin{aligned} \frac{\partial}{\partial r} &= \frac{\cos\vartheta}{2}\left(\frac{\partial}{\partial a_1} - \frac{\partial}{\partial b_1}\right) + \frac{\sin\vartheta}{2}\left(\frac{\partial}{\partial a_2} - \frac{\partial}{\partial b_2}\right) \\ \frac{\partial}{\partial \vartheta} &= \frac{r\sin\vartheta}{2}\left(-\frac{\partial}{\partial a_1} + \frac{\partial}{\partial b_1}\right) + \frac{r\cos\vartheta}{2}\left(\frac{\partial}{\partial a_2} - \frac{\partial}{\partial b_2}\right) \end{aligned} \tag{4.21}$$

These transformation rules can be used in (4.15) to transform between components like $G_{r\vartheta}$ to those like $G_{a_1a_2}$.

The calulation of the G_{ij} and the Γ_{ij} components for $q_i = \{a_1, a_2, b_1, b_2\}$ all proceed in the same way. Here we'll illustrate the calculation steps for $G_{a_1a_2}$ and then quote the final expressions for the tensor components for the relative coordinates r and ϑ.

We first express the partial derivatives with respect to real and imaginary parts in terms of the complex partial derivatives

$$\frac{\partial}{\partial a_1} = \frac{\partial}{\partial a} + \frac{\partial}{\partial \bar{a}}, \qquad \frac{\partial}{\partial a_2} = i\left(\frac{\partial}{\partial a} - \frac{\partial}{\partial \bar{a}}\right), \tag{4.22}$$

and similarly for b. We then have, using (4.15) and (4.17)

$$G_{a_1a_2} = -\int d\bar{z}dz\, \frac{\partial_{a_1}\psi\partial_{a_2}\bar{\psi} - \partial_{a_1}\bar{\psi}\partial_{a_2}\psi}{(1+\bar{\psi}\psi)^2} = -\int d\bar{z}dz\ (-2i)\frac{\frac{\partial\psi}{\partial a}\cdot\frac{\partial\bar{\psi}}{\partial\bar{a}}}{(1+\bar{\psi}\psi)^2}. \tag{4.23}$$

Substituting the form of ψ from (4.17),

$$G_{a_1a_2} = -4\int dxdy\, \frac{(x-\frac{r}{2})^2 + y^2}{((x-\frac{r}{2})^2 + (x+\frac{r}{2})^2 + 2y^2)^2}. \tag{4.24}$$

Converting to polar coordinates, cutting off the ρ integral at C and using the condition $r \ll C$, we finally get

$$G_{a_1a_2} = -\int_0^{2\pi} d\varphi \int_a^C \rho d\rho\, \frac{1}{\rho^2 + (\frac{r}{2})^2} \approx -2\pi J \ln\frac{C}{r/2}. \tag{4.25}$$

Once again we see a logarithmic dependence on the constant C. Calculating all the other components of the gyrotropic and dissipation tensors and transforming them to G_{rr}, Γ_{rr}, $\Gamma_{\vartheta\vartheta}$ and $\Gamma_{r\vartheta}$ using (4.21), we obtain the following expressions:

$$\begin{aligned} G_{r\vartheta} &= -\pi r \left(1 + 2\ln\frac{C}{r/2}\right), \\ \Gamma_{rr} &= \alpha\pi \left(1 + 2\ln\frac{C}{r/2}\right), \\ \Gamma_{\vartheta\vartheta} &= \alpha\pi r^2 \left(1 + 2\ln\frac{C}{r/2}\right), \\ \Gamma_{r\vartheta} &= 0. \end{aligned} \tag{4.26}$$

4.3.5 Equations of Motion

The equations of motion for the two collective coordinates r and ϑ, in the framework of (3.16), are:

$$\begin{aligned} r &: G_{r\vartheta}\dot{\vartheta} - \Gamma_{rr}\dot{r} + F_r = 0, \\ \vartheta &: G_{\vartheta r}\dot{r} - \Gamma_{\vartheta\vartheta}\dot{\vartheta} = 0. \end{aligned} \tag{4.27}$$

Here we have used the fact that $\Gamma_{r\vartheta} = F_\vartheta = 0$ for a vortex-antivortex pair. We can simplify these equations by using the fact that the change in relative angle is a fast mode which is present even in an undamped system, i.e. when $\alpha = 0$. The change in relative separation, on the other hand, is purely dissipational and of $O(\alpha)$ and is thus a slow mode. Using expressions for the force (4.20) and the gyrotropic and viscosity

coefficients (4.26) in (4.27) we obtain

$$\begin{aligned} \dot{r} &= -\alpha r \left[\frac{-1 + \ln\left(\frac{2C}{r}\right)}{1 + 2\ln\left(\frac{2C}{r}\right)} \right] \\ \dot{\theta} &= -\left[\frac{-1 + \ln\left(\frac{2C}{r}\right)}{1 + 2\ln\left(\frac{2C}{r}\right)} \right] \end{aligned} \tag{4.28}$$

In both equations we have retained terms only up to the lowest non-vanishing order in the small parameter α. Because of the global rotational symmetry, the initial orientation can be set to zero: $\vartheta(t = 0) = 0$. The solution to the above equations will then depend only on the the initial separation $r(t = 0) = r_0$. Thus the general solution to $r(t)$ and hence $\vartheta(t)$ can be obtained by numerically integrating the first equation in (4.28) for a given initial separation.

4.3.6 Estimates

The second equation in (4.28) can be written as $\dot{\vartheta} = \dot{r}/\alpha r$ which can be readily integrated to give

$$\vartheta(t) = \frac{1}{\alpha} \ln \frac{r(t)}{r_0}. \tag{4.29}$$

In the limit of very small separation ($r \to 0$), the first equation in (4.28) reduces to $\dot{r} = -\alpha r/2$. This implies $r(t) \sim C_1 e^{-\alpha t/2}$. So, the relative separation decays exponentially with a characteristic time $t_c = 2/\alpha$ in this limit. Substituting this in (4.29), one finds that the relative orientation grows linearly $\vartheta(t) \sim C_2 - t/2$ and thus the angular velocity $\omega = \dot{\vartheta}$ approaches a constant value of $-1/2$ in this limit.

A qualitative picture of the dynamics in the large separation limit can also be easily obtained. In this limit, one can largely use the independent vortex and antivortex picture developed in Section 4.2. The gyrotropic tensor for the relative coordinates, obtained using the transformations (4.21), is $G_{r\vartheta} = -\pi r$. Motivated by the result for the dissipation tensor for a single vortex (4.8), one can estimate $\Gamma_{rr} \sim \ln r$. The relations $\Gamma_{\vartheta\vartheta} = r^2\Gamma_{rr}$ and $\Gamma_{r\vartheta} = 0$ seen in (4.26) follow from the symmetries of the vortex-antivortex configuration and are true in this limit as well.

The relative orientation $\vartheta(t)$, being a fast mode, can be well-approximated by the result derived in the non-dissipative case (4.13). Substituting all these expressions in the second equation in (4.27), one obtains an estimate for the velocity of approach $\dot{r} \sim -\alpha(\ln r)/r$. Thus the dynamics is qualitatively similar to that of a domain wall pair derived in Section 3.4.3: the initial approach is logarithmically slow which then transitions to a fast exponential approach at small separation. Moreover, the angular velocity of the pair approaches a limiting value in both cases.

4.4 Discussion

We presented analytical results from an ongoing project studying the annihilation of a vortex and an antivortex of opposite core polarities in a ferromagnetic thin film. Past numerical studies [47] had shown that such a vortex-antivortex pair approach each other in the presence of energy dissipation and ultimately annihilate to create

a uniform state of magnetization. The final annihilation process is accompanied by a burst of spin waves, which can be attributed to the unwinding of a skyrmion at the center of the system. In this chapter, we discussed two theoretical frameworks, based on the method of collective coordinates, addressing the behavior of the vortex-antivortex pair in two limiting cases.

In the limit of large separation, one can assume that the cores of the vortices move as rigid objects. Much of the results obtained for a single isolated vortex/antivortex can be applied in this limit. We argued that an effective theory in terms of two collective coordinates: the relative separation and the relative orientation of the pair can capture the essential features of the dynamics in this limit. We showed that in the absence of dissipation the two cores just circle around their common geometrical center. Adding dissipation would cause them to move toward the center in spiral paths. We are currently calculating the dissipation coefficients of this effective theory which can be used to numerically solve the equations of motion and predict the trajectory of the pair in this limit.

We then turned to the opposite situation: when the vortex and the antivortex are close to each other. We argued that in this limit the pair can be modeled as a Belavin-Polyakov (BP) soliton [8], which is a static configuration in the absence of anisotropy. In the limit of small separation, the anisotropy energy can be treated as a small perturbation which causes the vortex and the antivortex to attract each other. We derived the full equations of motion for the relative separation and orientation of

the pair in the presence of dissipation. A numerical solution of these equations will predict the trajectories of the vortex and the antivortex in the small separation limit.

In addition to completing the theoretical description, we are also currently working on micormagnetic simulations of this annihilation process using the micromagnetic solver OOMMF [46], which can be used to check the predictions of our effective theories in the two limits.

Chapter 5

Discussion

In this dissertation, we have presented theoretical studies of one and two dimensional magnetic systems involving multiple interacting topological solitons. In the first work presented, we have found a composite bound state of kinks (domain walls) in a system of parallel ferromagnetic spin-1/2 Ising chains in the presence of weak effective transverse field and weak antiferromagnetic inter-chain coupling. A model involving a single chain, which treats the inter-chain coupling at the mean field level, predicts a hierarchy of two-kink bound states on one chain. We showed that going beyond the mean field level reveals the existence of more complicated excited states that are bound states of two confined kink pairs on adjacent chains. Using the parameters for the quasi one-dimensional material $CoNb_2O_6$, we found that the lowest four-kink bound state has significant spectral weight. This finding supports the interpretation of an excitation of $CoNb_2O_6$, observed in high resolution time-domain

terahertz spectroscopy, as a four-kink bound state.

We have also studied the annihilation of two domain walls in a ferromagnetic wire with an easy axis using the method of collective coordinates. A minimal description of this process fundamentally requires the inclusion of hard modes, which has posed a significant challenge in past theoretical works. In addition to the parameters for two zero modes of the system corresponding to global translation and rotation, we used the relative separation and the relative twist of the two domain walls as collective coordinates for describing the annihilation process. The latter coordinates become ill-defined in the small separation limit as the two domain walls start to overlap. We found that the two conserved momenta of the system corresponding to the translational and rotational symmetries, that are always well-defined, can be used as proxies for separation and twist. Adding dissipation to the system weakly breaks these symmetries, causing the momenta to decrease with time and bringing the domain walls closer. Predictions of the effective theory thus obtained were found to be in excellent agreement with numerical micromagnetic simulations. Our basic theoretical approach will be applicable even in the presence of other weak interactions that break the symmetries of the system. We hope that similar approaches can be used to study the annihilation of other topological solitons.

We finally have applied these ideas to understand the annihilation process of a vortex and an antivortex in a ferromagnetic thin film. We discussed two theoretical models describing the dynamics of the pair in the large and small separation limits.

In the large separation limit the vortex cores behave as rigid objects moving under an inter-vortex Coulomb force. One can then use the relative separation and the relative orientation of the vortex cores as the two collective coordinates. In the small separation limit the vortex cores start to overlap, and hence deform, much like in the situation with domain walls. Starting from an exact solution found by Belavin and Polykov for the Heisenberg model, and treating the easy-plane anisotropy as a weak perturbation, we developed an effective theory of the dynamics in this limit using the same two collective coordinates: relative separation and orientation. We are currently working on the final part of the analytical calculations that would predict the trajectories of the vortex and the antivortex. We also plan to perform numerical micromagnetic simulations of the annihilation process to check the predictions of our effective theory.

Appendix A

Four-Kink Bound State: Details

A.1 Effective Model on Cubic Lattice

For a given momentum $-\pi \leq k \leq \pi$, the four-kink Hamiltonian H_4 in the $\{v, m, n\}$ basis looks like:

$$\begin{aligned} H_{4,k}\,|v,m,n\rangle = (8J + V(v,m,n))\,|v,m,n\rangle - \alpha \Bigg[& e^{-ik/4} \left\{ \left| v+\frac{1}{2}, m+1, n \right\rangle \right. \\ & \left. + \left| v+\frac{1}{2}, m-1, n \right\rangle + \left| v-\frac{1}{2}, m, n+1 \right\rangle + \left| v-\frac{1}{2}, m, n-1 \right\rangle \right\} \\ & + e^{ik/4} \left\{ \left| v-\frac{1}{2}, m-1, n \right\rangle + \left| v-\frac{1}{2}, m+1, n \right\rangle + \left| v+\frac{1}{2}, m, n-1 \right\rangle \right. \\ & \left. \left. + \left| v+\frac{1}{2}, m, n+1 \right\rangle \right\} \right] - \beta_0 \delta_{m,1} [e^{ik/2}\,|v-1,m,n\rangle + e^{-ik/2}\,|v+1,m,n\rangle] \\ & - \beta_0 \delta_{n,1} [e^{ik/2}\,|v+1,m,n\rangle + e^{-ik/2}\,|v-1,m,n\rangle] + \beta_1 (\delta_{m,1} + \delta_{n,1})\,|v,m,n\rangle \end{aligned} \tag{A.1}$$

Here we have suppressed the momentum index in the state vector for brevity of notation. $m > 0$ and $n > 0$ are two independent positive integers denoting the lengths of the spin clusters on the two adjacent chains. v is the separation between the centers-of-mass of the two clusters. It can take any integer value if $|m-n|$ is even and any half integer value if $|m-n|$ is odd.

So, we now have an effective model of a particle hopping on a simple cubic lattice with coordinates $\{v, m, n\}$ with hard walls at the $m = 0$ and $n = 0$ planes. To keep the calculation simple, we can allow v to assume any integer or half-integer value, regardless of the parity of $|m-n|$. This will double the Hilbert space of the problem by including a lot of unphysical states of the type $|v = 1, m = 1, n = 2\rangle$. But this won't be a problem since $H_{4,k}$ doesn't mix the physical and the unphysical sectors of the Hilbert space. As a result, one can easily check if an eigenstate is physical or not by looking at its overlap with states like $|v = 1, m = 1, n = 2\rangle$.

A.2 Spectral Weight

As noted earlier, to calculate the spectral weight of the four-kink bound state, we need to consider the tunneling processes between the two-kink and the four-kink Hilbert spaces. These processes are mediated by the α-terms in the Hamiltonian H_4. The function of these terms is to flip a single $|\uparrow\rangle$ to $|\downarrow\rangle$ and vice-versa. As a result, they can flip a spin in a completely aligned c-chain and thus create a kink-pair out

of the kink-vacuum. This provides a tunneling mechanism between the the four-kink and the two-kink bound states.

Here we will focus only on the $k = 0$ sector of the "two kink + four kink" Hilbert space: $\{|n,0\rangle, |0,n\rangle, |v;m,n\rangle\}$. Here $|n,0\rangle$ and $|0,n\rangle$ are states that have a spin-cluster of length n in the first and the second chain respectively. It is easy to see that the part of the Hamiltonian that connects the two- and four-kink states H_{24} has the following non-zero matrix elements:

$$\begin{aligned} \langle n,0|\, H_{24}\, |v;n',n''\rangle &= -\alpha\delta_{n,n'}\delta_{1,n''} \\ \langle 0,n|\, H_{24}\, |v;n',n''\rangle &= -\alpha\delta_{1,n'}\delta_{n,n''} \end{aligned} \tag{A.2}$$

Let us denote the hierarchy of two-kink energy eigenstates on the two chains as $|mi,0\rangle$ and $|0,mi\rangle$ where $i \in \mathbb{N}$ and the four-kink ground state as $\left|G^{(0)}\right\rangle$. These can be decomposed into the above basis as:

$$\begin{aligned} |mi,0\rangle &= \sum_n \langle n,0|mi,0\rangle\, |n,0\rangle \\ |0,mi\rangle &= \sum_n \langle 0,n|0,mi\rangle\, |0,n\rangle \\ \left|G^{(0)}\right\rangle &= \sum_{v,m,n} \langle v;m,n|G^{(0)}\rangle\, |v;m,n\rangle \end{aligned} \tag{A.3}$$

Now we can go ahead and calculate the contribution of the two-kink states to $\left|G^{(0)}\right\rangle$

using first order perturbation theory:

$$\left|G^{(1)}\right\rangle = \sum_{mi} \left[\frac{\langle mi,0|\, H_{24} \left|G^{(0)}\right\rangle |mi,0\rangle}{E_G^{(0)} - E_i} + \frac{\langle 0,mi|\, H_{24} \left|G^{(0)}\right\rangle |0,mi\rangle}{E_G^{(0)} - E_i} \right] \tag{A.4}$$

The incoming photon excites a single spin flip anywhere in the two chains: $|s\rangle = \frac{1}{\sqrt{2}}(|1,0\rangle + |0,1\rangle)$. So, the desired spectral weight is given by:

$$S = \frac{|\langle s|G^{(1)}\rangle|^2}{\langle G^{(0)}|G^{(0)}\rangle} \tag{A.5}$$

S can now be evaluated numerically using the matrix elements of H_{24} listed in (A.2) and the state vectors for the two- and four-kink bound states that we have already obtained numerically.

Appendix B

Exact Solution: Domain Wall Pair

B.1 Planar Case

To obtain the planar soliton we need to minimize

$$U[\theta,\phi] = \int_{-\infty}^{\infty} dz \left[\frac{1}{2}\left[\left(\frac{d\theta}{dz}\right)^2 + \sin^2\theta\left(\frac{d\phi}{dz}\right)^2\right] + \frac{1}{2}\sin^2\theta - \Omega(\cos\theta - 1)\right] \quad \text{(B.1)}$$

with respect to $\theta(z)$ and $\phi(z)$ and the boundary condition $\theta(\pm\infty) = 0$. For brevity we'll suppress the tilde on $\tilde{U}$ in this appendix. The condition $\delta U/\delta\phi = 0$ implies $\sin^2\theta\, d\phi/dz$ = constant. Together with the boundary condition for θ and the assumption that $d\phi/dz$ stays finite as $z \to \pm\infty$, this in turn implies that the soliton is confined to one azimuthal plane: $\phi(z) = \Phi$. Substituting this back into (B.1) obtains

an energy functional just involving $\theta(z)$:

$$U[\theta] = \int_{-\infty}^{\infty} dz \left[\frac{1}{2} \left(\frac{d\theta}{dz} \right)^2 + \frac{1}{2} \sin^2 \theta - \Omega(\cos\theta - 1) \right] \tag{B.2}$$

Minimization of this reduced potential energy can be simplified by using the standard trick: pretending z to be a time coordinate, one can think of (B.2) as a "Lagrangian" of a particle moving in an "external potential" $u(\theta) = -1/2 \sin^2 \theta + \Omega(\cos\theta - 1)$. Since this "Lagrangian" doesn't depend explicitly on the "time" z, the corresponding "energy" is a constant of motion:

$$\frac{1}{2} \left(\frac{d\theta}{dz} \right)^2 - \frac{1}{2} \sin^2 \theta + \Omega(\cos\theta - 1) = \text{const} \tag{B.3}$$

The boundary conditions $\theta(\pm\infty) = 0$ and $d\theta/dz(\pm\infty) = 0$ imply const $= 0$. This first order differential equation can now be easily solved to obtain the profile of the soliton $\theta(z)$.

The solution thus obtained is parametrized by the Lagrange multiplier Ω. But it is more convenient for our analysis to use the angular momentum J, or equivalently the separation $\zeta = -J/2$, as the parameter. To switch parameters, we can substitute the expression for $\cos\theta(z)$ into the definition of J. Evaluating the elementary integral, one obtains $\zeta = -J/2 = 2 \operatorname{arctanh} \sqrt{1+\Omega}$. Inverting this gives the angular velocity as a function of separation: $\Omega = \operatorname{sech}^2(\zeta/2)$. This expression can now be used to change the parameter in the solution from Ω to ζ.

B.2 General Case

To obtain the general configuration of a domain wall pair, we need to minimize the following potential energy

$$U[\theta,\phi]=\int_{-\infty}^{\infty}dz\left\{\frac{1}{2}\left[\left(\frac{d\theta}{dz}\right)^2+\sin^2\theta\left(\frac{d\phi}{dz}\right)^2\right]+\frac{1}{2}\sin^2\theta-\Omega(\cos\theta-1)+V(\cos\theta-1)\phi'\right\} \tag{B.4}$$

with respect to $\theta(z)$ and $\phi(z)$ and the boundary condition $\theta(\pm\infty)=0$. Starting from the condition $\delta U/\delta\phi=0$ and using similar arguments as in the previous section, one gets

$$\phi'=\frac{V}{1+\cos\theta}. \tag{B.5}$$

Substituting this back into (B.4) obtains an energy functional just involving $\theta(z)$:

$$U[\theta]=\int_{-\infty}^{\infty}dz\ \left[\frac{1}{2}\left(\frac{d\theta}{dz}\right)^2+\frac{1}{2}\sin^2\theta-\Omega(\cos\theta-1)-\frac{V^2}{2}\tan^2\frac{\theta}{2}\right] \tag{B.6}$$

Just like before, one can integrate the second order ordinary differential equation $\delta U/\delta\theta=0$ once to obtain the first order equation

$$\frac{1}{2}\left(\frac{d\theta}{dz}\right)^2-\frac{1}{2}\sin^2\theta+\Omega(\cos\theta-1)+\frac{V^2}{2}\tan^2\frac{\theta}{2}=\text{const} \tag{B.7}$$

The boundary conditions $\theta(\pm\infty)=0$ and $d\theta/dz(\pm\infty)=0$ imply const $=0$. This first order differential equation can now be easily solved to obtain the $\theta(z)$ profile of

the soliton. The function $\theta(z)$ can then be substituted into (B.5) and integrated to obtain $\phi(z)$.

Once again, we want to switch the parameters from $\{\Omega, V\}$ to $\{\zeta, \varphi\}$. To that end, we calculate the momenta in terms of the velocities like before:

$$\zeta = 2\tanh^{-1}\sqrt{\frac{a}{b}}, \quad \varphi = 2\,\mathrm{sgn}(V)\tan^{-1}\sqrt{\frac{a(b-2)}{b(2-a)}}. \tag{B.8}$$

where $a = 2 + \Omega - \sqrt{\Omega^2 + V^2}$ and $b = 2 + \Omega + \sqrt{\Omega^2 + V^2}$. These can be inverted to obtain

$$\dot{Z} = V = \frac{2\sin\varphi}{\sinh\zeta}, \quad \dot{\Phi} = \Omega = \frac{\sin^2\frac{\varphi}{2}}{\sinh^2\frac{\zeta}{2}} - \frac{\cos^2\frac{\varphi}{2}}{\cosh^2\frac{\zeta}{2}}. \tag{B.9}$$

Appendix C

Equations of Motion for Domain Wall Pair

Since $F_i = -\partial U/\partial q_i$, (3.38) can be integrated to obtain

$$U = \frac{4(\cosh\zeta - \cos\varphi)}{\sinh\zeta} \tag{C.1}$$

The $\Gamma_{ij}(\zeta, \varphi)$ functions form a symmetric 4×4 matrix. It is easy to see that this matrix splits up into two 2×2 matrices, the Z-Φ block and the ζ-φ block, since the remainig four off-diagonal terms are zero. To see this we first express Γ_{ij} in terms of $\theta(z)$ and $\phi(z)$.

$$\Gamma_{ij} = \alpha \int dz \left(\frac{\partial\theta}{\partial q_i}\frac{\partial\theta}{\partial q_j} + \sin^2\theta \frac{\partial\phi}{\partial q_i}\frac{\partial\phi}{\partial q_j} \right) \tag{C.2}$$

As seen from (3.29) to (3.31) above, $\theta(z)$ is even and $\phi(z)$ is odd. Hence if $j = \zeta$ or φ

$$\begin{aligned}\Gamma_{Zj} &= -\alpha \int dz \left(\frac{\partial\theta}{\partial z}\frac{\partial\theta}{\partial q_j} + \sin^2\theta \frac{\partial\phi}{\partial z}\frac{\partial\phi}{\partial q_j}\right) = 0 \\ \Gamma_{\Phi j} &= \alpha \int dz \, \sin^2\theta \frac{\partial\phi}{\partial q_j} = 0\end{aligned} \tag{C.3}$$

Only the Z-Φ block enters the equations of motion at $O(\alpha)$ and these functions involve only elementary integrals. Performing these integrals, one obtains

$$\begin{aligned}\Gamma_{Z\Phi} &= -4\alpha\zeta \frac{\sin\varphi}{\sinh\zeta}, \\ \Gamma_{\Phi\Phi} &= \alpha \left[(b-a)\ln\left|\frac{1+\sqrt{a/b}}{1-\sqrt{a/b}}\right| + 2\sqrt{ab} + 4(2-b)\tanh^{-1}\sqrt{\frac{a}{b}}\right], \\ \Gamma_{ZZ} &= 2\alpha U - \Gamma_{\Phi\Phi},\end{aligned} \tag{C.4}$$

where $a(\zeta,\varphi)$ and $b(\zeta,\varphi)$ are defined in (3.30).

The two coupled first-order differential equations for $\zeta(t)$ and $\varphi(t)$ in (3.41) can only be solved numerically. However, the large-t limit, when $\zeta, \varphi \to 0$, is analytically tractable. In this limit one can expand all the quantities up to the lowest non-vanishing order in the two relative coordinates. This gives

$$V = 2\varphi/\zeta \qquad \Omega = (\varphi/\zeta)^2 - 1 \tag{C.5a}$$

$$U = 2(\zeta^2 + \varphi^2)/\zeta \tag{C.5b}$$

$$\Gamma_{Z\Phi} = -4\alpha\varphi \qquad \Gamma_{\Phi\Phi} = 4\alpha\zeta \qquad \Gamma_{ZZ} = 4\alpha\varphi^2/\zeta \tag{C.5c}$$

(C.5a) implies the constraint $\Omega(t) = V(t)^2/4 - 1$ in this limit. Substituting these expressions in the equations of motion (3.41) gives

$$\begin{aligned} \dot{\varphi} &= -2\alpha(1 + \varphi^2/\zeta^2)\varphi \\ \dot{\zeta} &= -2\alpha(1 + \varphi^2/\zeta^2)\zeta \end{aligned} \tag{C.6}$$

These readily imply $\dot{V} = (\zeta\dot{\varphi} - \dot{\zeta}\varphi)/\zeta^2 = 0$. Hence both V and Ω approach constant values V_∞ and $\Omega_\infty = V_\infty^2/4 - 1$, the exact values of which depend on the choice of initial conditions ζ_0 and φ_0. This also implies that the two relative coordinates ζ and φ are decoupled in this limit and they both decay exponentially with the same time constant $\tau^{-1} = 2\alpha(2 + \Omega_\infty)$. The shape of the soliton in this limit can be obtained by expanding (3.31) to the lowest order terms in the relative coordinates.

$$\begin{aligned} f(z;\zeta,\varphi) &= -\Big(1 + \frac{\Omega_\infty}{2}\Big)\zeta^2 \operatorname{sech}^2\Big[\Big(1 + \frac{\Omega_\infty}{2}\Big)\zeta z\Big] \\ g(z;\zeta,\varphi) &= \frac{V_\infty}{2} z + \tan^{-1}\Big[\frac{\varphi}{2}\tanh\Big[\Big(1 + \frac{\Omega_\infty}{2}\Big)\zeta z\Big]\Big] \end{aligned} \tag{C.7}$$

The expression for $f = m_z(z) - 1$ shows that the profile has a characteristic width $w^{-1} = (1 + \Omega_\infty/2)\zeta$ which diverges as the uniform state is approached.

Appendix D

G_{ij} and Γ_{ij} in the Complex Representation

To use the complex representation of magnetization

$$\psi = \frac{m_x + i m_y}{1 + m_z} = \tan\frac{\theta}{2}\, e^{i\phi} \tag{D.1}$$

in our calculations involving collective coordinates, we need to express the gyrotropic tensor G_{ij} and the dissipation tensor Γ_{ij} in this representation. We will present the derivation for G_{ij} in this appendix. The derivation for Γ_{ij} is done along very similar lines.

Here we will consider a planar magnet characterized by $\mathbf{m}(x, y)$. We first need to write the vector expression for the gyrotropic tensor given in (3.16) in terms of the

polar angle $\theta(x, y)$ and the azimuthal angle $\phi(x, y)$. Using the relation

$$\mathbf{m} = (\sin\theta\cos\phi, \sin\theta\sin\phi, \cos\theta) \tag{D.2}$$

we obtain

$$G_{ij} = -\int dxdy \left[\frac{\partial\phi}{\partial q_i}\frac{\partial\cos\theta}{\partial q_j} - \frac{\partial\cos\theta}{\partial q_i}\frac{\partial\phi}{\partial q_j}\right] \tag{D.3}$$

We can calculate the total differentials of ψ and $\bar{\psi}$ from (D.1) as

$$d\psi = \frac{\psi}{\sin\theta}(d\theta + i\sin\theta\, d\phi),\ d\bar{\psi} = \frac{\psi}{\sin\theta}(d\theta - i\sin\theta\, d\phi). \tag{D.4}$$

This allows us to solve for $d\theta$ and $d\phi$ in terms of the complex differentials.

$$d\theta = \frac{\sin\theta}{2}\left(\frac{d\psi}{\psi} + \frac{d\bar{\psi}}{\bar{\psi}}\right) \tag{D.5}$$

$$d\phi = \frac{-i}{2}\left(\frac{d\psi}{\psi} - \frac{d\bar{\psi}}{\bar{\psi}}\right) \tag{D.6}$$

These can now be used to convert the partial derivatives of the polar and azimuthal angles in (D.3) to those of the complex fields ψ and $\bar{\psi}$, which yields the desired expression

$$G_{ij} = -\int d\bar{z}dz\, \frac{\partial_i\psi\partial_j\bar{\psi} - \partial_i\bar{\psi}\partial_j\psi}{(1+\bar{\psi}\psi)^2} \tag{D.7}$$

Bibliography

[1] W. Heisenberg, "Mehrkrperproblem und resonanz in der quantenmechanik," *Z. Phys.*, vol. 38, no. 6-7, pp. 411–426, 1926. [Online]. Available: http://dx.doi.org/10.1007/BF01397160

[2] P. A. M. Dirac, "Quantum mechanics of many-electron systems," *Proc. Roy. Soc. (London) A*, vol. 123, no. 792, pp. 714–733, 1929. [Online]. Available: http://rspa.royalsocietypublishing.org/content/123/792/714.short

[3] A. M. Kosevich, B. A. Ivanov, and A. S. Kovalev, "Magnetic solitons," *Phys. Rep.*, vol. 194, pp. 117–238, Oct. 1990. [Online]. Available: http://www.sciencedirect.com/science/article/pii/037015739090130T

[4] P. M. Chaikin and T. C. Lubensky, "Principles of condensed matter physics," *Cambridge University Press*, 2000.

[5] S. Hikami and T. Tsuneto, "Phase transition of quasi-two dimensional planar system," *Progress of Theoretical Physics*, vol. 63, no. 2, p. 387, 1980.

[Online]. Available: https://academic.oup.com/ptp/article/63/2/387/1887126/Phase-Transition-of-Quasi-Two-Dimensional-Planar

[6] D. L. Huber, "Dynamics of spin vortices in two-dimensional planar magnets," *Phys. Rev. B*, vol. 26, no. 7, p. 3758, 1982. [Online]. Available: https://journals.aps.org/prb/abstract/10.1103/PhysRevB.26.3758

[7] R. Rajaraman, "Solitons and instantons," *North-Holland Publishing Company*, 1982.

[8] A. A. Belavin and A. M. Polyakov, "Metastable states of two-dimensional isotropic ferromagnets," *JETP Letters*, vol. 22, p. 245, 1975. [Online]. Available: http://www.jetpletters.ac.ru/ps/1529/article_23383.shtml

[9] A. Altland and B. D. Simons, "Condensed matter field theory," *Cambridge University Press*, 2010.

[10] R. Coldea, D. A. Tennant, E. M. Wheeler, E. Wawrzynska, D. Prabhakaran, M. Telling, K. Habicht, P. Smeibidl, and K. Kiefer, "Quantum criticality in an ising chain: Experimental evidence for emergent e_8 symmetry," *Science*, vol. 327, no. 5962, pp. 177–180, 2010. [Online]. Available: http://science.sciencemag.org/content/327/5962/177

[11] C. Morris, R. V. Aguilar, A. Ghosh, S. Koohpayeh, J. Krizan, R. Cava, O. Tchernyshyov, T. McQueen, and N. Armitage, "Hierarchy of bound

states in the one-dimensional ferromagnetic ising chain $CoNb_2O_6$ investigated by high-resolution time-domain terahertz spectroscopy," *Physical Review Letters*, vol. 112, no. 13, p. 137403, 2014. [Online]. Available: https://journals.aps.org/prl/abstract/10.1103/PhysRevLett.112.137403

[12] S. Sachdev, "Quantum phase transitions, second edition," *Cambridge University Press*, 2011.

[13] P. Pfeuty, "The one-dimensional ising model with a transverse field," *Annals of Physics*, vol. 57, no. 1, pp. 79–90, 1970. [Online]. Available: http://www.sciencedirect.com/science/article/pii/0003491670902708

[14] S. Rutkevich, "Energy spectrum of bound-spinons in the quantum ising spin-chain ferromagnet," *Journal of Statistical Physics*, vol. 131, no. 5, pp. 917–939, 2008. [Online]. Available: https://link.springer.com/article/10.1007/s10955-008-9495-1

[15] J. B. Torrence and M. Tinkham, "Magnon bound states in anisotropic linear chains," *Physical Review*, vol. 187, no. 2, p. 587, 1969. [Online]. Available: https://journals.aps.org/pr/abstract/10.1103/PhysRev.187.587

[16] ——, "Excitation of multiple-magnon bound states in $CoCl_2.2H_2O$," *Physical Review*, vol. 187, no. 2, p. 595, 1969. [Online]. Available: https://journals.aps.org/pr/abstract/10.1103/PhysRev.187.595

[17] B. M. McCoy and T. T. Wu, "Two-dimensional ising field theory in a magnetic field: Breakup of the cut in the two-point function," *Phys. Rev. D*, vol. 18, no. 4, p. 1259, 1978. [Online]. Available: https://journals.aps.org/prd/abstract/10.1103/PhysRevD.18.1259

[18] C. Heid, H. Weitzel, P. Burlet, M. Bonnet, W. Gonschorek, T. Vogt, J. Norwig, and H. Fuess, "Magnetic phase diagram of $CoNb_2O_6$: A neutron diffraction study," *Journal of Magnetism and Magnetic Materials*, vol. 151, no. 1-2, pp. 123–131, 1995. [Online]. Available: http://www.sciencedirect.com/science/article/pii/0304885395003940

[19] S. Kobayashi, S. Mitsuda, and K. Prokes, "Low-temperature magnetic phase transitions of the geometrically frustrated isosceles triangular ising antiferromagnet $CoNb_2O_6$," *Physical Review B*, vol. 63, no. 2, p. 024415, 2000. [Online]. Available: https://journals.aps.org/prb/abstract/10.1103/PhysRevB.63.024415

[20] T. Hanawa, K. Shinkawa, M. Ishikawa, K. Miyatani, K. Saito, and K. Kohn, "Anisotropic specific heat of $CoNb_2O_6$ in magnetic fields," *Journal of the Physical Society of Japan*, vol. 63, no. 7, pp. 2706–2715, 1994. [Online]. Available: http://journals.jps.jp/doi/10.1143/JPSJ.63.2706

[21] W.Scharf, H.Weitzel, I.Yaeger, I.Maartense, and B.M.Wanklyn, "Magnetic structures of $CoNb_2O_6$," *Journal of Magnetism and Magnetic Materials*, vol. 13,

pp. 121–124, 1979. [Online]. Available: http://www.sciencedirect.com/science/article/pii/0304885379900441?via%3Dihub

[22] S. S. P. Parkin, M. Hayashi, and L. Thomas, "Magnetic domain-wall racetrack memory," *Science*, vol. 320, no. 5873, p. 190, 2008. [Online]. Available: http://science.sciencemag.org/content/320/5873/190

[23] L. D. Landau and E. M. Lifshitz, *Phys. Z. Sow.*, vol. 8, p. 153, 1935.

[24] T. Gilbert, "A phenomenological theory of damping in ferromagnetic materials," *IEEE Trans. Magn.*, vol. 40, no. 6, pp. 3443–3449, 2004. [Online]. Available: http://ieeexplore.ieee.org/document/1353448/

[25] N. L. Schryer and L. R. Walker, "The motion of 180° domain walls in uniform dc magnetic fields," *J. Appl. Phys*, vol. 45, no. 12, pp. 5406–5421, 1974. [Online]. Available: http://aip.scitation.org/doi/abs/10.1063/1.1663252

[26] O. A. Tretiakov, D. Clarke, G.-W. Chern, Y. B. Bazaliy, and O. Tchernyshyov, "Dynamics of domain walls in magnetic nanostrips," *Phys. Rev. Lett.*, vol. 100, p. 127204, Mar 2008. [Online]. Available: http://link.aps.org/doi/10.1103/PhysRevLett.100.127204

[27] B. A. Ivanov and V. A. Stephanovich, "Two-dimensional soliton dynamics in ferromagnets," *Phys. Lett. A*, vol. 141, no. 1, pp. 89 – 94, 1989. [Online]. Available: http://www.sciencedirect.com/science/article/pii/0375960189904532

[28] K. Y. Guslienko, X. F. Han, D. J. Keavney, R. Divan, and S. D. Bader, "Magnetic vortex core dynamics in cylindrical ferromagnetic dots," *Phys. Rev. Lett.*, vol. 96, p. 067205, Feb 2006. [Online]. Available: http://link.aps.org/doi/10.1103/PhysRevLett.96.067205

[29] C. H. Wong and Y. Tserkovnyak, "Dissipative dynamics of magnetic solitons in metals," *Phys. Rev. B*, vol. 81, p. 060404, Feb 2010. [Online]. Available: http://link.aps.org/doi/10.1103/PhysRevB.81.060404

[30] I. Makhfudz, B. Krüger, and O. Tchernyshyov, "Inertia and chiral edge modes of a skyrmion magnetic bubble," *Phys. Rev. Lett.*, vol. 109, p. 217201, Nov 2012. [Online]. Available: http://link.aps.org/doi/10.1103/PhysRevLett.109.217201

[31] S. K. Kim and Y. Tserkovnyak, "Landau-lifshitz theory of thermomagnonic torque," *Phys. Rev. B*, vol. 92, p. 020410, Jul 2015. [Online]. Available: http://link.aps.org/doi/10.1103/PhysRevB.92.020410

[32] B. A. Ivanov and A. K. Kolezhuk, "Solitons with internal degrees of freedom in 1d heisenberg antiferromagnets," *Phys. Rev. Lett.*, vol. 74, pp. 1859–1862, Mar 1995. [Online]. Available: http://link.aps.org/doi/10.1103/PhysRevLett.74.1859

[33] E. G. Tveten, A. Qaiumzadeh, O. A. Tretiakov, and A. Brataas, "Staggered dynamics in antiferromagnets by collective coordinates," *Phys. Rev. Lett.*, vol. 110, p. 127208, Mar 2013. [Online]. Available: https://journals.aps.org/prl/abstract/10.1103/PhysRevLett.110.127208

[34] S. K. Kim, Y. Tserkovnyak, and O. Tchernyshyov, "Propulsion of a domain wall in an antiferromagnet by magnons," *Phys. Rev. B*, vol. 90, p. 104406, Sep 2014. [Online]. Available: http://link.aps.org/doi/10.1103/PhysRevB.90.104406

[35] E. G. Tveten, T. Müller, J. Linder, and A. Brataas, "Intrinsic magnetization of antiferromagnetic textures," *Phys. Rev. B*, vol. 93, p. 104408, Mar 2016. [Online]. Available: http://link.aps.org/doi/10.1103/PhysRevB.93.104408

[36] D. J. Clarke, O. A. Tretiakov, G.-W. Chern, Y. B. Bazaliy, and O. Tchernyshyov, "Dynamics of a vortex domain wall in a magnetic nanostrip: Application of the collective-coordinate approach," *Phys. Rev. B*, vol. 78, p. 134412, Oct 2008. [Online]. Available: http://link.aps.org/doi/10.1103/PhysRevB.78.134412

[37] A. Ghosh, K. S. Huang, and O. Tchernyshyov, "Annihilation of domain walls in a ferromagnetic wire," *Physcal Review B*, vol. 95, no. 18, p. 180408, 2017. [Online]. Available: https://journals.aps.org/prb/abstract/10.1103/PhysRevB.95.180408

[38] O. Tchernyshyov, "Conserved momenta of a ferromagnetic soliton," *Annals of Physics*, vol. 363, pp. 98–113, 2015. [Online]. Available: http://www.sciencedirect.com/science/article/pii/S0003491615003395

[39] J. C. Slonczewski, "Theory of domainwall motion in magnetic films and platelets," *Journal of Applied Physics*, vol. 44, p. 1759, 1973. [Online]. Available: http://aip.scitation.org/doi/abs/10.1063/1.1662444

[40] A. A. Thiele, "On the momentum of ferromagnetic domains," *Journal of Applied Physics*, vol. 47, p. 2759, 1976. [Online]. Available: http://aip.scitation.org/doi/abs/10.1063/1.323005

[41] F. D. M. Haldane, "Geometrical interpretation of momentum and crystal momentum of classical and quantum ferromagnetic heisenberg chains," *Phys. Rev. Lett.*, vol. 57, pp. 1488–1491, Sep 1986. [Online]. Available: http://link.aps.org/doi/10.1103/PhysRevLett.57.1488

[42] G. E. Volovik, "Linear momentum in ferromagnets," *Journal of Physics C: Solid State Physics*, vol. 20, no. 7, p. L83L87, 1987. [Online]. Available: http://iopscience.iop.org/article/10.1088/0022-3719/20/7/003/meta

[43] N. Papanicolaou and T. N. Tomaras, "Dynamics of magnetic vortices," *Nuclear Physics B*, vol. 360, no. 2-3, pp. 425–462, 1991. [Online]. Available: http://www.sciencedirect.com/science/article/pii/055032139190410Y?via%3Dihub

[44] A. M. Kosevich, B. A. Ivanov, and A. S. Kovalev, "Nonlinear localized magnetization wave of a ferromagnet as a bound state of a large number of magnons," *JETP Lett.*, vol. 25, no. 11, pp. 486–489, Jun. 1977. [Online]. Available: http://www.jetpletters.ac.ru/ps/1415/article_21475.shtml

[45] K. A. Long and A. R. Bishop, "Nonlinear excitations in classical ferromagnetic chains," *J. Phys. A: Math. Gen.*, vol. 12, no. 8, p. 1325, 1979. [Online]. Available: http://stacks.iop.org/0305-4470/12/i=8/a=025

[46] M. J. Donahue and D. G. Porter, "Oommf user's guide, version 1.0," *National Institute of Standards and Technology Report No. NISTIR 6376, math.nist.gov/oommf*, 1999.

[47] R. Hertel and C. M. Schneider, "Exchange explosions: Magnetization dynamics during vortex-antivortex annihilation," *Phys. Rev. Lett.*, vol. 97, no. 17, p. 177202, 2006. [Online]. Available: https://journals.aps.org/prl/abstract/10.1103/PhysRevLett.97.177202

[48] T. Apostol, "Mathematical analysis, second edition," *Addison-Wesley*, 1974.

Vita

Anirban Ghosh was born in West Bengal, India on October 5, 1984. He received the M. Sc. degree in Physics from the Indian Institute of Technology, Kharagpur in 2008, and enrolled in the Physics Ph.D. program at the Johns Hopkins University in the same year. Although initially pursuing theoretical particle physics, he got interested in the theory of magnetism in 2011. His research since then has focused on the properties of interacting topological solitons in classical and quantum magnets.

In addition to doing research in the theory of condensed matter, he maintains a keen interest in science teaching and communication. He has been a teaching assistant for a variety of physics courses at Hopkins and received the E J Rhee Teaching Award in 2014.